Dynamics and control of photon transport in coupled cavities

By

Nilakantha Meher

(Enrolment No. PHYS 02 2013 04 0001)

Indira Gandhi Centre for Atomic Research, Kalpakkam, India.

A thesis submitted to the

Board of Studies in Physical Sciences

in partial fulfillment of requirements

for the Degree of

DOCTOR OF PHILOSOPHY

of

HOMI BHABHA NATIONAL INSTITUTE

May, 2018

Homi Bhabha National Institute

Recommendations of the Viva Voce Board

As members of the Viva Voce Committee, we certify that we have read the dissertation prepared by **Nilakantha Meher** entitled **"Dynamics and control of photon transport in coupled cavities"** and recommend that it may be accepted as fulfilling the thesis requirement for the award of Degree of Doctor of Philosophy.

________________________ Date: Nov 19, 2018
(Chairman- Dr. G. Amarendra)

________________________ Date: 19/Nov/18
(Guide/Convener- Dr. S. Sivakumar)

Tarak Nath Dey
________________________ Date: 19/11/18
(External Examiner - Dr. Tarak Nath Dey)

________________________ Date: 19/Nov./18
(Member 1: Dr. Arul Lakshminarayan)

________________________ Date: 19/Nov/18
(Member 2: Dr. G. Raghavan)

________________________ Date: 19/11/2018
(Member 3: Dr. T. R. Ravindran)

Final approval and acceptance of this thesis is contingent upon the candidate's submission of the final copies of the thesis to HBNI.

I hereby certify that, I have read this thesis prepared under my direction and recommend that it may be accepted as fulfilling the thesis requirement.

Date: 19/Nov/18

Place: Kalpakkam

(Dr. S. Sivakumar)

STATEMENT BY AUTHOR

This dissertation has been submitted in partial fulfillment of requirements for an advanced degree at Homi Bhabha National Institute (HBNI) and is deposited in the Library to be made available to borrowers under rules of the HBNI.

Brief quotations from this dissertation are allowable without special permission, provided that accurate acknowledgment of source is made. Requests for permission for extended quotation from or reproduction of this manuscript in whole or in part may be granted by the Competent Authority of HBNI when in his or her judgment the proposed use of the material is in the interests of scholarship. In all other instances, however, permission must be obtained from the author.

Date: 19/11/2018
Place: Kalpakkam

Nilakantha Meher

DECLARATION

I, hereby declare that the investigation presented in the thesis has been carried out by me. The work is original and has not been submitted earlier as a whole or in part for a degree / diploma at this or any other Institution / University.

NMeher

Nilakantha Meher

List of Publications

PUBLICATIONS

(a). Published

1. **N. Meher** and S. Sivakumar, "Quantum interference induced photon localization and delocalization in Kerr-type nonlinear cavities," J. Opt. Soc. Am. B, 33, 1233-1241 (2016).

2. **N. Meher**, S. Sivakumar and P. K. Panigrahi, "Duality and quantum state engineering in cavity arrays," Scientific Reports 7, 9251 (2017).

3. **N. Meher** and S. Sivakumar, "Number state filtered coherent states," Quantum Information Processing 17, 233 (2018).

4. **N. Meher** and S. Sivakumar, "Atomic switch for control of heat transfer in coupled cavities," arXiv:1804.01897 [quant-ph].

(b). Other publications

(i) Conference/Symposium:

1. **N. Meher** and S. Sivakumar, "Nonintegrability and quantum fluctuations in a quantum optical model," National Laser Symposium 23 (2014), Tirupati. ISBN: 9788190332156 CP-04-04.

2. **N. Meher** and S. Sivakumar, "Generation of W state via quantum control of hopping strength in cavities in arrays," Young Quantum 2015, HRI, Allahabad.

3. **N. Meher**, S. Sivakumar and S. Kanmani, "Investigation on Wu-Anandan Matrix for separability," International conference on Light Quanta: Modern Perspectives and Applications, Allahbad, PA.11 (2015).

4. **N. Meher** and S. Sivakumar, "Localization and delocalization dynamics of photons in linearly coupled cavity arrays," in 13th International Conference on Fiber Optics and Photonics, OSA Technical Digest (online) (Optical Society of America, 2016), paper Th3A.73.

N. Meher

Nilakantha Meher

To

Maa and Bapa

Acknowledgments

It is a pleasure to express my sincere and heartfelt gratitude to Prof. S. Sivakumar for his excellent guidance and encouragement. His unbounded motivation and kindness ensured that I never felt frustration in my Ph.D life. I have always admired his deep insights and ability to present complicated ideas in simpler ways, which I can only hope to imitate. Not only have I benefited from the opportunity to learn about research from an expert in quantum optics, but also got the opportunity to learn quantum mechanics, statistical physics, mathematical physics and quantum optics from his amazing lectures. He allowed me to conduct problem sessions and teach some parts in the courses on quantum mechanics and mathematical physics courses offered by HBNI. It helped me a lot in understanding these subjects.

I would like to extend my sincere thanks to the doctoral committee members Prof. G. Amarendra, Prof. Arul Lakshminarayan, Prof. G. Raghavan and Prof. T. R. Ravindran for their comments and suggestions. I would like to thank Prof. N. V. Chandra Shekar, Dean and Prof. B. V. R. Tata, former Dean, Physical Sciences for their support.

I make a special mention of Prof. Prasanta K. Panigrahi, IISER Kolkata, for fruitful discussions and collaboration.

The unconditional love, encouragement and blessings of my parents helped me to overcome many barriers to reach the milestone of Ph.D. But for my brothers Santosh and Ashok, and sister Reena, I could not have become what I am now. They taught and guided me right from my school days. I thank all my family members, especially, my brother-in-law (jijaji) Jiten whose encouragement and support mean a lot to me.

I am in debted of my teachers for their excellent teaching and support.

My special thanks to all the members of the Materials Science Group, especially, Mr. S. Kanmani, Dr. Awadhesh Mani, Dr. Tripura Sundari and Dr. Sandip K. Dhara for their suggestions and encouragement during my stay at IGCAR. I extend my gratitude to Mr. Kanmani for his excellent lectures on mathematical physics.

I thank all my Bakwaas brothers Srinivasan, Radhakrishna, Anees, Manan, Karthickeyan, Subrat, Deepak, Mahendran, Devidas, Vinod and Dhilipan for their encouragement all these years. I extend my thanks to all my Hataash batchmates-cum-friends Padmalochan, Radhikesh, Irshad, Lakshmanan, Vairavel, Zaibudeen, Manoj and Madhushmita for their friendship and help. Acknowledgment would be incomplete without thanking my Hataash juniors-cum-friends Binaya (Iron Man), Alok(Hulk), Gopinath(Hawkeye), Santanu(Dr. Strange), Pradosh, Anil, Dilip(Captain America), Bijaya, Prasant, Sudarshan, Alaka(Makhmali), Arpita(Changi), Shradha (Chulubuli), Parvathy, Ijee (Nali), Pragnya (Kenjdi), Akshaya (Chaain) and Rajitha(Chuin) for their care and concern towards me. Special thanks to all my well wishers and friends in the JRF enclave. I also thank my school and college friends, especially, Rajesh, Pandav, Brushabh, Bibek, Bhikari, Radhe, Soubhagya, Sumanta, Himanshu, Anil, Dinabandhu, Dillip, Manas, Lokanath, Soumendra.

I would like to acknowledge the Department of Atomic Energy for the research fellowship. I extend my gratitude to our director Dr. A. K. Bhadhuri, Dr. M. Saibaba and Dr. Lakshmi Narasimman for their support. I would also like to thank the office staff of MSG, especially Ms. Vidhya and Ms. Kavya for their assistance.

Abstract

Controlled transfer of photonic qubits is essential for implementing quantum information protocols in cavity arrays. A basic requirement for effecting such a transfer is to tailor the system parameters such as the cavity frequencies, couplings, detunings, etc. Moreover, cavities containing atom or nonlinear medium can be considered that have additional control parameters, namely, the atomic state and nonlinearity. Controlled dynamics of photon transfer in a cavity array by appropriate choices of these parameters is established in this thesis.

Perfect transfer of a single photon in an array is not possible if the cavity couplings are homogeneous. A duality relation between two systems, namely, $N-1$ photons in two coupled cavities and a single photon in N cavities is employed to arrive at the required coupling strengths and nonlinearities in the array so that controlled and perfect photon transfer is possible between any two cavities in the array. Every transition in the two-cavity system has a dual phenomenon in terms of photon transport in the array. The condition for perfect transfer of photon enables transfer of photonic qubit between any two cavities in the array. Possibility of high fidelity generation of generalized NOON states in the two coupled cavities, which are dual to the Bell states of the photon in the cavity array, is established.

If the cavity array has more number of photons, localization and delocalization of photons are possible. These two features are analogous to the bunching and antibunching of photons. Occurrence of localization and delocalization of photons in linear cavities are explained *via* quantum interference. The role of the relative phase and entanglement in the initial superposition is discussed. Complete localization and delocalization of product states, which are absent in linear cavities, is possible in Kerr nonlinear cavities. Dynamics of photon transfer in dissipative structures is another topic discussed in this thesis. A system of two coupled cavities connected between two thermal reservoirs is considered. Embedding a dispersively interacting single atom in any one of the cavities brings a controllable flow of heat energy through the array. The thermal current through a system of two coupled cavities containing a single atom depends on the atomic state. By switching the state of the atom from its excited state to the ground state, the system changes from a thermal conductor to an insulator. In addition, by properly tuning the atomic state and system-reservoir parameters, direction of current can be reversed, thereby violating the second law of thermodynamics. It is shown that a large thermal rectification is achievable in this system by tuning the cavity-reservoir and cavity-atom couplings. Partial recovery of diffusive heat transport in an array of N cavities containing one dispersively coupled atom is also established.

Contents

List of Figures

Chapter 1

Cavity quantum optics

Quantum theory is presently the best description of nature. Formulated to understand the atomic spectrum, it is believed to be the formalism that can be used to understand nature at all scales, from the substructure of elementary particles to the entire universe. On the pragmatic side, many technological marvels such as the semiconductor devices, lasers, quantum-interference devices, etc are direct applications of quantum theory. The formalism continues to inspire new ideas. Quantum information processing is a recent example which promises features such as the teleportation, unbreakable codes, exponentially faster computation, etc which are not possible within the ambit of the classical physics [1]. An essential ingredient in all these is the ability to control the evolution of the system to achieve the desired result. Many experiments have been performed to show that it is indeed possible to design the evolution to gain control over the dynamics of atoms, ions and photons [2–6]. Apart from the practical applications, fundamental issues of quantum theory can also be addressed using these controllable systems. This thesis focuses on photon transfer in coupled cavities with a view to show the possibility of quantum control in such systems.

This chapter provides a review of the canonical field quantization in a cavity, various properties of cavities and cavity arrays. States of the electromangetic field such as the number states and thermal states are introduced. Cavities containing material medium or atom, in particular, Kerr medium and two-level atoms, are discussed. Inclusion of Kerr medium provides for control of quantum evolution of the cavity field. Dissipative processes are important as they are unavoidable. A review of some of the formalisms used in the study of dissipation in quantum systems is included.

1.1 Electromagnetic field

Space-time evolution of the electromagnetic field in vacuum is described by the Maxwell's equations, which are

$$\vec{\nabla} \cdot \vec{E}(\vec{r}, t) = 0, \tag{1.1a}$$

$$\vec{\nabla} \cdot \vec{B}(\vec{r}, t) = 0, \tag{1.1b}$$

$$\vec{\nabla} \times \vec{E}(\vec{r}, t) = -\tfrac{\partial}{\partial t}\vec{B}(\vec{r}, t), \tag{1.1c}$$

and
$$\vec{\nabla} \times \vec{B}(\vec{r}, t) = \mu_0 \epsilon_0 \tfrac{\partial}{\partial t}\vec{E}(\vec{r}, t), \tag{1.1d}$$

where μ_0 and ϵ_0 are respectively the permeability and the permittivity of the free space. A consequence of these equations is that the electric and magnetic fields satisfy

$$\vec{\nabla}^2 \vec{X}(\vec{r}, t) = \frac{1}{c^2}\frac{\partial^2}{\partial t^2}\vec{X}(\vec{r}, t), \tag{1.2}$$

where $\vec{X}(\vec{r}, t)$ can be $\vec{E}(\vec{r}, t)$ or $\vec{B}(\vec{r}, t)$. These equations imply that the electromagnetic wave propagates in free space with speed c. Another consequence of the Eqns. 1.1$(a - d)$ is that the fields $\vec{E}$ and $\vec{B}$ are transverse, *i.e.*, $\vec{E}$, $\vec{B}$ and the direction of propagation are mutually perpendicular to each other. These equations can be modified to include source terms as well. If boundary conditions are imposed on the fields, these equations can describe fields in confined geometry as well.

An important case is the description of the electromagnetic field between two perfectly conducting plates separated by a length L (cavity) as shown in Fig. 1.1. In the limit of large L, the field corresponds to the electromagnetic field in free space. The field is assumed to be propagating along z-direction and the electric field is polarized in

x-direction, *i.e.*, $\vec{E}(r,t) = \hat{e}_x E_x(r,t)$, where $\hat{e}_x$ is the polarization direction.

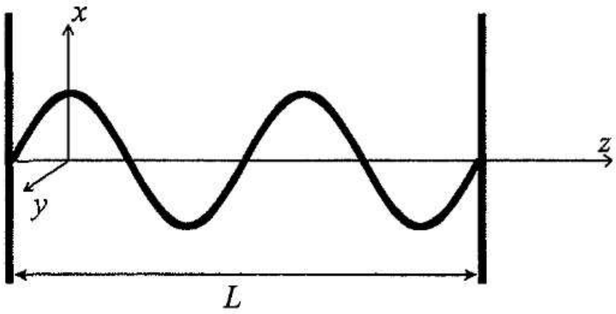

Figure 1.1 – Two parallel conducting surfaces located at $z = 0$ and $z = L$, forms a cavity. Electromagnetic field is propagating along z-axis and polarized along x-axis.

As the walls are perfectly conducting, the electric field vanishes at the boundaries at $z = 0$ and $z = L$. In order to write the explicit form of $\vec{E}$ for the cavity field, consider the fundamental modes of the electromagnetic field. Fundamental modes are the eigenfunctions of the spatial part of the wave equation. Any arbitrary distribution of the electric field inside the cavity can be expressed as a linear combination of these fundamental modes [7],

$$E_x(z,t) = \sum_{j=1}^{\infty} A_j q_j(t) \sin(k_j z), \tag{1.3}$$

where q_j is the amplitude of the jth fundamental mode with the dimension of length and $k_j = j\pi/L$ is the magnitude of the wave vector. The amplitude q_j plays the role of the canonical position for an oscillator. The expansion coefficient $A_j = \left(\frac{2\omega_j}{V\epsilon_0}\right)^{\frac{1}{2}}$ where ω_j is the frequency of jth fundamental mode and V is the modal volume. These modes satisfy the orthogonality relation

$$\int_0^L \sin(k_n z)\sin(k_m z)dz = \frac{L}{2}\delta_{nm}. \tag{1.4}$$

Boundary conditions on the electric field restrict the possible frequencies to

$$\omega_j = \frac{j\pi c}{L}. \tag{1.5}$$

These are the resonance frequencies of the cavity. Separation between two successive resonance frequencies is $\pi c/L$, which is negligible if L is large.

Similarly, the magnetic field inside the cavity is

$$B_y(z,t) = \sum_j A_j \left(\frac{p_j(t)\epsilon_0\mu_0}{k_j} \right) \cos(k_j z). \tag{1.6}$$

Here $p_j(t) = \dot{q}_j(t)$ is analogous to the canonical momentum for a particle in the Hamiltonian dynamics.

The Hamiltonian for the electromagnetic field is

$$H = \frac{1}{2}\int dV \left[\epsilon_0 E_x^2(z,t) + \frac{1}{\mu_0} B_y^2(z,t) \right], \tag{1.7}$$

which is the energy of the field. Using the expressions for E_x and B_y respectively from Eqn. 1.3 and 1.6, the total Hamiltonian is

$$H = \frac{1}{2}\sum_j \left(p_j^2(t) + \omega_j^2 \; q_j^2(t) \right). \tag{1.8}$$

The Hamiltonian has the same structure as that for a set of independent harmonic oscillators. In essence, each fundamental mode of the electromagnetic field is equivalent to an oscillator. The electric field and the magnetic field are equivalent to the position and the momentum respectively.

1.2 Quantization of electromagnetic field in cavity

Many experiments in optics are explainable by treating the electromagnetic field as classical [8]. However, there are a few notable experimental outcomes such as the black-body spectrum, spontaneous emission, lamb shift, resonance fluorescence, squeezed states, etc., that require quantization of the electromagnetic field [7]. As the cavity field is equivalent to a harmonic oscillator, quantization of the electromagnetic field is straightforward. Quantization provides an elegant way of understanding the classical wave picture of the field in terms of quantum picture. This indicates that the field is made up of field quanta which can be created and annihilated.

It can be inferred from the wave equation given in Eqn. 1.2 that the respective amplitudes, namely, q and p of the electric and magnetic fields obey the classical equations of motion of a harmonic oscillator. The canonical variables $q(t)$ and $p(t)$ are represented by self-adjoint operators $\hat{q}$ and $\hat{p}$ which satisfy the commutation relation $[\hat{q}, \hat{p}] = i\hbar I$. For further analysis, it is advantageous to define

$$\begin{aligned} \hat{a}_j &= \frac{1}{\sqrt{2\hbar\omega_j}}(\omega_j \hat{q}_j + i\hat{p}_j), \\ \hat{a}_j^\dagger &= \frac{1}{\sqrt{2\hbar\omega_j}}(\omega_j \hat{q}_j - i\hat{p}_j), \end{aligned} \tag{1.9}$$

which satisfy $[\hat{a}_j, \hat{a}_k^\dagger] = I\delta_{j,k}$. The operators $\hat{a}_j$ and $\hat{a}_j^\dagger$ are called the creation and annihilation operators respectively. In terms of these operators, the Hamiltonian for the quantized electromagnetic field is

$$\hat{H} = \sum_j \hbar\omega_j \left(\hat{a}_j^\dagger \hat{a}_j + \frac{1}{2} \right). \tag{1.10}$$

The term $1/2\hbar\omega_j$ corresponds to the energy of the vacuum of the jth mode.

The electric and magnetic field operators are

$$\hat{E}_x(z,t) = \sum_j \left(\frac{\hbar\omega_j}{\epsilon_0 V}\right)^{1/2} (\hat{a}_j + \hat{a}_j^\dagger) \sin k_j z,$$

$$\text{and} \qquad \hat{B}_y(z,t) = \sum_j \frac{\mu_0}{k_j} \left(\frac{\epsilon_0 \hbar\omega_j^3}{V}\right)^{1/2} \frac{1}{i} (\hat{a}_j - \hat{a}_j^\dagger) \cos k_j z, \tag{1.11}$$

respectively.

1.3 Quantum states of electromagnetic field

As noted in the previous section, each mode of electromagnetic field inside the cavity is equivalent to a harmonic oscillator. These independent modes are described in their respective Hilbert spaces. The collection of modes is described in the tensor product space of the respective Hilbert spaces corresponding to the modes. A single mode electromagnetic field has specific spatial distribution of the electric field decided by the geometry of the cavity and the boundary conditions. The amplitude of the shape function is subjected to canonical quantization as described in the previous section.

1.3.1 Number states

The Hamiltonian for a single mode field is

$$\hat{H} = \hbar\omega \left(\hat{a}^\dagger \hat{a} + \frac{1}{2}\right). \tag{1.12}$$

The eigenvalue equation for this Hamiltonian is

$$\hat{H} |n\rangle = E_n |n\rangle, \qquad n = 0, 1, 2, 3, ... \tag{1.13}$$

where $E_n = (n + 1/2)\hbar\omega$ is the energy of the nth excited state of the field. The state $|n\rangle$ corresponds to the eigenstate having n photons with total energy $(n + 1/2)\hbar\omega$. These eigenstates are called number states as they correspond to states of definite number of photons. Being the eigenstates of the self-adjoint operator $\hat{H}$, the number states $\{|n\rangle\}$ form a complete basis for the Hilbert space associated with the single mode field. Consequently, these states satisfy the completeness relation

$$\sum_{n=1}^{\infty} |n\rangle \langle n| = I. \tag{1.14}$$

Any state of that single mode field can be expressed as a superposition of the number states.

The action of the creation and annihilation operators on a number state $|n\rangle$ is

$$\begin{aligned} \hat{a}\,|n\rangle &= \sqrt{n}\,|n-1\rangle\,, \qquad \hat{a}\,|0\rangle = 0, \\ \hat{a}^{\dagger}\,|n\rangle &= \sqrt{n+1}\,|n+1\rangle\,. \end{aligned} \tag{1.15}$$

The reason for naming $\hat{a}$ as annihilation operator is that it changes a n-photon state to $(n-1)$-photon state. Similarly, the creation operator $\hat{a}^{\dagger}$ changes the n-photon state to $(n+1)$-photon state. Expectation value of operator $\hat{a}^{\dagger}\hat{a}$ in a number state gives the number of photons in the electromagnetic field, *i.e.*, $\langle n|\,\hat{a}^{\dagger}\hat{a}\,|n\rangle = n$. Hence, $\hat{n} = \hat{a}^{\dagger}\hat{a}$ is called the number operator.

The expectation value of the electric field in the number state is

$$\langle n|\,\hat{E}_x(z,t)\,|n\rangle \propto \langle n|\,(\hat{a}+\hat{a}^{\dagger})\,|n\rangle = 0, \tag{1.16}$$

and the fluctuation in the electric field is

$$\Delta E_x = \sqrt{\langle \hat{E}_x^2(z,t)\rangle - \langle \hat{E}_x(z,t)\rangle^2} = \sqrt{2}\left(\frac{\hbar\omega}{\epsilon_0 V}\right)^{1/4} |\sin kz| \left(n+\frac{1}{2}\right)^{1/2}. \tag{1.17}$$

Interestingly, fluctuation is non-zero even if $n = 0$. This is the vacuum fluctuation which is responsible for various effects such as the spontaneous emission, Lamb-shift, Casimir force, etc [9]. The fluctuations of the electric field in a number state are non-zero due to the fact that the electric field operator $\hat{E}_x$ does not commute with the number operator $\hat{a}^\dagger\hat{a}$. They satisfy the uncertainty relation [10]

$$\Delta\hat{n}\Delta\hat{E}_x \geq \frac{1}{2}\left(\frac{\hbar\omega}{\epsilon_0 V}\right)^{1/2} |\sin(kz)||\langle\hat{a}^\dagger - \hat{a}\rangle|. \tag{1.18}$$

This uncertainty bound implies that the state of the electromagnetic field does not lead to a well localized point in the phase space. However, it is useful to define two dimensionless quadrature operators analogous to the position and momentum operators, in order to describe the phase space properties of the field. Quadrature operators are defined as $\hat{X}_1 = (\hat{a} + \hat{a}^\dagger)/2$ and $\hat{X}_2 = (\hat{a} - \hat{a}^\dagger)/2i$. The uncertainties in $\hat{X}_1$ and $\hat{X}_2$ for the state $|n\rangle$ are

$$\langle(\Delta\hat{X}_1)^2\rangle = \langle(\Delta\hat{X}_2)^2\rangle = \frac{1}{4}(2n+1), \tag{1.19}$$

which increase with n. Note that the vacuum state $|0\rangle$ minimizes the uncertainty as

$$\langle(\Delta\hat{X}_1)^2\rangle = \langle(\Delta\hat{X}_2)^2\rangle = \frac{1}{4}. \tag{1.20}$$

1.3.2 Thermal states

The electromagnetic radiation from an object at a non-zero temperature is called thermal light. The density operator for the single mode electromagnetic field inside a cavity at temperature T is

$$\hat{\rho}_{th} = \frac{\exp(-\hat{H}/k_B T)}{\sum_n \exp(-\hat{H}/k_B T)}, \tag{1.21}$$

where $\hat{H} = (1/2 + \hat{a}^\dagger\hat{a})\hbar\omega$.

In the number state representation, the density matrix for thermal state is

$$\hat{\rho}_{th} = \frac{1}{1+\bar{n}} \sum_{n=0}^{\infty} \left(\frac{\bar{n}}{1+\bar{n}} \right)^n |n\rangle \langle n| \,, \tag{1.22}$$

where the average number of photons in the cavity field is the Bose-Einstein (BE) distribution

$$\bar{n} = \frac{1}{\exp(\hbar\omega/k_B T) - 1}. \tag{1.23}$$

According to the statistical distribution of the occupation of the energy levels, the probability of finding n quanta in the mode is

$$P_n = \frac{\exp(-E_n/k_B T)}{\sum_n \exp(-E_n/k_B T)}, \tag{1.24}$$

where $E_n = (n+1/2)\hbar\omega$ for harmonic oscillator and Boltzmann constant $k_B = 1.38 \times 10^{-23}$J/K. This probability can be expressed as

$$P_n = \frac{\bar{n}^n}{(1+\bar{n})^{n+1}}, \tag{1.25}$$

in terms of the mean photon number. Thus, temperature and mean photon number are equivalent parameters for the equilibrium distribution.

Photon number fluctuation in the thermal state is

$$\langle (\Delta n)^2 \rangle = \bar{n} + \bar{n}^2, \tag{1.26}$$

which is larger than the average number of photons in the field.

1.4 Cavity

A cavity is an arrangement of mirrors that confines light of certain resonance frequencies. The electromagnetic field inside the cavity satisfies suitable boundary conditions such as the vanishing of the electric field at the mirrors. The resonance frequencies given in Eqn. 1.5 for a planar cavity are dependent on the cavity length (L) which can be adjusted by using a shear piezo-actuator [11]. The tunability of the cavity resonance frequency allows to realize active tunable devices such as the microdisk lasers, modulators, optical switches, filters for optical communication etc. [12, 13]. A cavity containing a suitable material medium such as a two-level atom or Kerr medium offers a wide range of potential applications.

For understanding the basic properties of a cavity, consider a planar cavity consisting of two mirrors M_1 and M_2 with reflectivities R_1 and R_2 respectively. This arrangement is also known as Fabry-Perot cavity. A schematic diagram of a single Fabry-Perot cavity is given in the Fig. 1.2.

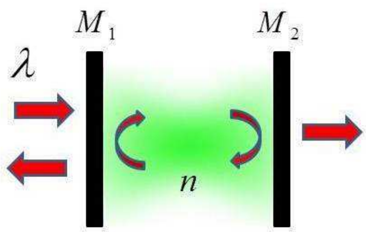

Figure 1.2 – A Fabry-Perot cavity of length L with two parallel mirrors M_1 and M_2. The refractive index of the medium inside the cavity is n.

The mirrors are separated by a distance L. The cavity can be empty or filled with a medium of refractive index n. The properties of the cavity are determined by shining a light of wavelength λ and collecting the transmitted light. In the absence of absorption and scattering losses, the transmittivity of the cavity is [14]

$$T = \frac{1}{1 + (4F^2/\pi^2)\sin^2(\phi/2)}, \tag{1.27}$$

where $\phi = 4\pi nL/\lambda$ is the round-trip phase shift. Quality of the cavity is measured by its finesse F defined as

$$F = \frac{\pi(R_1R_2)^{1/4}}{1-\sqrt{R_1R_2}}. \tag{1.28}$$

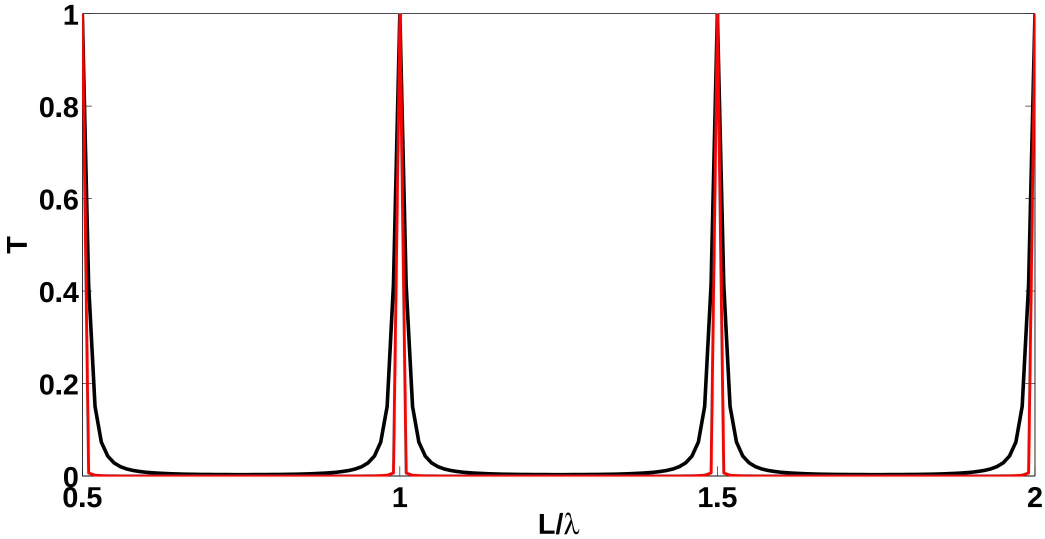

Figure 1.3 – Transmission profile of a Fabry-Perot cavity as a function of L/λ for reflectivities of the mirrors $R_1 = R_2 = 0.9$ (black) and $R_1 = R_2 = 0.99$ (red). The refractive index of the medium inside the cavity is taken as $n = 1$.

Transmission profile of a Fabry-Perot cavity is shown as a function of L/λ in Fig. 1.3. There is complete transmission if the cavity length is a half-integral multiple of λ, *i.e.*, $\phi = 2\pi m$, where m is an integer. The finesse of the cavity can be calculated from the full-width at half-maximum of the spectrum peak,

$$F = \frac{2\pi}{\Delta\phi_{FWHM}} = \frac{2\pi(m+1) - 2\pi m}{\Delta\phi_{FWHM}}. \tag{1.29}$$

Hence, finesse is also defined as the ratio of the separation between two adjacent maxima to the half-width which parametrizes the resolving power or spectral resolution of the cavity. For an ideal cavity, *i.e*, $R_1 = R_2 = 1$, the full-width at half-maximum becomes zero. This, in turn, means that the finesse is infinity. The transmitted light will have a sharp resonance frequency and its integral overtones. This is an ideal condition.

Deviation from this ideal condition amounts to leakage of photons/energy from the cavity. This is quantified by the cavity loss rate γ defined as

$$\gamma = \frac{\omega}{Q}, \tag{1.30}$$

where Q is the quality factor of the cavity (Q-factor). The Q-factor is the ratio of the energy stored in the cavity to the energy loss per round-trip. Essentially, Q-factor of a cavity characterizes the capability of storing the energy. A cavity with large Q-factor stores photons for a long time. Such a high Q cavity is a suitable physical system for generating, storing and manipulating the states of the electromagnetic field [15]. Any state of the electromagnetic field is achievable from the vacuum state of the cavity by a sequence of operations [16]. The state of the field can be manipulated either by external driving or embedded atoms [17–19, 19–21]. By suitably tailoring the external driving or atom-field coupling strengths, cavity state can be evolved to a desired target state [22]. Experimental realization of these theoretical ideas requires ultrahigh-Q cavities. Such cavities are fabricated in various configurations such as the Fabry-Perot [23, 24], pillar [25], whispering gallery resonators [26, 27], photonic crystal [28, 29], etc [30–32]. These cavities are being used for realizing strong atom-field coupling [33], imaging of atoms beyond diffraction limit [34, 35], atom-cavity microscope [24], controlling light pulse propagation [36], atom-field entanglement [37], bio-sensor [38, 39], optical sensor [40], etc.

1.5 Coupled cavity modes

Many of the quantum information protocols, for instance, quantum state transfer, quantum dense coding and quantum cryptography involve transfer of a qubit through a quantum channel. Qubits can be realized with photons [41], spins [42], atoms [43–45], phonons [46], etc. Of these, photons have several advantages due to their transfer speed and absence of mutual interaction. Transfer of photonic qubit requires a quantum channel that should allow controllability and high fidelity transfer. Coupled cavities as quantum channels are suitable for realizing the aforementioned protocols [43, 47–50]. Technological progress in the fabrication of high finesse cavities has rendered it possible to couple several cavities to build an extended quantum network [29]. Coupling of cavities is established by different mechanism such as the evanescent wave [51, 52], inductive coupling and capacitive coupling [53], wave guide coupling [54], etc. Coupling leads to energy exchange between them. The rate of exchange of energy depends on the coupling strength (J), which in turn, depends on the overlap of the spatial profiles of resonant modes [55] as depicted in Fig. 1.4.

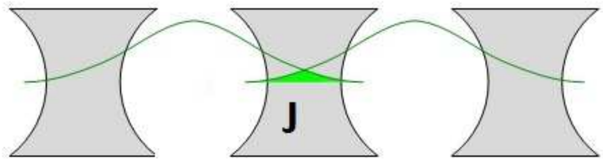

Figure 1.4 – Two coupled cavities with their spatial profile of resonant modes. The overlap of modes decide the coupling strength J.

The interaction energy for the cavities coupled *via* evanescent wave is [56, 57]

$$H_{int} = \int \epsilon E_1 E_2^* dV, \tag{1.31}$$

where ϵ is the relative permittivity profile for the coupled cavities.The range of integration extends over the coupled cavities. The two cavities are considered to be non-ideal in the sense that their electric field distributions extend beyond the cavity boundaries. Here E_1 and E_2 represent the electric fields of these cavities. If the cavities are ideal then the electric fields are confined within the respective cavities and the interaction energy vanishes.

The single mode electric field of the individual cavities in terms of the creation and annihilation operators is

$$\hat{E}_j = \sqrt{\frac{\hbar\omega_j}{2\epsilon_0\epsilon_{rj}V_j}}(\hat{a}_j + \hat{a}_j^\dagger)u_j(z), \qquad j = 1, 2 \tag{1.32}$$

where $u_j(z)$ is the mode function of the jth cavity in the absence of other cavity. Here ϵ_{rj} is the relative permittivity of the medium present and V_j is the mode volume of the jth cavity respectively.

The interaction Hamiltonian becomes

$$\begin{aligned}\hat{H}_{int} =& \sqrt{\frac{\hbar\omega_1}{2\epsilon_0\epsilon_{r1}V_1}}\sqrt{\frac{\hbar\omega_2}{2\epsilon_0\epsilon_{r2}V_2}}\int \epsilon(a_1 + a_1^\dagger)(a_2 + a_2^\dagger)u_1(z)u_2^*(z)dV, \\ =& J(\hat{a}_1 + \hat{a}_1^\dagger)(\hat{a}_2 + \hat{a}_2^\dagger),\end{aligned} \tag{1.33}$$

where

$$J = \sqrt{\frac{\hbar\omega_1}{2\epsilon_0\epsilon_{r1}V_1}}\sqrt{\frac{\hbar\omega_2}{2\epsilon_0\epsilon_{r2}V_2}}\int \epsilon u_1(z)u_2^*(z)dV. \tag{1.34}$$

The total Hamiltonian for the coupled cavities is

$$H = \hbar\omega_1\hat{a}_1^\dagger\hat{a}_1 + \hbar\omega_2\hat{a}_2^\dagger\hat{a}_2 + J(\hat{a}_1 + \hat{a}_1^\dagger)(\hat{a}_2 + \hat{a}_2^\dagger). \tag{1.35}$$

The evolution equations for the annihilation operators in resonant case ($\omega_1 = \omega_2 = \omega$) are [58]

$$\begin{pmatrix} \hat{a}_1(t) \\ \hat{a}_2(t) \end{pmatrix} = MAM \begin{pmatrix} \hat{a}_1(0) \\ \hat{a}_2(0) \end{pmatrix} + MBM \begin{pmatrix} \hat{a}_1^\dagger(0) \\ \hat{a}_2^\dagger(0) \end{pmatrix}, \tag{1.36}$$

where

$$M = \frac{1}{\sqrt{2}} \begin{pmatrix} 1 & 1 \\ 1 & -1 \end{pmatrix},$$

$$A = \begin{pmatrix} \alpha_x^2 e^{-i\sqrt{\omega^2+2J\omega}t} - \beta_x^2 e^{i\sqrt{\omega^2+2J\omega}t} & 0 \\ 0 & \alpha_y^2 e^{-i\sqrt{\omega^2-2J\omega}t} - \beta_y^2 e^{i\sqrt{\omega^2-2J\omega}t} \end{pmatrix},$$

$$B = \begin{pmatrix} -2i\alpha_x\beta_x \sin\sqrt{\omega^2+2J\omega}t & 0 \\ 0 & -2i\alpha_y\beta_y \sin\sqrt{\omega^2-2J\omega}t \end{pmatrix}.$$

Here

$$\alpha_x = \frac{\sqrt{\omega^2+2J\omega}+\omega}{2\sqrt{\omega}(\omega^2+2J\omega)^{1/4}}, \alpha_y = \frac{\sqrt{\omega^2-2J\omega}+\omega}{2\sqrt{\omega}(\omega^2-2J\omega)^{1/4}}, \beta_x = \frac{\sqrt{\omega^2+2J\omega}-\omega}{2\sqrt{\omega}(\omega^2+2J\omega)^{1/4}},$$

$$\text{and} \qquad \beta_y = \frac{\sqrt{\omega^2-2J\omega}-\omega}{2\sqrt{\omega}(\omega^2-2J\omega)^{1/4}}.$$

If $2J/\omega << 1$, then $\beta_x \approx 0 + \mathcal{O}(2J/\omega)$, $\beta_y \approx 0 + \mathcal{O}(2J/\omega)$, $\alpha_x \approx 1 + \mathcal{O}(2J/\omega)$ and $\alpha_y \approx 1 + \mathcal{O}(2J/\omega)$. Therefore, in the first order approximation, B becomes a null matrix and

$$A = \begin{pmatrix} e^{-i(\omega+J)t} & 0 \\ 0 & e^{-i(\omega-J)t} \end{pmatrix}. \tag{1.37}$$

Now, the equations of motion given in Eqn. 1.36 become

$$a_1(t) \approx e^{-i\omega t}[\cos Jt\ a_1(0) - i\sin Jt\ a_2(0)], \tag{1.38}$$

$$a_2(t) \approx e^{-i\omega t}[\cos Jt\ a_2(0) - i\sin Jt\ a_1(0)]. \tag{1.39}$$

These evolution equations are identical to the ones generated by the Hamiltonian

$$\hat{H} = \hbar\omega\hat{a}_1^\dagger\hat{a}_1 + \hbar\omega\hat{a}_2^\dagger\hat{a}_2 + J(\hat{a}_1^\dagger\hat{a}_2 + \hat{a}_1\hat{a}_2^\dagger). \tag{1.40}$$

Hence, in the limit $2J/\omega << 1$, the dynamics generated by the Hamiltonian given in Eqn. 1.35 is similar to the dynamics generated by the Hamiltonian given in Eqn. 1.40. In other words, the counter rorating terms do not affect the dynamics significantly[59].

In the non-resonant case, the equations of motion for the annihilation operators (using the Hamiltonian given in Eqn. 1.35) are

$$\begin{aligned}\frac{d}{dt}a_1 &= -i\omega_1 a_1 - iJ(a_2 + a_2^\dagger),\\ \frac{d}{dt}a_2 &= -i\omega_2 a_2 - iJ(a_1 + a_1^\dagger).\end{aligned} \tag{1.41}$$

In the weak coupling limit, *i.e.*, $2J/\omega_1, 2J/\omega_2 << 1$, the annihilation operators evolve as

$$a_1(t) \approx a_1(0)e^{-i\omega_1 t} \text{ and } a_2(t) \approx a_2(0)e^{-i\omega_2 t}. \tag{1.42}$$

Therefore,

$$\begin{aligned}&\langle \hat{a}_i \hat{a}_j \rangle_t \propto \exp(-i(\omega_i + \omega_j)t)\langle \hat{a}_i \hat{a}_j \rangle_0,\\ &\langle \hat{a}_i^\dagger \hat{a}_j^\dagger \rangle_t \propto \exp(i(\omega_i + \omega_j)t)\langle \hat{a}_i^\dagger \hat{a}_j^\dagger \rangle_0,\\ \text{and}\qquad &\langle \hat{a}_i \hat{a}_j^\dagger \rangle_t \propto \exp(-i(\omega_i - \omega_j)t)\langle \hat{a}_i \hat{a}_j^\dagger \rangle_0,\end{aligned} \tag{1.43}$$

where $i, j = 1, 2$. In the near resonant case, *i.e.*, $\omega_1 \approx \omega_2$, the terms $\langle \hat{a}_i \hat{a}_j \rangle_t$ and $\langle \hat{a}_i^\dagger \hat{a}_j^\dagger \rangle_t$ oscillate many times during a single oscillation of $\langle \hat{a}_i \hat{a}_j^\dagger \rangle$. As a result, time averages of $\langle \hat{a}_i \hat{a}_j \rangle$ and $\langle \hat{a}_i^\dagger \hat{a}_j^\dagger \rangle$ are small compared to $\langle \hat{a}_i \hat{a}_j^\dagger \rangle$ [58]. Neglecting these highly oscillating terms from the Hamiltonian given in Eqn. 1.35 is known as the rotating wave approximation (RWA). In this approximation, the Hamiltonian given in Eqn. 1.35 becomes

$$\hat{H} = \hbar\omega_1 \hat{a}_1^\dagger \hat{a}_1 + \hbar\omega_1 \hat{a}_2^\dagger \hat{a}_2 + J(\hat{a}_1^\dagger \hat{a}_2 + \hat{a}_1 \hat{a}_2^\dagger). \tag{1.44}$$

Due to the coupling between the cavities, photons in any one of the cavities propagate to other cavity [50, 60, 61]. One way of controlling the coupling strength J is by altering the distance between the cavities [29, 51, 62].

The Hamiltonian given in Eqn. 1.44 describes many physical systems such as the coupled phonic crystal cavities [29], coupled whispering-gallery cavities [51], coupled superconducting strip line resonators [53], driven optomechanical cavity in red detuned regime [63], single photon scattering from microsphere resonator in subwavelength limit [64] and a pair of trapped ions [65]. Photonic crystal cavities are coupled *via* evanescent wave field [29]. The overlap of cavity mode functions allow exchange of energy [55].

In the case of superconducting stripline resonators, coupling occurs *via* mutual inductance and mutual capacitance. The coupling strength between two superconducting strip line resonators is [53]

$$J_{SR} = \frac{\omega_0}{2}\sqrt{\frac{C^2}{(1+C)(1+2C)}\left(1+\frac{1}{\nu}\frac{C^2}{1-C^2}\right)} - \frac{\omega_0}{2\nu}\frac{L}{1-L^2}\sqrt{\frac{1+C}{1+2C}\frac{\nu(1-L^2)}{\nu(1-L^2)+L^2}}. \tag{1.45}$$

The first term arises due to capacitive coupling and the second term corresponds to inductive coupling. The quantities C and L are proportional to conductance and inductance of the resonator respectively, ω_0 is the frequency of both the resonators and ν is a geometric factor.

In case of optomechanical system, an optical field is coupled to a mechanical resonator *via* radiation pressure[63]. In this case coupling strength is

$$J_{opt} = \frac{\omega}{L}\sqrt{\frac{P_{in}}{\hbar\omega_d}}\sqrt{\frac{\gamma}{\gamma^2+4\delta^2}}, \tag{1.46}$$

where ω is the resonance frequency, L is the length of the cavity and γ is the decay

Table 1.1 – Experimental parameters

Systems	Resonance frequencies (Hz)	Coupling strengths(Hz)	Q-factor	Ref.
Photonic crystal cavity	3.33×10^{14}	1.3×10^{12}	2500	[29]
Photonic crystal cavity	1.169×10^{14}	1.1×10^{10}	10^5	[52]
Superconducting resonator	6.65×10^{9}	1.2×10^{9}	10^4-10^6	[53, 66]
Optomechanical cavity	65×10^{6}	1.6×10^{6}	4.33	[67]

rate of the cavity. Laser input power is P_{in} and its frequency is ω_d. The detuning between the cavity and the laser is $\delta = \omega - \omega_d$.

Currently achievable values of resonance frequencies, Q-factors and coupling strengths are listed in Table. 1.1.

1.6 Open quantum system

An ideal system is characterized by its complete isolation from all possible influences of the environment. Its dynamics is governed by a unitary transformation. The total energy of an isolated system remains constant during time evolution. However, complete isolation of a system from its surrounding is not possible. Interaction between a system and the environment which has large number of degrees of freedom (environment) leads to a dissipative dynamics of the system. Such systems are called open quantum systems.

Consider a damped harmonic oscillator whose equations of motion are

$$\dot{q} = \frac{p}{m},$$
$$\dot{p} = -m\omega^2 q - \gamma p, \tag{1.47}$$

where q and p are position and momentum of the oscillator. The natural frequency of the oscillator is ω. The damping rate in the system is γ. Equivalently, q satisfies

$$\ddot{q} + \gamma\dot{q} + \omega^2 q = 0. \tag{1.48}$$

To see the problem of describing the damped oscillator quantum mechanically, the classical variables q and p are replaced by the operators $\hat{q}$ and $\hat{p}$ satisfying $[\hat{q}, \hat{p}] = i\hbar$. The Heisenberg equations of motion for $\hat{q}$ and $\hat{p}$ are similar to those of the classical equations of motion given in Eqn. 1.47. On using the solutions of the Heisenberg equations, the commutation relation between $\hat{q}$ and $\hat{p}$ satisfies

$$[\hat{q}(t), \hat{p}(t)] = e^{-\gamma t} i\hbar. \tag{1.49}$$

For $t > 0$, the commutation relation deviates from the canonical commutation between $\hat{q}$ and $\hat{p}$. An immediate consequence is that the Heisenberg uncertainty relation becomes

$$\Delta\hat{q}\Delta\hat{p} \geq \frac{1}{2}\hbar e^{-\gamma t}. \tag{1.50}$$

This is erroneous as quantum mechanics limits the product of $\Delta\hat{q}\Delta\hat{p}$ to be greater than or equal to $\hbar/2$. Hence, replacing the classical variables by operators is not a suitable prescription to quantize the damped oscillator.

There are several approaches for incorporating dissipation in quantum systems. For instance, quantum master equation and Monte-Carlo wavefunction are the most used approaches. The results produced in this thesis are based on the master equation method. A review of this approach is presented here.

1.6.1 Master equation method

One of the most commonly used approaches in the description of open quantum systems is the quantum master equation [68]. In this method, the evolution equation for the reduced density matrix of the system is obtained by tracing over the variables of the reservoir. Two versions of quantum master equations, one due to Redfield [69] and another due to Lindblad [70] are known. An important characteristic of the Lindblad approach is that it preserves the positivity of the density matrix of the system.

In order to derive the evolution equation for the reduced density matrix, consider the Hamiltonian of the system and reservoir,

$$\hat{H} = \hat{H}_s + \hat{H}_r + \hat{H}_{sr}, \tag{1.51}$$

where $\hat{H}_s$ and $\hat{H}_r$ are the Hamiltonians for system (S) and reservoir (R) respectively. Interaction between the system and the reservoir is $\hat{H}_{sr}$. By incorporating the reservoir variables, the canonical commutation relation between $\hat{q}$ and $\hat{p}$ is preserved during time-evolution [71].

Let the density matrix of (system+reservoir) be ρ. Its evolution equation is governed by the quantum Liouville equation

$$\frac{d}{dt}\rho(t) = \frac{1}{i\hbar}[\hat{H}, \rho]. \tag{1.52}$$

This evolution is unitary as (system+reservoir) is closed. Tracing over the reservoir variables gives the reduced density matrix for the system:

$$\rho_s = Tr_r(\rho). \tag{1.53}$$

Expectation value of a system observable is calculated as

$$\langle \hat{O} \rangle = \mathrm{Tr}_s(\hat{O}\rho_s). \tag{1.54}$$

Hence, it is necessary to derive an evolution equation for the reduced density matrix. The density matrix ρ in interaction picture is defined to be

$$\tilde{\rho}(t) = e^{-i/\hbar(\hat{H}_s+\hat{H}_r)t}\rho(t)e^{i/\hbar(\hat{H}_s+\hat{H}_r)t}, \tag{1.55}$$

which satisfies

$$\frac{d}{dt}\tilde{\rho}(t) = \frac{1}{i\hbar}[\hat{H}'_{sr}(t), \tilde{\rho}], \tag{1.56}$$

where $\hat{H}'_{sr} = e^{i/\hbar(\hat{H}_s+\hat{H}_r)t}\hat{H}_{sr}e^{-i/\hbar(\hat{H}_s+\hat{H}_r)t}$.

The equivalent integral form is

$$\tilde{\rho}(t) = \rho(0) + \frac{1}{i\hbar}\int_0^t dt'[\hat{H}'_{sr}(t'), \tilde{\rho}(t')], \tag{1.57}$$

which is more suited for the present purpose. Substituting this in Eqn. 1.56,

$$\frac{d}{dt}\tilde{\rho}(t) = \frac{1}{i\hbar}[\hat{H}'_{sr}(t), \rho(0)] - \frac{1}{\hbar^2}\int_0^t dt'[\hat{H}'_{sr}(t), [\hat{H}'_{sr}(t'), \tilde{\rho}(t')]]. \tag{1.58}$$

The system and reservoir are initially uncorrelated so that

$$\tilde{\rho}(0) = \rho(0) = \tilde{\rho}_s(0)\tilde{\rho}_r(0). \tag{1.59}$$

On tracing over the reservoir variables, Eqn. 1.58 gives the following evolution equation for the reduced density matrix of the system

$$\frac{d}{dt}\tilde{\rho}_s = -\frac{1}{\hbar^2}\int_0^t dt' \mathrm{Tr}_r\{[\hat{H}'_{sr}(t), [\hat{H}'_{sr}(t'), \tilde{\rho}(t')]]\}, \tag{1.60}$$

where $\mathrm{Tr}_r\{[\hat{H}'_{sr}(t), \rho(0)]\} = 0$ due to the assumption $\mathrm{Tr}_r(\hat{H}_{sr}\rho_r) = 0$. In the Born approximation,

$$\tilde{\rho}(t) = \tilde{\rho}_s(t)\rho_r, \tag{1.61}$$

which amounts to saying that the state of the system evolves due to the interaction of the system with the reservoir while remaining uncorrelated. Additionally, neglecting the higher order terms in $\hat{H}_{sr}$ yields

$$\frac{d}{dt}\tilde{\rho}_s = -\frac{1}{\hbar^2}\int_0^t dt' \mathrm{Tr}_r\{[\hat{H}'_{sr}(t), [\hat{H}'_{sr}(t'), \tilde{\rho}_s(t')\rho_r]]\}. \tag{1.62}$$

Note that the state of the system at time t depends on the state at earlier times. Under the Markov approximation, the state $\tilde{\rho}_s(t')$ under the integral is replaced by $\tilde{\rho}_s(t)$. With this substitution, the above equation becomes

$$\frac{d}{dt}\tilde{\rho}_s = -\frac{1}{\hbar^2}\int_0^{t'} dt' \mathrm{Tr}_r\{[\hat{H}'_{sr}(t), [\hat{H}'_{sr}(t'), \tilde{\rho}_s(t)\rho_r]]\}. \tag{1.63}$$

which is the master equation for $\tilde{\rho}_s$.

Consider a single harmonic oscillator interacting with a reservoir. The later is a collection of oscillators. Hamiltonians for the system and the reservoir are

$$\hat{H}_s = \hbar\omega\hat{a}^\dagger\hat{a}, \quad \hat{H}_r = \sum_{j=0}^{\infty}\hbar\omega_j\hat{b}_j^\dagger\hat{b}_j, \tag{1.64}$$

respectively and the interaction between them is

$$\hat{H}_{sr} = \sum_j \hbar(k_j \hat{a}_j^\dagger \hat{b} + k_j^* \hat{a}_j \hat{b}_j^\dagger). \tag{1.65}$$

Here $\hat{a}$ is the annihilation operator of the system and its adjoint is $\hat{a}^\dagger$. The annihilation (creation) operator for the jth mode of the reservoir is $\hat{b}_j(\hat{b}_j^\dagger)$.

The state of the reservoir in thermal equilibrium at temperature T is

$$\rho_r = \prod_j e^{-i\hbar\omega_j \hat{b}_j^\dagger \hat{b}_j / k_B T}(1 - e^{-i\hbar\omega_j / k_B T}). \tag{1.66}$$

Assuming a delta correlated reservoir, *i.e.*,

$$\langle \hat{b}_i(t)\hat{b}_j(t')\rangle_r \propto \delta(t - t'), \tag{1.67}$$

the master equation given in Eqn. 1.63 for the harmonic oscillator is

$$\dot{\tilde{\rho}}_s = -i\hbar\omega[\hat{a}^\dagger\hat{a}, \rho_s] + \frac{\gamma(\bar{n}+1)}{2}(2\hat{a}\rho_s\hat{a}^\dagger - \hat{a}^\dagger\hat{a}\rho_s - \rho_s\hat{a}^\dagger\hat{a}) + \frac{\gamma\bar{n}}{2}(2\hat{a}^\dagger\rho_s\hat{a} - \hat{a}\hat{a}^\dagger\rho_s - \rho_s\hat{a}\hat{a}^\dagger), \tag{1.68}$$

which is the Lindblad equation for $\tilde{\rho}_s$. The average number of photons $\bar{n}$ in the reservoir is

$$\bar{n} = \frac{1}{e^{\hbar\omega/k_B T} - 1}. \tag{1.69}$$

The coupling constants k_j are related to the decay rate γ through the relation [72]

$$\gamma = 2\pi \sum_j k_j^2 \delta(\omega_j - \omega). \tag{1.70}$$

First term in the expression given in Eqn. 1.68 corresponds to the unitary evolution (no dissipation and decoherence) of the quantum state ρ_s. Second term refers to the energy dissipation from the system to the reservoir and the last term corresponds to absorption of energy by the system from the reservoir [68].

1.7 Two-level atom inside a cavity

A single atom in the free space interacts with a continuum of modes of the electromagnetic field. On de-excitation from one of its higher energy levels to a lower energy level, the atom emits a photon to this continuum. This is an irreversible process. The rate of emission is decided by the density of modes of the field. In three dimensions, the density of modes is proportional to ω^2 where ω is the frequency of electromagnetic field (appendix C of ref. [14]). Interaction between the atom and the field can be tailored by modifying the mode density, which is possible in a cavity. For instance, both the direction and rate of spontaneous emission from an atom in a cavity can be controlled [73]. The rate of spontaneous can be controlled by tuning the cavity resonance frequency and atom-field coupling strength, known as Purcell effect [74]. Strong light-matter interaction is achieved by increasing the finesse (Q-factor) of the cavity [43, 75, 76]. Cavity mitigates the effect of dissipation on atoms so that atom-photon entanglement is possible [77]. Control of spontaneous emission has been used for quantum encryption [78], quantum computation [79], etc.

A cavity with a two-level atom provides an exceptional setting for understanding light-matter interaction [80–82]. The Hamiltonian of an electron of charge $-e$ interacting with an external field is

$$\hat{H} = \frac{1}{2m}[\hat{P} + e\hat{A}(\vec{r}, t)]^2 - e\Phi(\vec{r}, t) + V(r). \tag{1.71}$$

Here $V(r)$ is the Coulomb interaction potential between the nucleus and the electron separated by a distance $r = |\vec{r}|$. Further, $\hat{A}(\vec{r}, t)$ and $\Phi(\vec{r}, t)$ are the vector and scalar potentials respectively. Under the dipole approximation, *i.e.*, wavelength of the electromagnetic field is much larger than the atomic size, the Hamiltonian becomes

$$H = \frac{1}{2m}\hat{P}^2 + V(r) - \hat{d}\cdot\hat{E}(t). \tag{1.72}$$

Here $\hat{d} = e\hat{r}$ is the dipole moment and the electric field $\hat{E}(t) = \partial\hat{A}/\partial t$.

Let $|e\rangle$ and $|g\rangle$ represent the excited and ground states respectively for the atom. The raising and lowering operators for the atomic system are $\hat{\sigma}_+ = |e\rangle\langle g|$ and $\hat{\sigma}_- = |g\rangle\langle e|$ respectively. The energy operator for the atom is $\hat{\sigma}_z = |e\rangle\langle e| - |g\rangle\langle g|$. Using the expression for electric field operator $\hat{E}$ from Eqn. 1.11 and $\hat{d} = d\,|e\rangle\langle g| + d\,|g\rangle\langle e|$ where d is real, the Hamiltonian becomes

$$\hat{H} = \frac{1}{2}\hbar\omega_0\hat{\sigma}_z + \hbar\omega\hat{a}^\dagger\hat{a} + g(\hat{\sigma}_+ + \hat{\sigma}_-)(\hat{a} + \hat{a}^\dagger). \tag{1.73}$$

The atom-field coupling strength is $g = -d_{eg}(\hbar\omega/\epsilon_0 V)^{1/2}\sin kz$ where d_{eg} is the matrix element of dipole moment operator that represents the strength of the dipole transition. This Hamiltonian, known as the quantum Rabi Hamiltonian [10], contains the energy non-conserving terms $\hat{\sigma}_+\hat{a}^\dagger$ and $\hat{\sigma}_-\hat{a}$. However, as these terms are fast oscillating their time-averages are vanishingly small. Therefore, the Hamiltonian given in Eqn. 1.73 becomes

$$\hat{H} = \frac{1}{2}\hbar\omega_0\hat{\sigma}_z + \hbar\omega\hat{a}^\dagger\hat{a} + g(\hat{\sigma}_+\hat{a} + \hat{\sigma}_-\hat{a}^\dagger). \tag{1.74}$$

This is the Jaynes-Cummings Hamiltonian to describe atom-field interaction when the coupling strength g is weak ($g << \omega, \omega_0$) and $\omega_0 \approx \omega$ [82]. The excitation number operator $\hat{N} = \hat{\sigma}_z + \hat{a}^\dagger\hat{a}$ is a conserved quantity. The Hilbert space naturally splits into distinct invariant subspaces corresponding to different excitation numbers. Therefore, the unitary dynamics of the system is restricted to subspace corresponding to a given number of excitations in the initial state.

In the dispersive limit, *i.e.*, $(\omega_0 - \omega) >> g$, the above Hamiltonian becomes [83]

$$\hat{H} = \frac{\hbar\omega_0}{2}\hat{\sigma}_z + \hbar\omega\hat{a}^\dagger\hat{a} + \chi(\hat{\sigma}_+\hat{\sigma}_- + \hat{\sigma}_z\hat{a}^\dagger\hat{a}). \tag{1.75}$$

Due to large detuning, the atom and the field do not exchange energy. However, the presence of the atom shifts the cavity resonance frequency [83]. There are several advantages of nonresonant atom-field interactions than the resonant one. For instance, generation of cat states [83, 84], controlled superposition of number states [85], photon number-dependent phase gate [20], optical nonlinearity [86], etc. are possible with nonresonant interaction.

Coupled cavity array can be a conduit for transmitting photons. Embedding an atom in a cavity affects the propagation of photons in the array [87–89]. The transmission and reflection probabilities depend on the atomic resonance frequency and atom-cavity coupling strength. If there is an atom in each of the cavities in the array, the system becomes strongly correlated [90]. Such a system is useful to explore the equilibrium and nonequilibrium phase transitions. An interesting feature of this system is the interplay between the atom-field coupling strength and the inter-cavity interaction strengths [90], making it possible to study interesting phenomena such as the transition from Mott insulator phase (excitations localized on each site) to superfluidity (excitations delocalized in the array) phase [91–93], localization-delocalization of excitations [94, 95], etc. In this system, by properly tuning the atom and cavity resonance frequencies, transfer a superposition of polaritonic states is possible which may be useful for quantum information processing [96].

1.8 Kerr medium inside a cavity

Energy levels of the quantized electromagnetic field in an empty cavity are equi-spaced. Anharmonicity in the levels arises on incorporating a nonlinear medium, especially, Kerr medium inside the cavity. The cavity with Kerr nonlinearity is to be referred as 'Kerr cavity' in subsequent discussions. The energy of the electromagnetic field in a Kerr cavity is proportional to the square of number of photons. This anharmonicity gives rise to many interesting phenomena such as the photon blockade [86, 97–101], bunching and antibunching of photons [102, 103], quantum phase transitions [104], slow light [105], etc. The feature that is responsible for the aforementioned phenomena is the strong photon-photon interaction which is possible in the presence of nonlinearity [86]. This strong interaction requires extra energy to populate n photons in a Kerr cavity than in an empty cavity.

Consider a driven cavity containing a nonlinear dispersive medium. Polarization of the medium is

$$P = \chi^{(1)}\hat{E} + \chi^{(2)}\hat{E}\hat{E} + \chi^{(3)}\hat{E}\hat{E}\hat{E} + \cdots , \tag{1.76}$$

where $\chi^{(n)}$ is $(n+1)$th rank susceptibility tensor. The energy of the electromagnetic field inside the cavity is

$$H = \int_V d^3r \frac{1}{2}(\vec{D}\cdot\vec{E} + \vec{H}\cdot\vec{B}), \tag{1.77}$$

where V is the mode volume, $\vec{D} = \epsilon_0\vec{E} + \vec{P}$ and $\vec{H} = 1/\mu_0\vec{B}$. If the field is propagating along z-direction and polarization is along the x-direction, then $\vec{E} = (E(z,t),0,0)$, $\vec{B} = (0,B(z,t),0)$, $\vec{H} = (1/\mu_0 B(z,t),0,0)$ and the electric flux density $\vec{D} = (\epsilon_0 E + P, 0, 0)$. If the medium is centro-symmetric and the driving is intense then the third-order nonlinearity is larger than the linear $\left(\chi^{(1)}\right)$ and second-order $\left(\chi^{(2)}\right)$ susceptibilities. With this assumption, the Hamiltonian given in Eqn. 1.77 becomes [106]

$$H = \int_V d^3r \frac{1}{2}\left[\left(\epsilon |E|^2 + \frac{1}{\mu_0}|B|^2\right) + \chi^{(3)}|E|^4\right]. \tag{1.78}$$

Under the rotating wave approximation, the corresponding quantum Hamiltonian is [107]

$$\hat{H} = \hbar\omega \hat{a}^\dagger \hat{a} + \hbar\chi \hat{a}^{\dagger 2}\hat{a}^2, \tag{1.79}$$

where

$$\chi \approx \frac{3\hbar\omega^2\chi^{(3)}}{4\epsilon_0\epsilon_r^2}\int |u(r)|^4 \, d^3r = \frac{3\hbar\omega^2\chi^{(3)}}{4\epsilon_0 V_{\text{eff}}\epsilon_r^2}, \tag{1.80}$$

is the strength of Kerr nonlinearity. The effective cavity mode volume $V_{\text{eff}}^{-1} = \int |u(r)|^4 \, d^3r$ [108]. The mode function $u(r)$ satisfies $\int [u^*(r)(1+\chi^{(3)}/\epsilon)u(r)]d^3r = 1$.

Recently, Fushman et. al. achieved large Kerr coefficients by embedding quantum dots in photonic crystal [109]. The achieved value $\chi^{(3)} = 2.4 \times 10^{-10}\text{m}^2/\text{V}^2$ is many orders of magnitude larger than the optical nonlinearities in solids. The lowest mode volume that has been achieved so far is $\sim 10^{-23}\text{m}^3$ [109]. Using the experimental values $\omega \approx 10^{14}\text{Hz}, \chi^{(3)} = 2.4 \times 10^{-10}\text{m}^2/\text{V}^2, V_{\text{eff}} = 10^{-20}\text{m}^3, \epsilon_r = 13.1$ (for GaAs), the Kerr nonlinear strength is calculated from Eqn. 1.80 to be $\chi \approx 1.2 \times 10^{13}\text{Hz}$.

The Hamiltonian for an array of N cavities, each containing a Kerr medium, is

$$\hat{H}_{Kerr} = \sum_{j=}^{N} \omega_j \hat{a}_j^\dagger \hat{a}_j + \chi_j \hat{a}_j^{\dagger 2} a_j^2 + \sum_{j}^{N-1} J_j(\hat{a}_j^\dagger \hat{a}_{j+1} + \hat{a}_j \hat{a}_{j+1}^\dagger). \tag{1.81}$$

Here ω_j and χ_j are the resonance frequency and Kerr strength of jth cavity. The strength of coupling between the jth and $(j+1)$th cavity is J_j.

1.9 Motivation and outline

Array of coupled cavities is considered suitable for implementing quantum information protocols, generation of non-classical states of the electromagnetic field, testing the foundational aspects of quantum theory, etc. Cavity arrays provide desirable features such as scalability and control, in addition to being a system that can sustain photons for sufficiently long duration without being lost due to dissipation. What are the control parameters that can be made available in an array to steer the transfer of photons? It is known that in the case of identical cavities with uniform inter-cavity coupling, transfer of photon beyond three cavities does not happen with high probability. This is a serious impediment if cavity arrays are to be used for practical applications. In this thesis, it is shown that it is indeed possible to have array configurations wherein the restriction on the number of cavities is not necessary.

The thesis is organized into six chapters. A brief introduction to the contents of the chapters is presented below.

Perfect transfer of a single photon between any two cavities in an array is discussed in Chapter 2. The conditions that determine the suitable values of the coupling strengths and Kerr nonlinear strengths are derived by using a duality relation. The duality relation is established between "$N-1$ photons in two coupled cavities" and "single photon in an array of N cavities". Single photon transfer also means that it is possible to transfer states of the form $\alpha|0\rangle + \beta|1\rangle$.

Chapter 3 discusses the two photon localization and delocalization in a linear cavity array. The emergence of localization and delocalization of photons is shown to be the consequence of quantum interference. Importance of entanglement and relative phase present in the initial state to bring about localization and delocalization is discussed.

Studies on the localization and delocalization dynamics in Kerr nonlinear cavities with intensity-dependent couplings are presented in Chapter 4. State switching condition which relates the nonlinear strength and cavity detuning is derived for evolving a localized product state to a delocalized state.

Controlled transfer of heat through two coupled cavities containing a single atom is discussed in Chapter 5. The thermal current in the cavity array is shown to be controllable by the atom. Atom acts as a switch for controlling both magnitude and direction of heat current. By proper choices of the system parameters and atomic state, large thermal rectification is possible. Violation of the Fourier's law of heat conduction and its partial recovery are also discussed.

Summary of the results and possibility of further exploration of the present work are discussed in Chapter 6.

Chapter 2

Controlled transfer of photon in cavity array

2.1 Introduction

Photons are excellent information carriers as they do not interact with each other and fairly resilient under decoherence [104]. Currently available technology already allows photons as elementary units in quantum information processing protocols such as the quantum teleportation [110], quantum state transfer [47, 50, 111], quantum dense coding [112], quantum cryptography [113], etc. at the laboratory level. An outstanding challenge is to achieve a process for controlled, perfect and coherent transfer of photons in order to realize the aforementioned protocols. In addition, availability of such a process will help in designing experiments for understanding subtilities of quantum phase transition [91, 93, 114], generating entangled states [115–117], simulating many-body systems [55, 104, 118], etc. A coupled network is a basic building block to realize these ideas mainly due to the controllability of couplings, scalability, addressability.

Cavities provide insulation against environment induced decoherence. By and large, the requisite conditions for controlled transfer of photon can be achieved by tailoring the cavity resonance frequencies [119, 120] or coupling strengths [121] in cavity arrays. Controllable transport of photons is also possible by including suitable medium inside the cavities. For instance, photon transport can be controlled by embedding two-level or three-level atoms in the cavities [87–89]. Essentially, the resonance frequencies of the filled cavities are different from the empty cavities which affect the reflection and transmission of photons. Also, the magnitude of atom-cavity coupling dynamically changes the transport properties [60]. Embedded atoms in the array provide for a controllable transport of photon. Inclusion of Kerr medium inside the cavities leads to photon-photon interaction even at a few photons level [86, 122]. This offers a wide range of possibilities for realizing various interesting phenomena such as the photon blockade [86, 123], quantum phase transition [55, 104, 124], bunching and antibunching of photons [94, 125], etc.

This chapter discusses about perfect and controlled transfer of a photon in a cavity array. An array with homogeneous coupling forbids perfect transfer of a single photon due to the nonlinear dispersion in the array. One way of realizing a perfect transfer is to choose the coupling strengths and resonance frequencies. Appropriate choices of the coupling strengths and resonance frequencies are derived *via* a duality relation between two systems, namely, "$N-1$ photons in two coupled cavities" and "single photon in N coupled cavities". This provides a condition which relates the parameters of one system to those of the other. This modification in the coupling strengths and resonance frequencies allows transfer of a single photon between two symmetrically located cavities. In order to steer the perfect transfer between any two cavities in the array, Kerr nonlinearity is included in each cavity. Duality holds for the nonlinear cavities too. This is employed to arrive at a state switching condition which ensures a perfect transfer of photon between any two cavities. Further, this condition enables perfect transfer of quantum states of the form $\alpha\left|0\right\rangle + \beta\left|1\right\rangle$, where $\left|0\right\rangle$ and $\left|1\right\rangle$ are respectively the vacuum state and single photon state. Generation of NOON-type states is possible in the system of two coupled cavities with $N-1$ photons.

This chapter is organized as follows. Transfer of a single photon in a homogeneously coupled cavity array is discussed in Section. 2.2. Duality between "$N-1$ photons in two coupled cavities" and "single photon in N coupled cavities" is established in Section. 2.3. Controlled transfer of a single photon between any two cavities in the array is discussed in Section. 2.4. Generation of NOON type states is presented in Section. 2.5. A protocol for quantum state transfer is introduced in Section. 2.6. Experimental feasibility of the scheme and the chapter summary are given in Sections. 2.7 and 2.8 respectively.

2.2 Coupled cavity array

Consider a system of an array of N linearly coupled cavities. The Hamiltonian for the system is

$$\hat{H} = \sum_{l=1}^{N} \tilde{\omega}_l \hat{b}_l^\dagger \hat{b}_l + \sum_{l=1}^{N-1} \tilde{J}_l (\hat{b}_l^\dagger \hat{b}_{l+1} + \hat{b}_l \hat{b}_{l+1}^\dagger), \tag{2.1}$$

where $\tilde{\omega}_l$ is the cavity resonance frequency of the lth cavity, $\hat{b}_l$ and $\hat{b}_l^\dagger$ are respectively the annihilation and creation operators. The coupling strength between the lth and $(l+1)$th cavities in the array is $\tilde{J}_l$. All the coupling strengths and frequencies are expressed in terms of frequency of the first cavity. In the plots, the frequency of the first cavity is set to unity.

Consider the simplest situation where all the coupling strengths $\tilde{J}_l$ are equal $(= J)$ and the cavities are identical, *i.e.*, all the resonance frequencies are equal $(= \omega)$. This array is said to be homogeneous. In this case, the Hamiltonian conserves the number of excitations as $[\hat{H}, \sum_{l=1}^{N} \hat{b}_l^\dagger \hat{b}_l] = 0$. Hence, the Hamiltonian can be diagonalized in the subspace corresponding to different excitation numbers. Normal mode operators for the cavity array are

$$\hat{c}_k(t) = \sum_{j=1}^{N} \hat{b}_j(t) S(j,k), \tag{2.2}$$

so that the inverse transformation is

$$\hat{b}_j(t) = \sum_{k=1}^{N} \hat{c}_k(t) S(j,k). \tag{2.3}$$

The transformation matrix $S(j,k)$ is

$$S(j,k) = \sqrt{\frac{2}{N+1}} \sin\left(\frac{j\pi k}{N+1}\right). \tag{2.4}$$

Using the orthogonality relation

$$\sum_{j=1}^{N} \sin\left(\frac{j\pi k}{N+1}\right) \sin\left(\frac{j\pi m}{N+1}\right) = \frac{N+1}{2}\delta_{km}, \tag{2.5}$$

the Hamiltonian for an array of resonant cavities with homogeneous coupling is

$$\hat{H} = \sum_{k=1}^{N} \Omega_k \hat{c}_k^\dagger \hat{c}_k, \tag{2.6}$$

where $\hat{c}_k$ and $\hat{c}_k^\dagger$ are the creation and annihilation operators for the kth normal mode. The Hamiltonian in the normal mode coordinates corresponds to a collection of independent oscillators. The normal mode frequencies are

$$\Omega_k = \left(\omega + 2J\cos\frac{\pi k}{N+1}\right). \quad k = 1,2,3,....,N \tag{2.7}$$

The evolution equation for kth normal mode operator is

$$\frac{d}{dt}\hat{c}_k = i[\hat{H}, \hat{c}_k] = i\left[\sum_{n=1}^{N} \Omega_n \hat{c}_n^\dagger \hat{c}_n, \hat{c}_k\right] = -i\Omega_k \hat{c}_k. \tag{2.8}$$

The solution of the above equation is

$$\hat{c}_k(t) = e^{-i\Omega_k t}\hat{c}_k(0). \tag{2.9}$$

Using inverse transformation given in Eqn. 2.3, the annihilation operator for the jth mode is

$$\hat{b}_j(t) = \sum_{l=1}^{N}\sum_{k=1}^{N} e^{-i\Omega_k t}\hat{b}_l(0)S(l,k)S(j,k). \tag{2.10}$$

The average number of photons in the j-th cavity at time t is given by

$$\langle n_j\rangle_t = \langle \hat{b}_j^{\dagger}\hat{b}_j\rangle_t = \sum_{l=1}^{N} |G_{jl}|^2 \langle \hat{b}_l^{\dagger}\hat{b}_l\rangle_0, \tag{2.11}$$

where

$$G_{jl} = \frac{2}{N+1}\sum_{k=1}^{N} e^{-i(\omega+2J\cos(\frac{\pi k}{N+1}))t} \sin\left(\frac{j\pi k}{N+1}\right)\sin\left(\frac{l\pi k}{N+1}\right). \tag{2.12}$$

In order to investigate the photon transfer properties, consider a single photon in the first cavity which implies $\langle \hat{b}_l^{\dagger}\hat{b}_l\rangle_0 = \delta_{1,l}$. Then

$$\langle n_N\rangle_t = \langle \hat{b}_N^{\dagger}\hat{b}_N\rangle_t = |G_{N1}|^2 = \left|\frac{2}{N+1}\sum_{k=1}^{N} e^{-i(\omega+2J\cos(\frac{\pi k}{N+1}))t} \sin\left(\frac{N\pi k}{N+1}\right)\sin\left(\frac{\pi k}{N+1}\right)\right|^2, \tag{2.13}$$

is the average photon number in the last cavity. Perfect transfer of a photon to the end cavity corresponds to having $\langle n_N\rangle_t = 1$ at some time t.

Time evolution $\langle n_N\rangle$ for arrays with N =3, 4, 5 and 10 cavities respectively are shown in Fig. 2.1. From the figure it is clear that complete transfer occurs if the array has three cavities. Maximum of $|G_{N1}|^2$ decreases with increasing number of cavities. This is inferred from Eqn. 2.12 on noting that for large N, $\sin(Nk\pi/N+1) \approx \sin(k\pi) = 0$

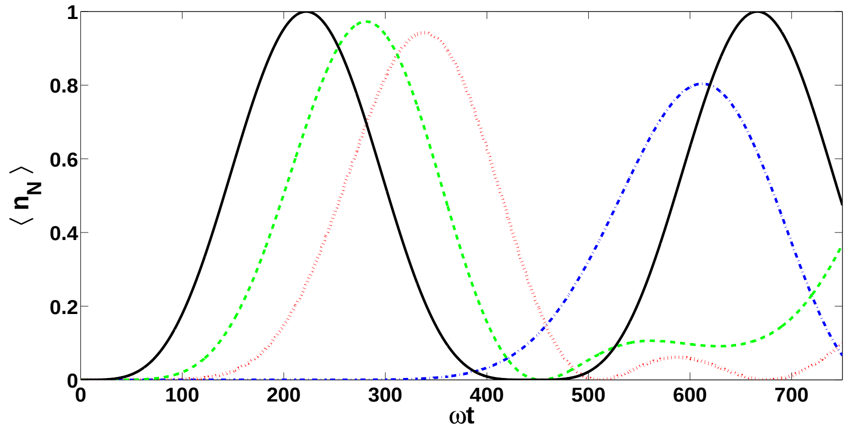

Figure 2.1 – Average number of photon in the end cavity as a function of ωt in homogeneous cavity array. Number of cavities in the array is N =3 (solid line), 4 (dashed), 5 (dotted) and 10 (dot-dashed). All the cavities are identical and homogeneously coupled with coupling strength $J/\omega = 0.01$.

and G_{N1} tends to zero. What happens in the limit of large N is that during the time evolution a single photon is shared by all the cavities. Hence, detecting the photon in any of the cavities with unit probability is not possible.

It is to be noted that the dispersion relation is linear if the array contains less than four cavities. For two cavities, the normal mode frequencies are $\Omega_1 = \omega + J$ and $\Omega_2 = \omega - J$ which lie on a straight line. Similarly, the normal mode frequencies for three cavities are $\Omega_1 = \omega + \sqrt{2}J, \Omega_2 = \omega$, and $\Omega_3 = \omega - \sqrt{2}J$. These are also collinear. In order to understand the inhibition of complete transfer of single photon in array having more than three cavities, the normal mode frequencies are shown in Fig. 2.2 for $N = 4$ and $N = 10$. Due to this nonlinear dispersion relation, any propagating wave undergoes dispersion. Consequently, complete transfer does not occur if the homogeneous array has more than three cavities.

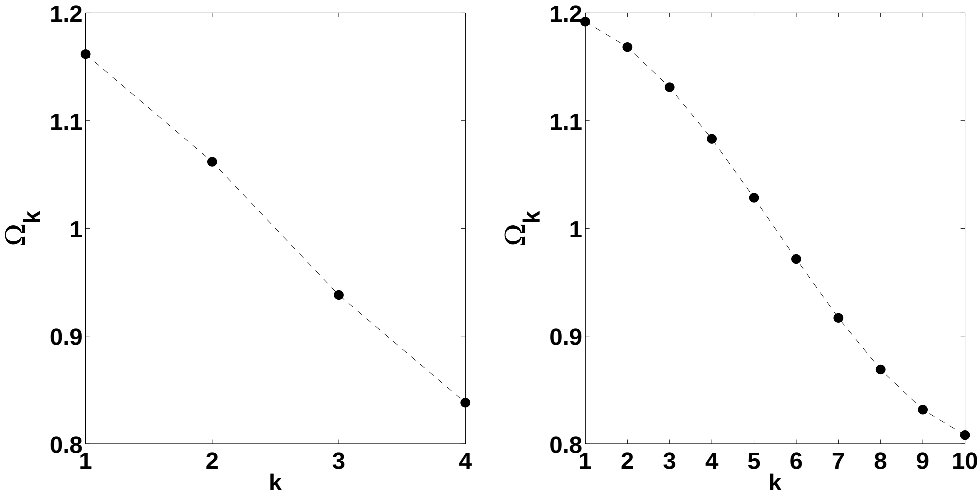

Figure 2.2 – Normal mode frequencies Ω_k as a function of k for $(a)N = 4$ and $(b)N = 10$. Here $\omega = 1$ and $J = 0.1$.

2.3 Duality between two coupled cavities and an array of cavities

Prefect transfer of a single photon from one end to the other end in an array with homogeneous coupling is prohibited by the nonlinear dispersion. Complete transfer of a single photon demands a correct combinations of the coupling strengths and cavity resonance frequencies of the cavities. In order to derive the conditions for a perfect transfer, a duality relation between "$N-1$ photons in two coupled cavities" and "single photon in N cavities" is established.

The concept of duality has been extensively discussed in various branches of physics to facilitate understanding of nontrivial aspects of one system in terms of easily accessible features of the other [126]. One of the simplest examples that can be considered is the distribution of N photons in g levels for deriving the Planck's blackbody spectrum. The indistinguishable nature of photons requires that the number of photons and the number of levels to be occupied by them are considered together. The number of possible ways of distributing is $(N + g - 1)!/N!(g - 1)!$. It is interesting to note that the result is the same if there are $g-1$ photons and $N+1$ levels. This possibility of interchanging the roles of the number of particles and the number of levels is a duality. Another example of duality is the Euler characteristic $V-E+F=2$, where V, E and F refer to the number of vertices, edges and faces respectively of a convex solid. In this expression the roles of V and F are interchangeable.

Consider a system of two linearly coupled cavities described by the Hamiltonian

$$\hat{H}_A = \omega_1 \hat{a}_1^\dagger \hat{a}_1 + \omega_2 \hat{a}_2^\dagger \hat{a}_2 + J\left[\hat{a}_1^\dagger \hat{a}_2 + \hat{a}_1 \hat{a}_2^\dagger\right]. \tag{2.14}$$

Here ω_1 and ω_2 are the resonance frequencies of the respective cavities and J is the coupling strength. Suffix A has been used to refer to this system of two coupled cavities. Here $\hat{a}_{1(2)}$ and $\hat{a}_{1(2)}^\dagger$ are the annihilation and creation operators for the first (respectively, second) cavity. Let $|n+1\rangle$ represent the bipartite state $|N-1-n, n\rangle$ of the two cavities corresponding to $N-n-1$ photons in the first cavity and n photons in the second cavity. The total number of photons in the two cavities is $N-1$. If the number of photons is $N-1$, the Hamiltonian is

$$\hat{H}_A = \sum_{n=0}^{N-1} \Omega_{n+1} |n+1\rangle\langle n+1| + \sum_{n=0}^{N-2} J_{n+1}(|n+1\rangle\langle n+2| + |n+2\rangle\langle n+1|), \tag{2.15}$$

where $\Omega_{n+1} = [(N-1-n)\omega_1 + n\omega_2]$ and $J_{n+1} = \sqrt{(n+1)(N-1-n)}J$.

At resonance (detuning $\Delta = \omega_1 - \omega_2 = 0$), the eigenvectors of $\hat{H}_A$ are

$$|X_n\rangle = \frac{1}{\sqrt{2^{N-1}}} \sum_{k=0}^{N-1-n} \sum_{k'=0}^{n} (-1)^{k'}\, {}^{N-1-n}C_k\, {}^{n}C_{k'} \sqrt{\frac{{}^{N-1}C_n}{{}^{N-1}C_r}}\, |N-r, r\rangle, \tag{2.16}$$

with corresponding eigenvalues $E_n = (N-1)\omega + (N-1-2n)J$. The index $r = n+k-k'$.

Now, consider the Hamiltonian for N coupled cavities

$$\hat{H}_B = \sum_{l=1}^{N} \tilde{\omega}_l \hat{b}_l^{\dagger} \hat{b}_l + \sum_{l=1}^{N-1} \tilde{J}_l (\hat{b}_l^{\dagger} \hat{b}_{l+1} + \hat{b}_l \hat{b}_{l+1}^{\dagger}). \tag{2.17}$$

Suffix B has been used to refer to this array of N cavities.

For a single photon in the array, the possible states are $|l\rangle\rangle$ which represents one photon in the lth cavity while the other cavities are in their respective vacuua. Then the Hamiltonian is

$$\hat{H}_B = \sum_{l=1}^{N} \tilde{\omega}_l \, |l\rangle\rangle\langle\langle l| + \sum_{l=1}^{N-1} \tilde{J}_l (|l\rangle\rangle\langle\langle l+1| + |l+1\rangle\rangle\langle\langle l|). \tag{2.18}$$

Duality between the two systems described by $\hat{H}_A$ and $\hat{H}_B$ respectively is identified if

$$\begin{aligned} \tilde{J}_l &= \sqrt{l(N-l)}J, \\ \tilde{\omega_l} &= [(N-l)\omega_1 + (l-1)\omega_2], \end{aligned} \tag{2.19}$$

and $l = n+1$. This is termed as the duality condition. With this identification the two systems are equivalent. It is easy to see that the states

$$|X_n\rangle\rangle = \frac{1}{\sqrt{2^{N-1}}} \sum_{k=0}^{N-1-n} \sum_{k'=0}^{n} (-1)^{k'} \, {}^{N-1-n}C_k \, {}^{n}C_{k'} \sqrt{\frac{{}^{N-1}C_n}{{}^{N-1}C_r}} \, |r+1\rangle\rangle, \tag{2.20}$$

are the eigenvectors of $\hat{H}_B$ with eigenvalues $E_n = (N-1)\omega + (N-1-2n)J$, where $r = n + k - k'$.

The transition $|N-1-n, n\rangle \rightarrow |N-2-n, n+1\rangle$ in the system of two cavities corresponds to photon transport from $|n+1\rangle\rangle \rightarrow |n+2\rangle\rangle$ in the array. In essence, transitions in the two-cavity system are equivalent to transport of a photon across the cavities in the array.

As the total number of photons is conserved by $\hat{H}_A$, the subspace of states corresponding to a given number of photons is an invariant subspace. If the initial state belongs to the invariant subspace, the time-evolved state also belongs to the same subspace. Therefore, the Hamiltonian is finite dimensional as far as evolution within the invariant space is concerned.

If the initial state of the two cavity system at resonance is $|N-1-n, n\rangle$, it evolves to

$$\begin{aligned} e^{-i\hat{H}_A t}\,|N-1-n, n\rangle =& e^{-i(N-1)\omega t} \sum_{k=0}^{N-1-n} \sum_{l=0}^{n} \binom{N-1-n}{k} \binom{n}{l} (\cos Jt)^{N-1-(k+l)} \\ & \times (-i \sin Jt)^{k+l} \sqrt{\binom{N-1}{n} \Big/ \binom{N-1}{p}}\, |N-1-p, p\rangle\,, \end{aligned} \tag{2.21}$$

at time t, where $p = n+k-l$. It is worth noting that the time-evolved state represents an atomic coherent state [127]. At $t = \pi/2J$, the time-evolved state is $|n, N-1-n\rangle$ corresponding to swapping the number of photons in the cavities. Time evolution of the respective probabilities for $|N-1, 0\rangle$ to become $|0, N-1\rangle$ corresponding to $N = 2, 4$ and 6 are shown in Fig. 2.3.

Complete transfer of photon between the end cavities of the array corresponds to $|N-1, 0\rangle \rightarrow |0, N-1\rangle$ transition in the coupled cavity system. By the duality between $\hat{H}_A$ and $\hat{H}_B$, the profiles shown in Fig. 2.3 also represent the probability of transferring a photon from one end to the other in an array of $2, 4$ and 6 cavities respectively. It may be noted that the probabilities attain their peak value of unity corresponding to perfect transport of a photon between the end cavities at time

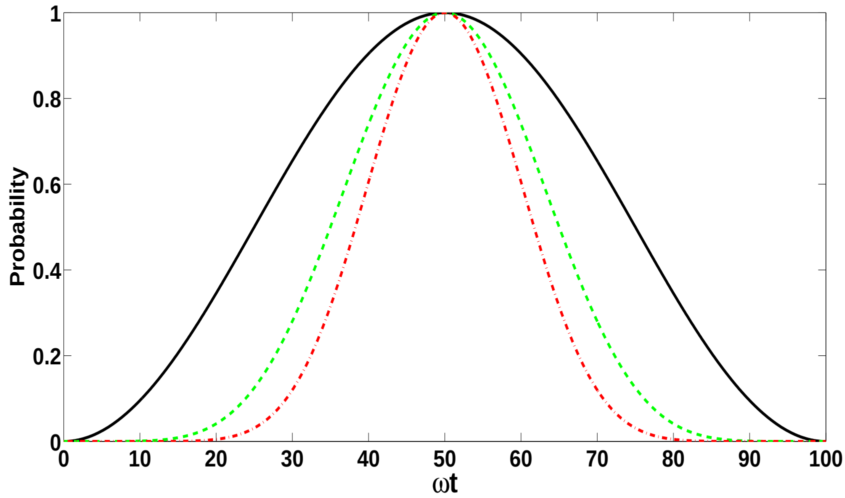

Figure 2.3 – Time evolution of probability for the coupled cavities to be in $|0, N-1\rangle$ on evolution from the initial state $|N-1, 0\rangle$, with $J/\omega = 10^{-2}\pi$. By duality, these profiles show the probability of detecting a single photon in Nth (end) cavity in the cavity array. Different curves correspond to $N = 2$ (continuous), 4 (dashed) and 6 (dot-dashed).

$t = \pi/2J$. This comes from the fact that the site dependent couplings make the dispersion relation linear which resulting in dispersionless transport.

It is to be further noted that complete transition is possible only between the states $|N-1-n, n\rangle$ and $|n, N-1-n\rangle$ of the coupled cavities. Analogously, complete transfer of a single photon occurs only between $(n+1)$th and $(N-n)$th cavities in the array. The choice for the coupling strengths given in Eqn. 2.19, therefore, allows perfect transfer of a photon between two symmetrically located cavities.

2.4 Quantum state engineering

Complete transfer of a photon between two symmetrically located cavities is possible if the system parameters of the array satisfy the duality relation given in Eqn. 2.19. This is equivalent to the transition between the states $|N-1-n, n\rangle$ and $|n, N-1-n\rangle$ in the coupled cavity system. Transferring a photon between any two arbitrary cavities in the array requires the transition between the states $|m, n\rangle$ to $|p, q\rangle$, where $m + n = p + q = N - 1$. With linear coupling, it is not possible to achieve perfect transition between two arbitrary states.

To see if nonlinearity helps in steering the evolution of states to achieve perfect transfer and complete transition, Kerr-type nonlinearity is considered. Analysis of two coupled nonlinear cavities is presented here. The Hamiltonian for the system is

$$\hat{H}'_A = \omega_1 \hat{a}_1^\dagger \hat{a}_1 + \omega_2 \hat{a}_2^\dagger \hat{a}_2 + \chi_1 \hat{a}_1^{\dagger 2} \hat{a}_1^2 + \chi_2 \hat{a}_2^{\dagger 2} \hat{a}_2^2 + J \left[\hat{a}_1^\dagger \hat{a}_2 + \hat{a}_1 \hat{a}_2^\dagger \right], \tag{2.22}$$

which describes two linearly coupled Kerr cavities. The term $\hat{a}_i^{\dagger 2} \hat{a}_i^2$ corresponds to the Kerr nonlinearity in ith cavity with Kerr strength χ_i.

If it is required to evolve from $|m, n\rangle$ to $|p, q\rangle$, consider the superposition $|X_\pm\rangle = 1/\sqrt{2}(|m, n\rangle \pm |p, q\rangle)$. These two states become approximate eigenstates of $\hat{H}'_A$ if $J << \chi_1, \chi_2, \omega_1, \omega_2$, and

$$\Delta = \frac{(p(p-1) - m(m-1))\chi_1 + (q(q-1) - n(n-1))\chi_2}{m-p}. \tag{2.23}$$

This condition is equivalent to

$$\langle m, n|\hat{H}'_A|m, n\rangle = \langle p, q|\hat{H}'_A|p, q\rangle. \tag{2.24}$$

This equality of average energies in the two states is another way of stating the requirement that the states $|X_\pm\rangle$ are approximate eigenstates of $\hat{H}'_A$. In the discussion that follows it is assumed that $\chi_1 = \chi_2 = \chi > 0$ and the condition Eqn. 2.23 simplifies to

$$\Delta = 2\chi(n - p). \tag{2.25}$$

If the initial state is $|m, n\rangle = 1/\sqrt{2}(|X_+\rangle + |X_-\rangle)$, the state of the system at a later time is

$$|\psi(t)\rangle \approx \left[\cos\left(\theta_a t\right)|m,n\rangle - i\sin\left(\theta_a t\right)|p,q\rangle\right], \tag{2.26}$$

with $\theta_a = (\lambda_s^a - \lambda_n^a)/2$. Here λ_s^a and λ_n^a are the eigenvalues of $\hat{H}'_A$ corresponding to the approximate eigenvectors $|X_+\rangle$ and $|X_-\rangle$ respectively. The expressions for these eigenvalues λ_s^a and λ_n^a up to first order correction are

$$\begin{aligned}
\lambda_s^a &= (m+p)\omega_1 + (n+q)\omega_2 + (m(m-1)+n(n-1)+p(p-1)+q(q-1))\chi \\
&+ \frac{J}{2}[\sqrt{p(q+1)}\delta_{m,p-1}\delta_{n,q+1} + \sqrt{q(p+1)}\delta_{m,p+1}\delta_{n,q-1}] \\
&+ \frac{J}{2}[\sqrt{m(n+1)}\delta_{p,m-1}\delta_{q,n+1} + \sqrt{n(m+1)}\delta_{p,m+1}\delta_{q,n-1}], \\
\lambda_n^a &= (m+p)\omega_1 + (n+q)\omega_2 + (m(m-1)+n(n-1)+p(p-1)+q(q-1))\chi \\
&- \frac{J}{2}[\sqrt{p(q+1)}\delta_{m,p-1}\delta_{n,q+1} + \sqrt{q(p+1)}\delta_{m,p+1}\delta_{n,q-1}] \\
&- \frac{J}{2}[\sqrt{m(n+1)}\delta_{p,m-1}\delta_{q,n+1} + \sqrt{n(m+1)}\delta_{p,m+1}\delta_{q,n-1}].
\end{aligned} \tag{2.27}$$

At $t = \pi/(\lambda_s^a - \lambda_n^a)$, the time-evolved state is $|p,q\rangle$. This is the minimum time required to switch from $|m,n\rangle$ to $|p,q\rangle$, referred as the state switching time (T_s). Thus, the state switching (SS) condition given in Eqn. 2.25 ensures that there is perfect transfer from the initial state $|m,n\rangle$ to the desired final state $|p,q\rangle$.

It is immediate that the detuning Δ and the nonlinear coupling strength χ can be properly chosen for a given value for $n-p$. As the value of n is specified in the initial state $|m,n\rangle$, the two parameters Δ and χ fix the number of photons (s) that can be transferred so that the target state is $|p = m \pm s, q = n \mp s\rangle$. It needs to be emphasized that for given values of Δ and χ satisfying the SS condition, not more than two states have their average energies equal as shown in Fig. 2.4. Once these parameters are fixed, probability of transition to any state other than the target state

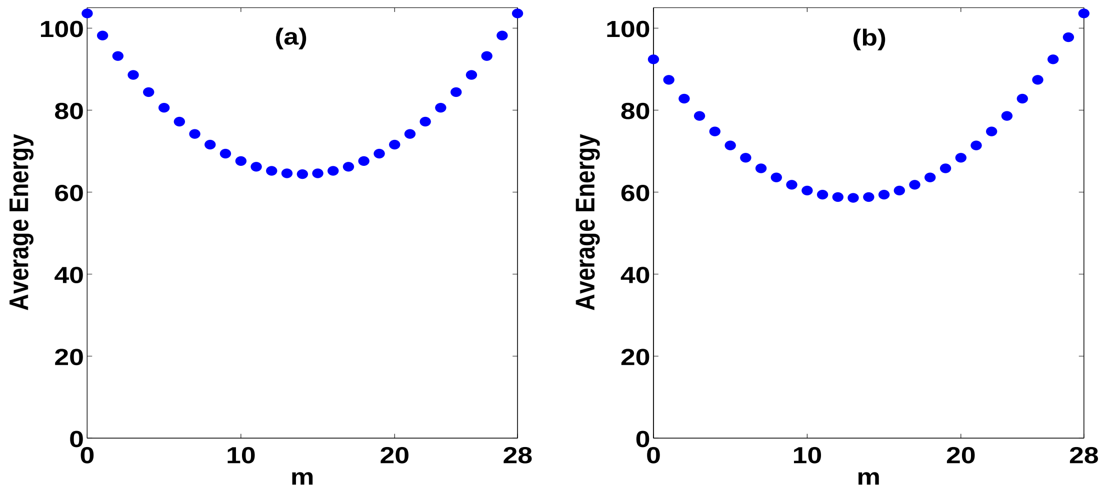

Figure 2.4 – Average energy $\langle m,n|\, \hat{H}'_A \,|m,n\rangle$ as a function of m, with $\Delta/\omega_1 = 0, \chi/\omega_1 = 0.1$ (Left) and $\Delta/\omega_1 = 0.4, \chi/\omega_1 = 0.1$ (Right).

is negligible. Hence, Δ and χ provide the requisite control to steer the system from the initial state $|m,n\rangle$ to the final state $|p,q\rangle$.

In Fig. 2.4, $\langle m,n|\, \hat{H}'_A \,|m,n\rangle$ is plotted as a function of m keeping $m + n = 28$. From Fig. 2.4(a), it is seen that every state has only one partner state with equal average energy in the resonant case. So, SS can occur between these partner states. It is observed from Fig. 2.4(b) that not every state has a partner state with equal average energy in the nonresonant case. Essentially, states without partner states are approximate eigenstates of $\hat{H}'_A$ and, therefore, do not evolve. This brings out another control aspect available in the system, namely, the possibility of inhibiting the evolution of certain states with properly chosen values of the control parameters χ and Δ.

Consider the initial state of the coupled cavity system to be $|50\rangle$. In Fig. 2.5, the probability of detecting the system in the state $|14\rangle$ at later times is shown when the required SS condition is satisfied. The values have been generated from the approximate evolved state $|\psi(t)\rangle$ and also by exact numerical solution for the evolution due to $\hat{H}'_A$. It is seen that photons are exchanged periodically, driving the system between $|14\rangle$ and $|50\rangle$, while transfer to other states is insignificant. In order to effect

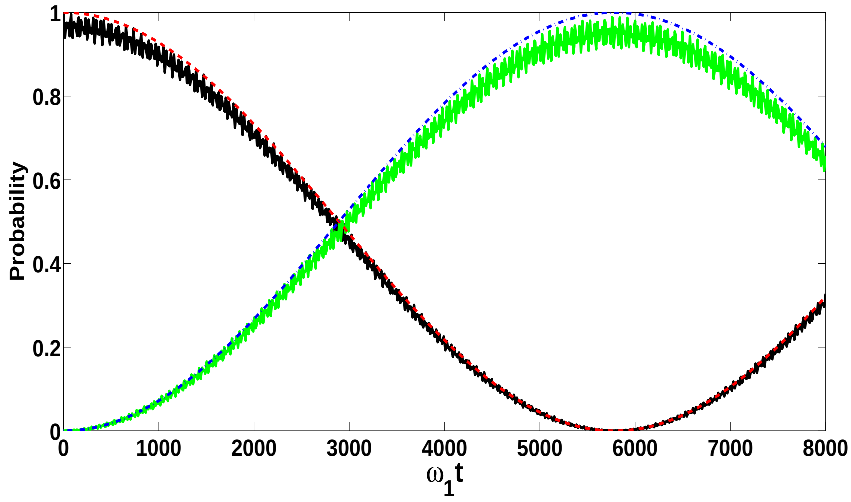

Figure 2.5 – Probability of detecting the state $|14\rangle$ from $|50\rangle$ as a function of $\omega_1 t$. Detecting other states are practically zero. Continuous black (dashed) and continuous green (dot-dashed) line corresponds to P_{50} and P_{14} calculated numerically (approximate analytical solution $|\psi(t)\rangle$). Here $\Delta/\omega_1 = -0.2$, $\chi/\omega_1 = 0.1$, $J/\omega_1 = 0.035$.

transition to other states from the initial state $|50\rangle$, the value of Δ has to be different. The maximum probabilities of detecting the target state $|p, q\rangle$ with $p = 1, 2, 3, 4, 5$ and $p + q = 5$ from $|50\rangle$ are shown in Fig. 2.6 as a function of Δ. The value of χ has been chosen to be 0.1. Depending on the value of detuning, exchange of photons is precisely controlled to reach different target states.

The discussion so far has been to steer the coupled cavities in an initial state $|m, n\rangle$ to a desired target state $|p, q\rangle$ using the Kerr nonlinearity in the cavities. But its duality relation with the cavity array points to the possibility of transferring a photon from any cavity in the array to any specified target cavity without populating the other cavities in the array.

A duality relation of the two cavity system with the cavity array system is possible in this nonlinear case too. Consider the nonlinear cavity array Hamiltonian

$$\hat{H}'_B = \sum_{l=1}^{N} \tilde{\omega}_l \hat{b}_l^\dagger \hat{b}_l + \tilde{\chi}_l (\hat{b}_l^\dagger \hat{b}_l)^2 + \sum_{l=1}^{N-1} \sqrt{l(N-l)} J (\hat{b}_l^\dagger \hat{b}_{l+1} + \hat{b}_l \hat{b}_{l+1}^\dagger), \tag{2.28}$$

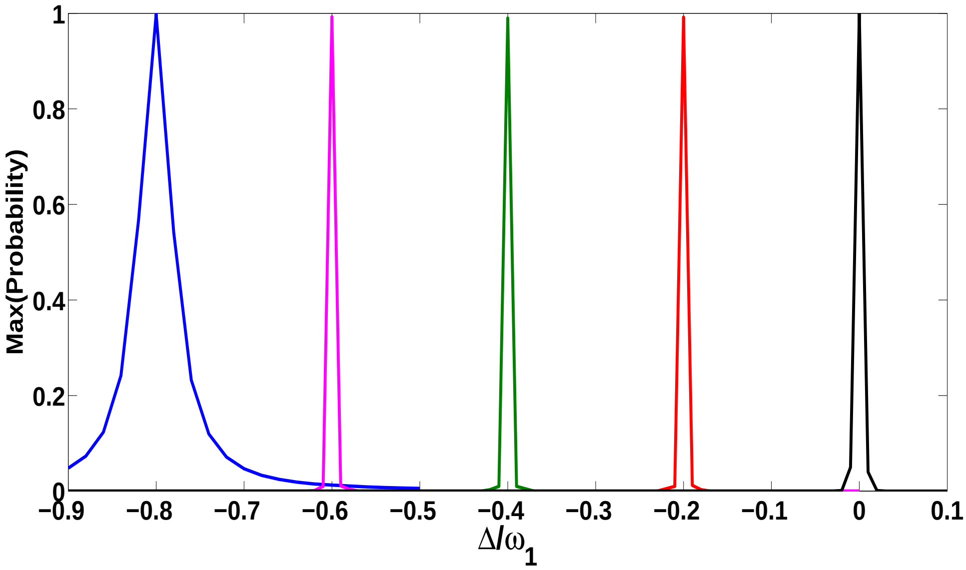

Figure 2.6 – Maximum probability of detecting quantum states $|p, q\rangle$ during the time evolution as a function of Δ/ω_1 for $\chi/\omega_1 = 0.1$ and $J/\omega_1 = 0.01$ from the initial state $|5, 0\rangle$. Note that complete switching occurs from $|5, 0\rangle$ to $|41\rangle$ (blue), $|32\rangle$ (magenta), $|23\rangle$ (green), $|14\rangle$(red) and $|05\rangle$ (black) at $\Delta = -8\chi$, $\Delta = -6\chi$, $\Delta = -4\chi$, $\Delta = -2\chi$ and $\Delta = 0$ respectively satisfying the relation given in Eqn. 2.25.

which includes Kerr nonlinearity in each cavity of the array and there is only one photon in the array. This is dual to $\hat{H}'_A$ if $\tilde{\omega}_{k+1} + \tilde{\chi}_{k+1} = (N-1-k)\omega_1 + k\omega_2 + [(N-1-k)(N-2-k)+k(k-1)]\chi$. With this identification, transitions among the levels in the two coupled Kerr cavities is mapped to transfer of photon in the Kerr cavity array.

In particular, transition from $|N-1-n, n\rangle$ to $|N-1-q, q\rangle$ in the coupled cavities corresponds to transferring a photon between $(n+1)$-cavity to $(q+1)$-cavity in the cavity array. The condition to realize the perfect transfer between these cavities is $\langle\langle n+1|\hat{H}'_B|n+1\rangle\rangle = \langle\langle q+1|\hat{H}'_B|q+1\rangle\rangle$ whose dual relation for the coupled cavities is given in Eqn. 2.24. For the Hamiltonian $\hat{H}'_B$, this condition yields

$$\begin{aligned}\tilde{\chi}_{k+1} + \tilde{\omega}_{k+1} = (N-1)\omega_1 &- 2k\chi(n+q+1-N)\\ &+ [(N-1-k)(N-2-k) + k(k-1)]\chi,\end{aligned} \tag{2.29}$$

which realizes perfect transfer of photon between the cavities. On employing cavity-dependent nonlinearity $\tilde{\chi}_l$, controlled transfer of photons between selected cavities is achievable. Such site-dependent nonlinearity has been realized recently by embedding quantum dots in photonic crystal cavities [128–130].

In the limit of weak coupling strength J, $\frac{1}{\sqrt{2}}(|n+1\rangle\rangle \pm |q+1\rangle\rangle)$ are eigenstates of $\hat{H}'_B$ and the corresponding eigenvalues are denoted by λ_s^b and λ_n^b. The expressions for these eigenvalues up to first order correction are

$$\begin{aligned}\lambda_s^b &= \omega_{n+1} + \omega_{q+1} + \chi_{n+1} + \chi_{q+1} + \frac{J}{2}(\delta_{n,q+1} + \delta_{n+1,q}),\\ \lambda_n^b &= \omega_{n+1} + \omega_{q+1} + \chi_{n+1} + \chi_{q+1} - \frac{J}{2}(\delta_{n,q+1} + \delta_{n+1,q}).\end{aligned} \tag{2.30}$$

The initial state $|n+1\rangle\rangle$ evolves under $\hat{H}'_B$ to

$$|\psi(t)\rangle\rangle \approx \cos(\theta_b t)\,|n+1\rangle\rangle - i\sin(\theta_b t)\,|q+1\rangle\rangle, \tag{2.31}$$

where $\theta_b = (\lambda_s^b - \lambda_n^b)/2$. It is seen that the photon is exchanged periodically between $(n+1)$th and $(q+1)$th cavities. An important feature of this process is that the other cavities in the array are not populated to any appreciable extent during the evolution. This conclusion is based on the observation that the states other than $|n+1\rangle\rangle$ and $|q+1\rangle\rangle$ do not contribute appreciably to $|\psi(t)\rangle\rangle$.

For the purpose of illustration, consider a single photon transfer probability from the 1st cavity to 5th cavity in an array of six cavities. Choosing $\omega_1 = 0.185$ and $\chi = 0.01538$, the SS condition in Eqn. 2.29 gives the nonlinear parameters $\tilde{\chi}_1/\tilde{\omega}_1 = 0.077, \tilde{\chi}_2/\tilde{\omega}_1 = 0, \tilde{\chi}_3/\tilde{\omega}_1 = 0.0307, \tilde{\chi}_4/\tilde{\omega}_1 = 0.0615, \tilde{\chi}_5/\tilde{\omega}_1 = 0.077, \tilde{\chi}_6/\tilde{\omega}_1 = 0$ for a given set of resonance frequencies $\tilde{\omega}_2/\tilde{\omega}_1 = 0.985, \tilde{\omega}_3/\tilde{\omega}_1 = 0.92, \tilde{\omega}_4/\tilde{\omega}_1 = 0.92, \tilde{\omega}_5/\tilde{\omega}_1 = 1, \tilde{\omega}_6/\tilde{\omega}_1 = 1.23$. With these values, probability for a single photon transfer is shown in Fig. 2.7. Note that the probability of detecting the photon in 5th cavity is unity.

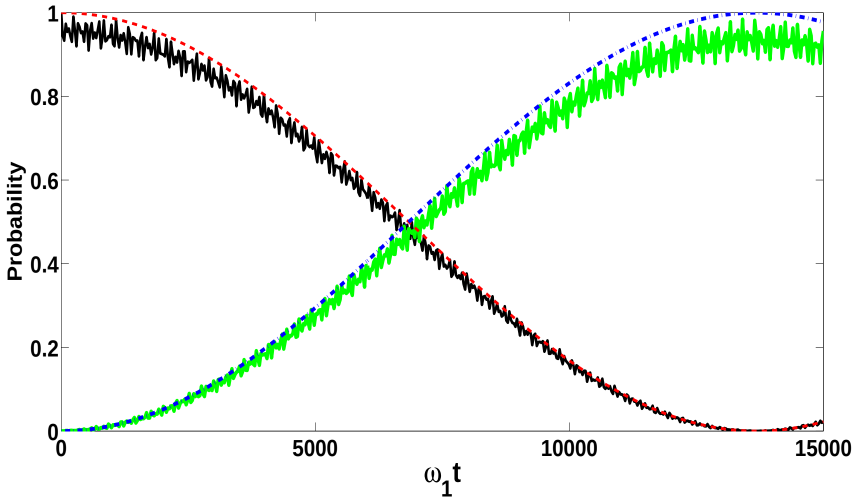

Figure 2.7 – Single photon detection probability in 1st and 5th cavities in an array of six cavities as a function of $\omega_1 t$. At time $t = \pi/(\lambda_s^b - \lambda_n^b)$, photon transferred from 1st cavity to 5th cavity with nearly unit probability. Black solid(dashed) and green solid(dot-dashed) line corresponds to P_1 and P_5 calculated numerically(approximate analytical state evolution $|\psi(t)\rangle\rangle$). Here P_m is the probability of finding the single photon in mth cavity. Setting $J/\omega_1 = 0.006$.

2.5 Entangled state generation

In the context of coupled cavities, generation of states of the form

$$|\Psi\rangle = \cos\theta\,|m,n\rangle + e^{i\phi}\sin\theta\,|p,q\rangle\,, \qquad (m+n = p+q = N) \tag{2.32}$$

is possible if the initial state is $|m,n\rangle$ and the target state is $|p,q\rangle$. If $m \neq p$ and $\theta \neq 0, \pm\pi/2$, then $|\Psi\rangle$ is entangled. These states are useful in the context of quantum metrology and imaging [131]. Additionally, if $m, q = N$ and $\theta = \pi/4$, the resultant state is

$$|\Psi\rangle = \frac{1}{\sqrt{2}}(|N0\rangle + e^{i\phi}\,|0N\rangle), \tag{2.33}$$

the generalized NOON state.

In order to generate NOON-type states given in Eqn. 2.32, consider the coupling term in the Hamiltonian $\hat{H}'_A$ to be $J\left[e^{i\eta}\hat{a}_1^\dagger\hat{a}_2 + e^{-i\eta}\hat{a}_1\hat{a}_2^\dagger\right]$, where the coupling constants are complex. Then the initial state $|m,n\rangle$ evolves to

$$|\psi(t)\rangle \approx \left[\cos(\theta_a t)|m,n\rangle - ie^{-i(q-n)\eta}\sin(\theta_a t)|p,q\rangle\right]. \tag{2.34}$$

The evolved state becomes $|\Psi\rangle$ given in Eqn. 2.33 if $\theta = \theta_a t$ and $\phi = -(\pi/2 + (q-n)\eta)$. This comes from the fact that the state switching condition given in Eqn. 2.25 ensures that transition occurs between the two states $|m,n\rangle$ and $|p,q\rangle$ only. No other state gets populated appreciably. Duality implies that in the case of the cavity array this is equivalent to generating the Bell state $|\psi\rangle\rangle = \cos\theta\,|n+1\rangle\rangle + e^{i\phi}\sin\theta\,|q+1\rangle\rangle$.

2.6 Quantum state transfer

Quantum state transfer is essential for transferring information encoded in quantum states. A qubit is sent by a sender to a receiver *via* a quantum channel. Sender prepares the quantum state $|\psi\rangle$ which encodes the information to be communicated to the receiver. Receiver reads out the state for the information. In the context of quantum state transfer in a cavity array, sender and receiver possess two different cavities in the array. The sender prepares the state $|\psi\rangle$ in his/her cavity which is to be transferred to the receiver cavity. The state of the system is

$$|\Psi\rangle = |\psi\rangle_S|0\rangle|0\rangle....|0\rangle|0\rangle_R|0\rangle|0\rangle..., \tag{2.35}$$

where the state of the sender's cavity is $|\psi\rangle$ and the other cavities are in their respective vacuua. Here 'S' stands for sender and 'R' stands for receiver. On evolution under a suitable Hamiltonian $\hat{H}$, if the state of the system after time t is

$$|\Psi(t)\rangle = |0\rangle_S|0\rangle|0\rangle....|0\rangle|\psi\rangle_R|0\rangle|0\rangle..., \tag{2.36}$$

the quantum state transfer is realized.

Perfect transfer of a single quantum between any two cavities in the array can be used for perfect transfer of quantum states. Consider the initial state of the cavity array to be

$$|\psi_{in}\rangle = \alpha|\text{vac}\rangle\rangle + \beta\,|n+1\rangle\rangle,$$

where

$$|\text{vac}\rangle\rangle = |0\rangle_1\,|0\rangle_2 \,....\, |0\rangle_N\,,$$
$$|n+1\rangle\rangle = |0\rangle_1\,|0\rangle_2 \,....\, |1\rangle_{n+1} \,...\, |0\rangle_N\,.$$

The state $|\psi_{in}\rangle$ corresponds to the $(n+1)$-th cavity in the superposition $\alpha|0\rangle + \beta|1\rangle$ and the other cavities are in their respective vacuua. If the SS condition is satisfied, the time-evolved state is

$$|\psi(t)\rangle = \alpha|\text{vac}\rangle\rangle + \beta e^{-i\lambda t}[\cos(\theta_b t)\,|n+1\rangle\rangle - ie^{-i\eta(q-n)}\sin(\theta_b t)\,|q+1\rangle\rangle], \tag{2.37}$$

where $\lambda = (\lambda_s^b + \lambda_n^b)/2$. At $t = \pi/2\theta_b$, the state of the $(q+1)$-th cavity is the superposition $\alpha|0\rangle + \beta|1\rangle$ and the other cavities are in their respective vacuua for the suitable value of η. Thus, the SS condition ensures the state of the field in the $(n+1)$-th cavity is transferred to the $(q+1)$-th cavity which signals perfect transfer.

2.7 Experimental feasibility

It is possible to implement the above scheme for photon transport and state transfer in arrays of high quality photonic crystal cavities (PCC) [132]. Typical values for the cavity resonance frequencies of PCC are in the range of mega-Hertz to tera-Hertz.

Other advantages of PCC are their high Q-values and low modal volume. The Q values of PCC are of the order of $\sim 10^6$ [133]. High value of Q implies that the dissipation is less. Kerr nonlinearity in PCC is realized by embedding two level atoms (quantum dots) in the cavities. The realizable nonlinearity is much larger compared to the optical nonlinearities in solids [109]. For these typical values, the effect of dissipation on the photon transport and state transfer is negligible. For the purpose of demonstration, an array of six identical cavities of resonance frequency 62.5 THz has been considered. The Kerr nonlinearity parameters $\tilde{\chi}_l$ are determined using the relation given in Eqn. 2.29 for $\chi = 1.25$ THz and $\omega_1 = 12.5$ THz. The coupling strength is chosen to be $J = 70$ GHz which is readily achievable in PCC [29]. The effect of dissipation is quantified by the fidelity between the state realized at the target cavity (penultimate cavity in this study) with and without considering dissipation. The state of the target cavity has been determined numerically by solving the Lindblad evolution equation and the estimated fidelity is 0.98. This clearly shows that the choice of the inter-cavity couplings and Kerr nonlinearities given by the duality principle is robust enough to achieve near perfect transfer with the currently available technology. Similar results are possible with other platforms such as the Josephson junction arrays [134–136].

2.8 Summary

Perfect transfer of a single photon in an array of homogeneously coupled cavities is forbidden if the array has more than three cavities. A duality relation between a system of single photon in an array of N linearly coupled cavities and another system of $N-1$ photons in two linearly coupled cavities identifies the correct combination of the coupling strengths and resonance frequencies for perfect transfer of a photon between two symmetrically located cavities in the array. In particular, the coupling strengths are required to be inhomogeneous. With this identification, transfer of a photon in the array is dynamically equivalent to the problem of sharing $N-1$ photons between the two linearly coupled cavities. Duality is extendable even if the cavities are of Kerr-type. This extended duality has identified the correct combination of the coupling strengths and local nonlinearities in the cavity array for complete photon transfer between any two selected cavities in the array. Additionally, this transfer is effected without populating the other cavities so that the transfer cannot be viewed as a contiguous hopping of photon from one cavity to the other. Another interesting result of the analysis is the possibility of perfect transfer of superpositions of the form $\alpha\,|0\rangle + \beta\,|1\rangle$ using a combination of Kerr nonlinearity and complex coupling strengths. This feature is important in the context of encoding and transfer of information. High fidelity generation of entangled states of the form $\cos\theta\,|m,n\rangle + e^{i\phi}\sin\theta\,|p,q\rangle$ in coupled cavities is another advantage of incorporating Kerr nonlinearity. Equivalently, Bell states in the cavity array are achievable with high fidelity. These results are pertinent in the context of quantum information processing in cavity arrays as they are scalable. The ideas presented here are applicable to coupled spin chains as well to achieve controlled transfer of states between any two spins in the chain.

Chapter 3

Quantum interference induced photon localization and delocalization

3.1 Introduction

Superposition principle is important in quantum mechanics [37]. Quantum interference, which is a consequence of superposition principle, is expected to arise when there is coherence in the state. The phenomenon of interference is almost ubiquitous. Occurrence of interference patterns in the Young's double slit experiment, lasing without inversion [137], electromagnetically induced transparency [138, 139], coherent population trapping [140], Hong-Ou-Mandel interferometery [141] and interference dip in neutron-nucleus scattering cross-section are some of the consequences of interference between transition amplitudes. In fact, interference between the multiple scattering of electron/photon in a disordered lattice leads to Anderson localization wherein the wavefunction of the particle gets spatially localized [142]. Localization of non-interacting particles such as photons is well understood in terms of the Anderson localization [143–146] which was originally formulated for non-interacting particles [147].

Localization and delocalization of photons in a linearly coupled cavity array are discussed in this chapter. An array of cavities containing two photons is considered.

If the two photons are detected in one of the cavities, it corresponds to two photon localization (TPL). If the two photons are detected in two different cavities, it is two-photon delocalization(TPD). The localization in this case does not arise due to any disorder unlike the Anderson localization. The occurrence of TPL and TPD is understood in terms of interference between various transition amplitudes, without requiring any disorder. It is seen that the relative phase and entanglement in the initial state are the factors responsible for the emergence of TPL and TPD. In the context of coupled cavities, TPL is analogous to the photon bunching while TPD corresponds to antibunching [148].

The organization of this chapter is as follows. The Hamiltonian for two coupled cavities and the dynamics generated by it are discussed in Section. 3.2. Importance of the relative phase in the initial state and inter-cavity detuning in the context of TPL and TPD is studied in Section. 3.3. Effects of dissipation and dephasing on TPL and TPD are explored in Section. 3.4. In Section. 3.5, localization and delocalization dynamics in an array of N cavities is discussed. Role of the array size on the delocalization process is investigated in Section. 3.6. Results are summarized in Section. 3.7.

3.2 Coupled cavities

Consider a system of two linearly coupled cavities whose resonance frequencies are ω_1 and ω_2 respectively. The Hamiltonian for the system is

$$\hat{H} = \omega_1 \hat{a}_1^\dagger \hat{a}_1 + \omega_2 \hat{a}_2^\dagger \hat{a}_2 + J\left[\hat{a}_1 \hat{a}_2^\dagger + \hat{a}_1^\dagger \hat{a}_2\right]. \tag{3.1}$$

Here $\hbar = 1$. The annihilation and creation operators for the two cavities are $\hat{a}_m$ and $\hat{a}_m^\dagger$ $(m = 1, 2)$. The first two terms in $\hat{H}$ correspond to two uncoupled linear cavities. The last term containing the coupling constant J describes the interaction between the two cavities. All the coupling strengths and frequencies are expressed in terms of frequency of the first cavity. In the plots, the frequency of the first cavity is set to unity.

For this Hamiltonian, the excitation number operator $\hat{N} = \hat{a}_1^\dagger \hat{a}_1 + \hat{a}_2^\dagger \hat{a}_2$ is a conserved quantity, *i.e.*, $[\hat{H}, \hat{N}] = 0$. The unitary dynamics due to $\hat{H}$ is restricted in an invariant subspace corresponding to a given number of excitations. Therefore, $\hat{H}$ can be diagonalized within the invariant subspace.

The eigenvalues of the Hamiltonian given in Eqn. 3.1, by restricting the total number of photons to be 2, are

$$\begin{aligned}
\lambda_1 &= \omega_1 + \omega_2, \\
\lambda_2 &= \omega_1 + \omega_2 - \sqrt{\Delta^2 + 4J^2}, \\
\lambda_3 &= \omega_1 + \omega_2 + \sqrt{\Delta^2 + 4J^2},
\end{aligned} \tag{3.2}$$

where $\Delta = \omega_1 - \omega_2$.

To discuss the occurrence of TPL and TPD, consider the state

$$|\psi(0)\rangle = C_1(0)\,|20\rangle + C_2(0)\,|11\rangle + C_3(0)\,|02\rangle\,, \tag{3.3}$$

where the probability amplitudes satisfy condition $|C_1(0)|^2 + |C_2(0)|^2 + |C_3(0)|^2 = 1$. Each of the superposed states in the initial state has two quanta. Therefore, the initial state belongs to the subspace spanned by the eigenstates of $\hat{N}$ corresponding to the eigenvalue 2. As a consequence, the time-evolved state also belongs to the invariant subspace.

The initial state $|\psi(0)\rangle$ evolves in time to

$$|\psi(t)\rangle = \frac{e^{-i(\omega_1+\omega_2)t}}{\Omega^2}[C_1(t)\,|20\rangle + C_2(t)\,|11\rangle + C_3(t)\,|02\rangle], \tag{3.4}$$

where

$$\begin{aligned} C_1(t) = &-[(4\omega_1^2 + 2J^2)C_1(0) + \sqrt{2}J(3\omega_1+\omega_2)C_2(0) + 2J^2C_3(0)]L_1 \\ &- i[2\omega_1 C_1(0) + \sqrt{2}JC_2(0)]L_2 + C_1(0)L_3, \end{aligned} \tag{3.5}$$

$$\begin{aligned} C_2(t) = &-[\sqrt{2}J(3\omega_1+\omega_2)C_1(0) + (4J^2 + (\omega_1+\omega_2)^2)C_2(0) + \sqrt{2}J(\omega_1+3\omega_2)C_3(0)]L_1 \\ &+ i[\sqrt{2}JC_1(0) + (\omega_1+\omega_2)C_2(0) + \sqrt{2}JC_3(0)]L_2 + C_2(0)L_3, \end{aligned} \tag{3.6}$$

$$\begin{aligned} C_3(t) = &-[(4\omega_2^2 + 2J^2)C_3(0) + \sqrt{2}J(\omega_1+3\omega_2)C_2(0) + 2J^2C_1(0)]L_1 \\ &- i[2\omega_2 C_3(0) + \sqrt{2}JC_2(0)]L_2 + C_3(0)L_3. \end{aligned} \tag{3.7}$$

Various terms occurring in the coefficients are

$$L_1 = 1 - \cos\Omega t, \tag{3.8}$$

$$L_2 = [2(\omega_1+\omega_2)(1-\cos\Omega t) - i\Omega\sin\Omega t)]\,, \tag{3.9}$$

$$L_3 = \left[(\omega_1+\omega_2)^2(\cos\Omega t - 1) + i(\omega_1+\omega_2)\Omega\sin\Omega t + \Omega^2\right]. \tag{3.10}$$

Here $\Omega = \sqrt{\Delta^2 + 4J^2}$.

Choosing $C_1(0) = \cos\theta$, $C_2(0) = 0$ and $C_3(0) = e^{i\phi}\sin\theta$ for the initial state, so that

$$|\psi(0)\rangle = |\theta,\phi\rangle = \cos\theta\,|20\rangle + e^{i\phi}\sin\theta\,|02\rangle\,, \tag{3.11}$$

makes it a TPL state. Upon detection, both the photons will be in one of the two cavities if $\theta \neq 0$ or $\pi/2$. Note that the state given in Eqn. 3.11 is a NOON-type state with $N = 2$.

For use in the subsequent discussions, define

$$\begin{aligned}
&|+\rangle &&= |\theta = \tfrac{\pi}{4}, \phi = 0\rangle = \tfrac{1}{\sqrt{2}}(|20\rangle + |02\rangle), \\
\text{and} \quad &|-\rangle &&= |\theta = \tfrac{\pi}{4}, \phi = \pi\rangle = \tfrac{1}{\sqrt{2}}(|20\rangle - |02\rangle).
\end{aligned} \tag{3.12}$$

It may be noted that the state $|+\rangle$ is symmetric under the exchange of photons, while $|-\rangle$ is antisymmetric. Both $|+\rangle$ and $|-\rangle$ are entangled states.

3.3 Localization and delocalization dynamics

To discuss in quantitative terms about TPL and TPD, relevant probabilities are defined: the probability of detecting the system to be in $|02\rangle$ or $|20\rangle$ is the localization probability $P_{|20\rangle+|02\rangle}$ and the probability of detecting the system in the state $|11\rangle$ is the delocalization probability $P_{|11\rangle}$. Perfect localization corresponds to the probability being unity for detecting both the photons in one of the cavities and zero for the other.

The time-evolved state given in Eqn. 3.4 is used to calculate the required probability amplitudes. With $\theta = \frac{\pi}{4}$, probability for TPD is

$$P_{|11\rangle}(t) = \frac{|C_2(t)|^2}{\Omega^4} = \frac{J^2}{\Omega^4}|i\Delta(1 - e^{i\phi})(1 - \cos\Omega t) - \Omega(1 + e^{i\phi})\sin\Omega t|^2. \tag{3.13}$$

If the relative phase $\phi = 0$, thereby implying $|\psi\rangle$=$|+\rangle$, then $P_{|11\rangle}$ is

$$P_{|11\rangle}(t) = \frac{4J^2}{4J^2 + \Delta^2}\sin^2\Omega t, \tag{3.14}$$

which varies between 0 and 1 periodically if the cavities are resonant ($\Delta = \omega_1 - \omega_2 = 0$).

On the other hand, if $\phi = \pi$, *i.e.*, $|\psi\rangle$=$|-\rangle$, then Eqn. 3.13 becomes

$$P_{|11\rangle}(t) = \frac{4J^2\Delta^2}{(4J^2+\Delta^2)^2}(1-\cos\Omega t)^2. \tag{3.15}$$

In the resonant case, $P_{|11\rangle}$ vanishes, irrespective of coupling strength J. In Fig. 3.1, the amplitudes of $P_{|11\rangle}$ given in Eqn. 3.14 and 3.15 are shown as a function of Δ/ω_1. These amplitudes correspond to the maximum values of $P_{|11\rangle}$ that can be achieved during time evolution.

In essence, for the state $|+\rangle$ ($\phi = 0$), constructive interference between the two transition amplitudes $C_{|20\rangle\to|11\rangle}$ and $C_{|02\rangle\to|11\rangle}$ enhances the probability of transition to $|11\rangle$. For the state $|-\rangle$ ($\phi = \pi$), the destructive interference between the two amplitudes makes the probability of detecting the system in $|11\rangle$ zero. It is to be pointed out that the initial state $|-\rangle$ is an eigenstate of $\hat{H}$ under resonance. As a consequence, the state does not change during evolution apart from acquiring an overall phase factor.

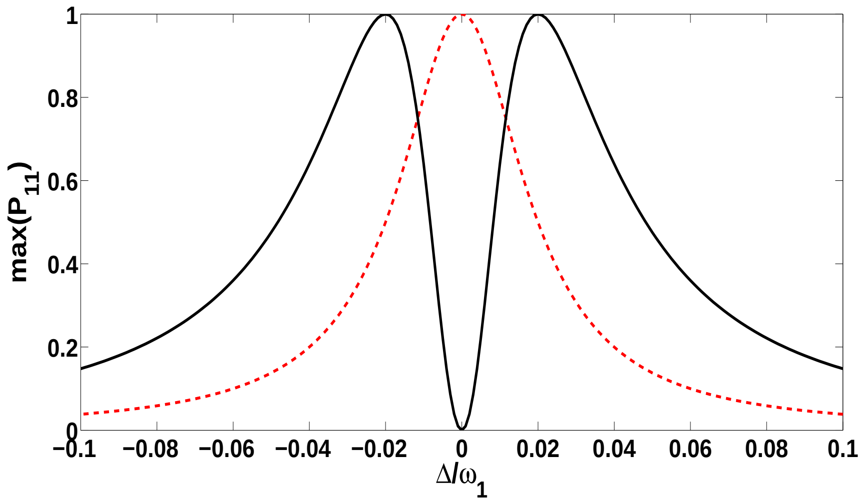

Figure 3.1 – Maximum achievable value of probability of delocalization $P_{|11\rangle}$ during time evolution is plotted as a function of cavity detuning Δ/ω_1. The two curves correspond to two different initial states, namely, $|+\rangle$ (dashed line) and $|-\rangle$ (continuous). Here $J/\omega_1 = 0.01$.

If $\Delta \neq 0$, the maximum value of the delocalization probability $P_{|11\rangle}$ for the state $|+\rangle$

is

$$\max(P_{|11\rangle}) = \frac{4J^2}{4J^2 + \Delta^2}, \tag{3.16}$$

which decreases with increasing detuning as seen from Fig. 3.1. However, the state $|-\rangle$ evolves to become a completely delocalized state, *i.e.,* $P_{|11\rangle} = 1$ due to constructive interference if $|\Delta| = 2J$, as seen from Eqn. 3.15. In Fig. 3.2, the maximum value of the delocalization probability for the state $|-\rangle$ is shown as a function of detuning for different choices of the coupling strength J. It is observed that the delocalization probability is unity for $|\Delta| = 2J$ and less than unity if $|\Delta| \neq 2J$.

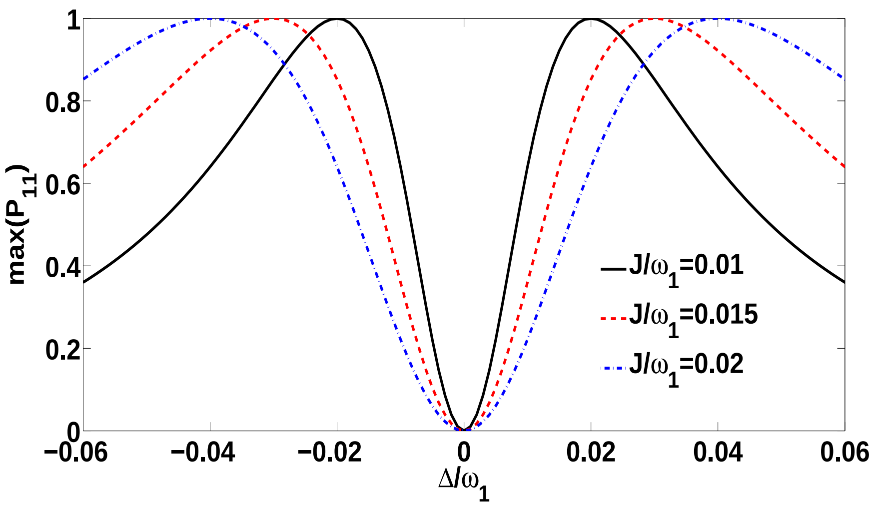

Figure 3.2 – Maximum of $P_{|11\rangle}$ during time evolution is shown as a function of cavity detuning Δ/ω_1 for the state $|-\rangle$. Complete delocalization occurs at $\Delta/\omega_1 = \pm 0.02$, ± 0.03, ± 0.04 for $J/\omega_1 = 0.01$, 0.015 and 0.02 respectively.

The discussion so far has been in the context of the entangled states $|+\rangle$ and $|-\rangle$. Considering the initial state to be one of the product states $|\psi\rangle = |20\rangle$ or $|02\rangle$ obtained by setting $\theta = 0$ or $\pi/2$ in Eqn. 3.11 respectively, the corresponding delocalization probabilities are

$$P_{|11\rangle}(\theta = 0) = \frac{2J^2}{\Omega^4} \left| [i\Delta(1 - \cos\Omega t) - \Omega \sin\Omega t] \right|^2,$$

$$\text{and} \qquad P_{|11\rangle}(\theta = \frac{\pi}{2}) = \frac{2J^2}{\Omega^4} \left| [i\Delta(1 - \cos\Omega t) + \Omega \sin\Omega t] \right|^2. \tag{3.17}$$

From Eqn. 3.17, the minimum time required to achieve the maximum value of delocalization probability ($P_{|11\rangle}$) is $T = \frac{1}{\Omega}\cos^{-1}(-\Delta^2/4J^2)$ if $|\Delta| \leq 2J$. The maximum value that $P_{|11\rangle}$ can attains is 1/2, and independent of Δ. However, if $\Delta > 2J$, minimum time to attain the maximum value of $P_{|11\rangle}$ is $T = \pi/\Omega$ and the corresponding maximum value is $8J^2\Delta^2/(4J^2 + \Delta^2)^2$. In Fig. 3.3, variation of the maximum delocalization probability is shown as a function of the detuning parameter Δ for the case $\theta = 0$. It is seen that the maximum value of $P_{|11\rangle}$ remains constant for $|\Delta| \leq 2J$ in each case: $J/\omega_1 = 0.01$ (continuous), 0.015 (dashed), 0.02 (dot-dashed). In short, for the initial state which is a localized product state, localization is dominant if $|\Delta| > 2J$.

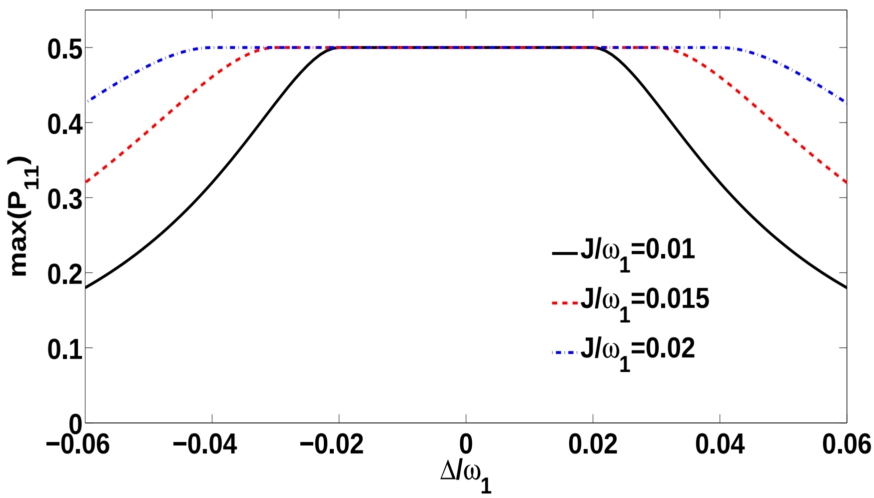

Figure 3.3 – Maximum of $P_{|11\rangle}$ during time evolution is shown as a function of cavity detuning Δ/ω_1 for the state $|20\rangle$. TPD probability starts decreasing at $\Delta/\omega_1 = \pm 0.02$, ± 0.03, ± 0.04 for $J/\omega_1 = 0.01$, 0.015 and 0.02 respectively. It is clear that for $|\Delta| > 2J$, TPL dominates over TPD.

3.4 TPD in presence of dissipation and dephasing

An ideal cavity evolves unitarily if it is completely isolated from the influences of the environment. In reality, there are unavoidable influences from the environment leading to dissipation and decoherence or dephasing. The dominant mechanism of dissipation is photon leakage. Dephasing is another aspect of system-environment interaction which leads to the decay of the off-diagonal elements of the density operator as the system looses its quantum coherence.

3.4.1 Effect of dissipation on TPD

Effects of dissipation are studied by coupling the system (coupled cavities) to zero temperature reservoirs and analyzing the master equation for the density operator of the system. In the presence of dissipation, the previously considered invariant subset of the Hilbert space is inadequate as the number of photons is not fixed. However, since the dissipative process does not increase the number of photons, only states with lower number of photons than what is contained in the initial state are to be considered. To facilitate writing down the master equation, relevant states are relabeled as follows: $|00\rangle \rightarrow |1\rangle\rangle, |10\rangle \rightarrow |2\rangle\rangle, |01\rangle \rightarrow |3\rangle\rangle, |20\rangle \rightarrow |4\rangle\rangle, |11\rangle \rightarrow |5\rangle\rangle, |02\rangle \rightarrow |6\rangle\rangle$, where double angular brackets are used to represent the various bipartite states of the two cavities. Using these as the basis states, the elements of the density operator are obtained by solving the master equation [149–152]

$$\frac{\partial \rho}{\partial t} = -i[\hat{H}, \rho] + \sum_{i,j=1}^{2} \frac{\gamma_{ij}}{2}(2\hat{a}_j \rho \hat{a}_i^\dagger - \hat{a}_i^\dagger \hat{a}_j \rho - \rho \hat{a}_i^\dagger \hat{a}_j). \tag{3.18}$$

Here γ_{11} and γ_{22} are decay rates of the first and second cavities respectively and, γ_{12} and γ_{21} are the cross-damping rates arising due to interference of transition amplitudes.

If $\gamma_{12} = \gamma_{21} = 0$ and $\gamma_{11} = \gamma_{22} = \gamma$, the localization probability is

$$P_{|20\rangle+|02\rangle}(t) = \frac{e^{-2\gamma t}}{\Omega^4}(|C_1(t)|^2 + |C_3(t)|^2). \tag{3.19}$$

The result shows that the TPL probability decreases exponentially in time at a rate that is twice the decay rate of the cavities. The suffix $|20\rangle + |02\rangle$ indicates that the probability corresponds to the case when the state of the system subsequent to measurement is a localized two photon state.

To bring out the effects of cross-damping, the master equation is solved numerically to get ρ_{44} and ρ_{66}, where $\rho_{ij} = \langle\langle i|\,\rho\,|j\rangle\rangle$. Referring to the convention given in the beginning of the subsection, it is immediate that ρ_{44} and ρ_{66} are the respective probabilities for detecting the system in $|20\rangle$ and $|02\rangle$. Therefore, $\rho_{44}+\rho_{66}$ is the localization probability when system evolves to a mixed state due to dissipation. The evolution equations for density matrix elements in the product basis $|m, n\rangle$ are

$$\frac{\partial \rho^{m,n}_{p,q}}{\partial t} = U + D + C; \tag{3.20}$$

where

$$\begin{aligned}
U =& -i[(m-p)\omega_1\rho^{m,n}_{p,q} + (n-q)\omega_2\rho^{m,n}_{p,q} + J\sqrt{m}\sqrt{n+1}\rho^{m-1,n+1}_{p,q} \\
&+ J\sqrt{n}\sqrt{m+1}\rho^{m+1,n-1}_{p,q} + J\sqrt{p}\sqrt{q+1}\rho^{m,n}_{p-1,q+1} + J\sqrt{q}\sqrt{p+1}\rho^{m,n}_{p+1,q-1}], \\
D =& \frac{\gamma_{11}}{2}[2\sqrt{(m+1)(p+1)}\rho^{m+1,n}_{p+1,q} - (m+p)\rho^{m,n}_{p,q}] \\
&+ \frac{\gamma_{22}}{2}[2\sqrt{(n+1)(q+1)}\rho^{m,n+1}_{p,q+1} - (n+q)\rho^{m,n}_{p,q}], \\
C =& \frac{\gamma_{12}}{2}[2\sqrt{(n+1)(p+1)}\rho^{m,n+1}_{p+1,q} - \sqrt{m(n+1)}\rho^{m-1,n+1}_{p,q} - \sqrt{q(p+1)}\rho^{m,n}_{p+1,q-1}] \\
&+ \frac{\gamma_{21}}{2}[2\sqrt{(m+1)(q+1)}\rho^{m+1,n}_{p,q+1} - \sqrt{n(m+1)}\rho^{m+1,n-1}_{p,q} - \sqrt{p(q+1)}\rho^{m,n}_{p-1,q+1}],
\end{aligned}$$

where $\rho^{g,h}_{i,j} = \langle g, h|\,\rho\,|i, j\rangle$. Here $m + n \leq 2$ and $p + q \leq 2$. Here U corresponds to the unitary part, D is the damping part and C is the cross damping part.

The explicit form of the evolution equations for $\rho_{44} = \langle 20|\,\rho\,|20\rangle$ and $\rho_{66} = \langle 02|\,\rho\,|02\rangle$ are

$$\dot{\rho}_{44} = -i[\sqrt{2}J(\rho_{54} - \rho_{45})] - 2\gamma_{11}\rho_{44} - \frac{\gamma_{12}}{\sqrt{2}}\rho_{54} - \frac{\gamma_{21}}{\sqrt{2}}\rho_{45}, \tag{3.21}$$

$$\dot{\rho}_{66} = -i[\sqrt{2}J(\rho_{56} - \rho_{65})] - 2\gamma_{22}\rho_{66} - \frac{\gamma_{12}}{\sqrt{2}}\rho_{65} - \frac{\gamma_{21}}{\sqrt{2}}\rho_{56}. \tag{3.22}$$

It is to be noted that the evolution of localization probabilities depends on evolution of off-diagonal elements. A typical evolution equation for an off-diagonal element, for instance, ρ_{45} is

$$\begin{aligned}\dot{\rho}_{45} &= -i[\Delta\rho_{45} + \sqrt{2}J(\rho_{55} - \rho_{44} - \rho_{46})] \\ &\quad - \left(\frac{3\gamma_{11}}{2} + \frac{\gamma_{22}}{2}\right)\rho_{45} - \frac{\gamma_{12}}{\sqrt{2}}(\rho_{55} + \rho_{44}) - \frac{\gamma_{21}}{\sqrt{2}}\rho_{46}, \end{aligned} \tag{3.23}$$

which indeed depends on the cavity frequencies. Hence, the evolution of ρ_{44} and ρ_{66} depend on the cavity frequencies also. Temporal evolution of TPL probability for the initial state $|+\rangle$ in the presence of dissipation is shown in Fig. 3.4. Resonant ($\Delta = 0$) and non-resonant ($\Delta \neq 0$) cases have been considered. In the resonant case, due to interference between the various transitions shown in Fig. 3.5, the probability of localization does not completely vanish. In non-resonant case, detuning renders the average energies $\langle 20|\,H\,|20\rangle$, $\langle 11|\,H\,|11\rangle$ and $\langle 02|\,H\,|02\rangle$ unequal, thereby making the transition amplitudes unequal in magnitude. As a result, perfect interference does not occur and localization probability decays to zero.

The above features differ if the initial state is $|-\rangle$ which is an eigenstate of $\hat{H}$. The localization probability decays $\sim e^{-2\gamma t}$ as shown in Fig. 3.6. Also, the localization probability decays to zero for any non-zero detuning due to unequal magnitudes of the transitions amplitudes between various states.

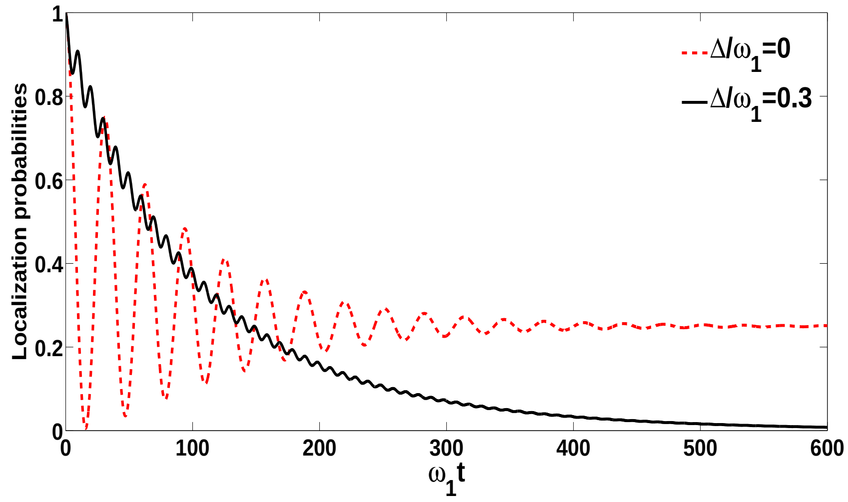

Figure 3.4 – Probability of localization $P_{|20\rangle+|02\rangle} = \rho_{44} + \rho_{66}$ is shown as a function of $\omega_1 t$ for the initial state $|+\rangle$. Here $J/\omega_1 = 0.05$ and $\gamma/\omega_1 = \gamma_{11}/\omega_1 = \gamma_{22}/\omega_1 = \gamma_{12}/\omega_1 = \gamma_{21}/\omega_1 = 0.005$. Dashed curve corresponds to $\Delta/\omega_1 = 0$ and the continuous line for $\Delta/\omega_1 = 0.3$.

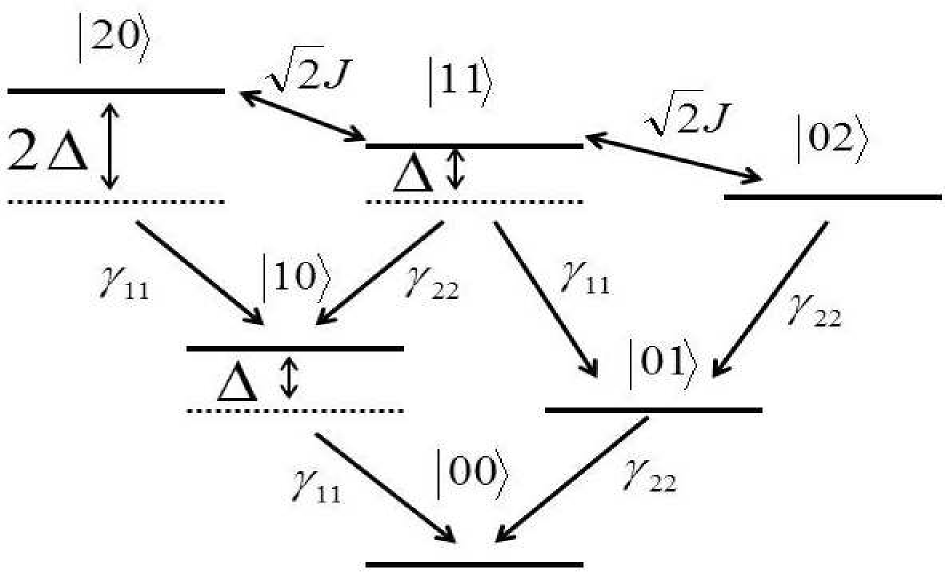

Figure 3.5 – Energy levels are labeled by the expectation value of the Hamiltonian $\hat{H}$ in the respective states. The inter-state decay rates are denoted by γ with appropriate suffixes. Here $\Delta = \omega_1 - \omega_2$.

In dissipative systems, energy decreases if there is no suitable external forcing. So, it is important to study the corresponding situation for the present system. Using the master equation given in Eqn. 3.18, the evolution equation for the expectation values of the relevant operators are obtained. These equations can be cast in the following

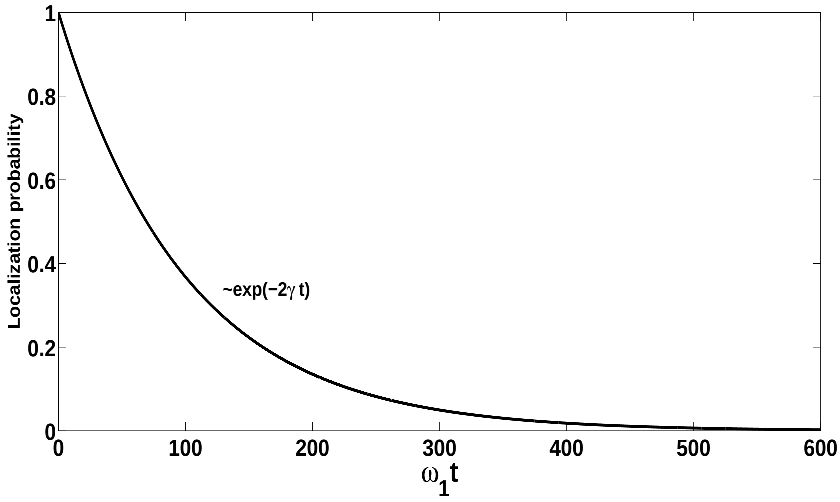

Figure 3.6 – Probability of localization $P_{|20\rangle+|02\rangle} = \rho_{44} + \rho_{66}$ is shown as a function of $\omega_1 t$ for the initial state $|-\rangle$. Values used are $J/\omega_1 = 0.05$,$\gamma/\omega_1 = 0.005$ and $\Delta/\omega_1 = 0$. Here $\gamma = \gamma_{11} = \gamma_{22} = \gamma_{12} = \gamma_{21}$.

form

$$\frac{d}{dt}\begin{pmatrix} \langle \hat{a}_1^\dagger \hat{a}_1\rangle \\ \langle \hat{a}_1^\dagger \hat{a}_2\rangle \\ \langle \hat{a}_1 \hat{a}_2^\dagger\rangle \\ \langle \hat{a}_2^\dagger \hat{a}_2\rangle \end{pmatrix} = \begin{pmatrix} -\gamma & \frac{-iJ}{\hbar}-\frac{\gamma}{2} & \frac{iJ}{\hbar}-\frac{\gamma}{2} & 0 \\ \frac{-iJ}{\hbar}-\frac{\gamma}{2} & -\gamma & 0 & \frac{iJ}{\hbar}-\frac{\gamma}{2} \\ \frac{iJ}{\hbar}-\frac{\gamma}{2} & 0 & -\gamma & \frac{-iJ}{\hbar}-\frac{\gamma}{2} \\ 0 & \frac{iJ}{\hbar}-\frac{\gamma}{2} & \frac{-iJ}{\hbar}-\frac{\gamma}{2} & -\gamma \end{pmatrix}\begin{pmatrix} \langle \hat{a}_1^\dagger \hat{a}_1\rangle \\ \langle \hat{a}_1^\dagger \hat{a}_2\rangle \\ \langle \hat{a}_1 \hat{a}_2^\dagger\rangle \\ \langle \hat{a}_2^\dagger \hat{a}_2\rangle \end{pmatrix}. \quad (3.24)$$

Here $\gamma = \gamma_{11} = \gamma_{22}$ and $\gamma_{12} = \gamma_{21} = \sqrt{\gamma_{11}\gamma_{22}}$ [153] and $\langle\hat{O}\rangle = \mathrm{Tr}[\rho(t)\hat{O}]$. The matrix differential equation is solved to get the average number of photons in the first and second cavities. The resultant expressions are is

$$\langle \hat{a}_1^\dagger \hat{a}_1\rangle_t = \frac{1}{4}[X_1(t)\langle \hat{a}_1^\dagger \hat{a}_1\rangle_0 + X_2(t)\langle \hat{a}_1^\dagger \hat{a}_2\rangle_0 + X_3(t)\langle \hat{a}_1 \hat{a}_2^\dagger\rangle_0 + X_4(t)\langle \hat{a}_2^\dagger \hat{a}_2\rangle_0], \quad (3.25)$$

$$\langle \hat{a}_2^\dagger \hat{a}_2\rangle_t = \frac{1}{4}[X_4(t)\langle \hat{a}_1^\dagger \hat{a}_1\rangle_0 + X_3(t)\langle \hat{a}_1^\dagger \hat{a}_2\rangle_0 + X_2(t)\langle \hat{a}_1 \hat{a}_2^\dagger\rangle_0 + X_1(t)\langle \hat{a}_2^\dagger \hat{a}_2\rangle_0]. \quad (3.26)$$

where

$$X_1(t) = 1 + 2e^{-\gamma t}\cos 2Jt + e^{-2\gamma t}, \tag{3.27}$$

$$X_2(t) = -1 + 2ie^{-\gamma t}\sin 2Jt + e^{-2\gamma t}, \tag{3.28}$$

$$X_3(t) = -1 - 2ie^{-\gamma t}\sin 2Jt + e^{-2\gamma t}, \tag{3.29}$$

$$X_4(t) = 1 - 2e^{-\gamma t}\cos 2Jt + e^{-2\gamma t}. \tag{3.30}$$

For the initial state $|\psi\rangle = \cos\theta\,|20\rangle + e^{i\phi}\sin\theta\,|02\rangle$,

$$\langle\hat{a}_1^\dagger\hat{a}_1\rangle_t = \frac{1}{2}[2e^{-\gamma t}\cos 2Jt\cos 2\theta + 1 + e^{-2\gamma t}], \tag{3.31}$$

$$\langle\hat{a}_2^\dagger\hat{a}_2\rangle_t = \frac{1}{2}[-2e^{-\gamma t}\cos 2Jt\cos 2\theta + 1 + e^{-2\gamma t}]. \tag{3.32}$$

It is clear from the expression that the evolution of the mean photon number is independent of the relative phase ϕ. If $\theta = \pi/4$, then

$$\langle\hat{a}_1^\dagger\hat{a}_1\rangle_t = \langle\hat{a}_2^\dagger\hat{a}_2\rangle_t = \frac{1}{2}[e^{-2\gamma t} + 1], \tag{3.33}$$

which saturates at $1/2$ for large t. Thus, quantum interference stabilizes the average number photons at a non-zero value in spite of dissipation. If the initial state is $|\psi_+\rangle = \frac{1}{\sqrt{2}}[|10\rangle + |01\rangle]$, then

$$\langle\hat{a}_1^\dagger\hat{a}_1\rangle_t = \langle\hat{a}_2^\dagger\hat{a}_2\rangle_t = \frac{e^{-2\gamma t}}{2}. \tag{3.34}$$

The average number of photons in the cavities decays to zero as t increases. Both the cavities lose energy at the same rate, a consequence of assuming resonance and equal damping.

If the initial state is $|\psi_-\rangle = \frac{1}{\sqrt{2}}(|10\rangle - |01\rangle)$, the average number of photons in the cavities are

$$\langle \hat{a}_1^\dagger \hat{a}_1 \rangle_t = \langle \hat{a}_2^\dagger \hat{a}_2 \rangle_t = \frac{1}{2}, \tag{3.35}$$

which is independent of time. The average values do not decrease to zero as the relative phase in the initial state is π which leads to destructive interference between the amplitudes corresponding to $|10\rangle \rightarrow |00\rangle$ and $|01\rangle \rightarrow |00\rangle$. In the present context, the initial state is either the symmetric state $|\psi_+\rangle$ or the antisymmetric state $|\psi_-\rangle$. The former decays at a rate 2γ while the later does not decay. This is analogous to the superradiance and subradiance that occur in the interaction between a three-level atom and the electromagnetic field [152]. Due to interference, the average photon number saturates at 1/2 though dissipation is present. It implies that quantum interference makes it possible to retain nonzero number of photons in the cavities in spite of dissipation.

3.4.2 Effect of dephasing on TPD

As seen in the previous section, the relative phase in the initial state plays a crucial role in TPD. In the presence of dephasing, the relative phases in the time-evolved state are randomized. It is natural to expect dephasing to affect TPD whose occurrence is sensitive to the relative phase. The master equation described in the previous section can be modified to incorporate dephasing by including the Lindblad term $\frac{\gamma_d}{2}\mathcal{D}(\hat{a}^\dagger \hat{a})\rho$ [98, 154], where $\mathcal{D}[\hat{o}]\rho = 2\hat{o}\rho\hat{o}^\dagger - \hat{o}^\dagger\hat{o}\rho - \rho\hat{o}^\dagger\hat{o}$. The master equation becomes

$$\frac{\partial \rho}{\partial t} = -i[\hat{H}, \rho] + \frac{\gamma_d}{2}\mathcal{D}[\hat{a}_1^\dagger \hat{a}_1]\rho + \frac{\gamma_d}{2}\mathcal{D}[\hat{a}_2^\dagger \hat{a}_2]\rho. \tag{3.36}$$

The Lindblad term accounts for the dephasing which leads to the decay of the off-diagonal elements in the density operator.

Evolution equations for the density matrix elements for the dephasing case can be expressed as

$$\frac{d}{dt}\begin{bmatrix}\rho_{44}\\ \rho_{45}\\ \rho_{46}\\ \rho_{54}\\ \rho_{55}\\ \rho_{56}\\ \rho_{64}\\ \rho_{65}\\ \rho_{66}\end{bmatrix} = \begin{bmatrix} 0 & B & 0 & -B & 0 & 0 & 0 & 0 & 0\\ B & A & B & 0 & -B & 0 & 0 & 0 & 0\\ 0 & B & C & 0 & 0 & -B & 0 & 0 & 0\\ -B & 0 & 0 & A^* & B & 0 & -B & 0 & 0\\ 0 & -B & 0 & B & 0 & B & 0 & -B & 0\\ 0 & 0 & -B & 0 & B & A & 0 & 0 & -B\\ 0 & 0 & 0 & -B & 0 & 0 & C^* & B & 0\\ 0 & 0 & 0 & 0 & -B & 0 & B & A^* & B\\ 0 & 0 & 0 & 0 & 0 & -B & 0 & B & 0\end{bmatrix}\begin{bmatrix}\rho_{44}\\ \rho_{45}\\ \rho_{46}\\ \rho_{54}\\ \rho_{55}\\ \rho_{56}\\ \rho_{64}\\ \rho_{65}\\ \rho_{66}\end{bmatrix}, \tag{3.37}$$

where $A = -i\Delta - \gamma_d$, $B = iJ\sqrt{2}$, $C = -2i\Delta - 4\gamma_d$.

To understand the effect of dephasing on delocalization, numerically obtained time-dependence of $P_{11} = \rho_{55}$, the probability of delocalization, is shown in Fig. 3.7 for the initial states $|-\rangle$ and $|+\rangle$. If the initial state is $|-\rangle$, the time evolved state is partially delocalized as ρ_{55} is less than unity. In the absence of dephasing, complete localization is possible due to destructive interference between the amplitudes corresponding to the transitions $|20\rangle \rightarrow |11\rangle$ and $|02\rangle \rightarrow |11\rangle$ in Section. 3.3. But dephasing randomizes the relative phases during time-evolution and suppresses the destructive interference.

Generally, in the presence of dephasing, the initial coherence is expected to vanish resulting in a steady state density operator. The steady-state solutions for the evolution equation given in Eqn. 3.37 are obtained by equating the time derivatives to zero. The first and last rows of the matrix in the above equation have two non-zero entries. This yields $\rho_{45} = \rho_{54}$ and $\rho_{56} = \rho_{65}$ respectively in the steady state. The

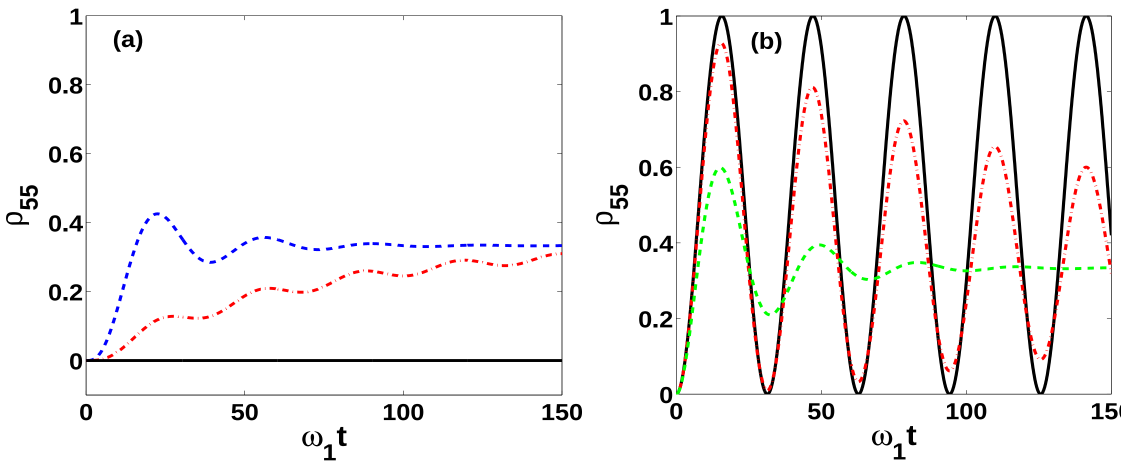

Figure 3.7 – Probability of delocalization ρ_{55} as a function of $\omega_1 t$ for (a) $|-\rangle$ and (b) $|+\rangle$. Curves correspond to different values of decay rate: $\gamma_d/\omega_1 = 0$ (continuous), 0.005 (dot-dashed) and 0.05 (dashed). For all the cases, $J/\omega_1 = 0.05$ and $\Delta/\omega_1 = 0$.

remaining steady state equations are

$$[-i\Delta - \gamma_d]\rho_{45} - i\sqrt{2}J(\rho_{55} - \rho_{44} - \rho_{46}) = 0, \tag{3.38}$$

$$[-2i\Delta - 4\gamma_d]\rho_{46} - i\sqrt{2}J(\rho_{56} - \rho_{45}) = 0, \tag{3.39}$$

$$[i\Delta - \gamma_d]\rho_{45} + i\sqrt{2}J(\rho_{55} - \rho_{44} - \rho_{64}) = 0, \tag{3.40}$$

$$[-i\Delta - \gamma_d]\rho_{56} - i\sqrt{2}J(\rho_{46} + \rho_{66} - \rho_{55}) = 0, \tag{3.41}$$

$$[2i\Delta - 4\gamma_d]\rho_{64} + i\sqrt{2}J(\rho_{56} - \rho_{45}) = 0, \tag{3.42}$$

$$[i\Delta - \gamma_d]\rho_{56} + i\sqrt{2}J(\rho_{64} + \rho_{66} - \rho_{55}) = 0. \tag{3.43}$$

Using the Cramer's rule for solving a system of linear equations, with the constraint $\rho_{44} + \rho_{55} + \rho_{66} = 1$, the steady state solutions are

$$\rho_{44} = \frac{1}{3}, \rho_{45} = 0, \rho_{46} = 0, \rho_{55} = \frac{1}{3}, \rho_{56} = 0, \rho_{64} = 0, \rho_{66} = \frac{1}{3}, \tag{3.44}$$

which are independent of Δ. It is also clear from Fig. 3.7(a) that the curves indeed saturate at 1/3. The initial state $|+\rangle$ also evolves to steady state density matrix in presence of dephasing as shown in Fig 3.7(b) .

The probabilities of TPD for different values of detuning are shown in Fig. 3.8 for the initial state $|-\rangle$. Comparing the profiles corresponding to the different values of Δ, it is clear that the rate of attaining steady state values is slow as Δ increases. Detuning slows down the process of attaining the steady state. Similar conclusion holds for the state $|+\rangle$ as the initial state.

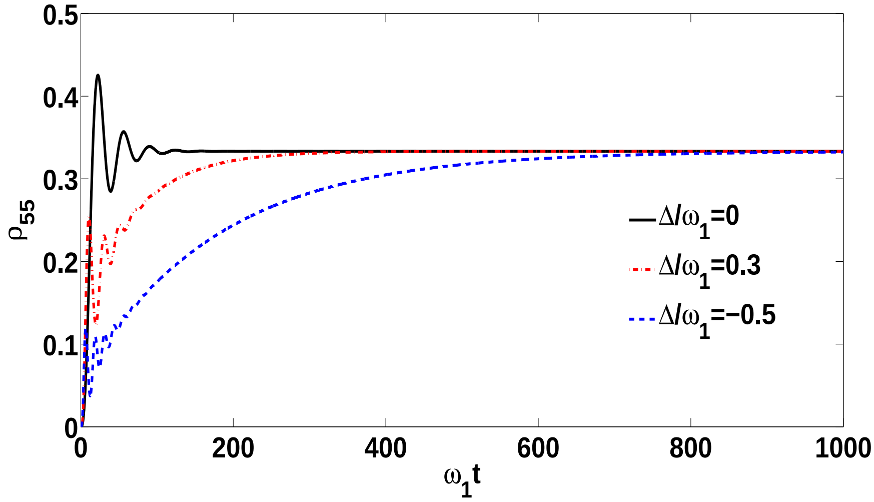

Figure 3.8 – Delocalization probability as a function of $\omega_1 t$ for $|-\rangle$ with various values of detuning. Continuous line for $\Delta/\omega_1 = 0$, dot-dashed line is for $\Delta/\omega_1 = 0.3$ and dashed line correspond to $\Delta/\omega_1 = -0.5$ with $J/\omega_1 = 0.05$ and $\gamma_d/\omega_1 = 0.05$.

3.4.3 Role of coherence on delocalization

For a better appreciation of the role of coherence, consider the realistic situation where an initial pure state is prepared with probability ϵ and a related random state (noise) with probability $1-\epsilon$. The total density matrix to represent the initial TPL state $|\psi\rangle$ and the added noise M is [155]

$$\rho = \epsilon\, |\psi\rangle \langle\psi| + (1-\epsilon)M, \tag{3.45}$$

where

$$|\psi\rangle = \cos\theta\,|20\rangle + e^{i\phi}\sin\theta\,|02\rangle\,, \tag{3.46}$$

$$M = \cos^2\theta\,|20\rangle\langle 20| + \sin^2\theta\,|02\rangle\langle 02|\,. \tag{3.47}$$

This is a mixed state for all $\epsilon < 1$. The state interpolates between the TPL state $|\psi\rangle$ ($\epsilon = 1$) which has coherence and the state M ($\epsilon = 0$) which has no coherence. Thus, ϵ measures the degree of coherence in the state ρ. To bring out the effect of initial coherence in the state given in Eqn. 3.45, the variation of the maximum of TPD probability as a function of ϵ is shown in Fig. 3.9. The value of θ is chosen to be $\frac{\pi}{4}$ which makes the superposition coefficients in the initial state to be of equal magnitude. The curves shown in the figure correspond to two values of ϕ, namely, 0 and π. In the later case, as ϵ increases the peak value of TPD probability ρ_{55} decreases and vanishes at $\epsilon = 1$. This is due to the destructive interference between the amplitudes for the two transitions, namely, $|20\rangle \to |11\rangle$ and $|02\rangle \to |11\rangle$. In the former case, the peak of TPD probability increases with ϵ due to constructive interference.

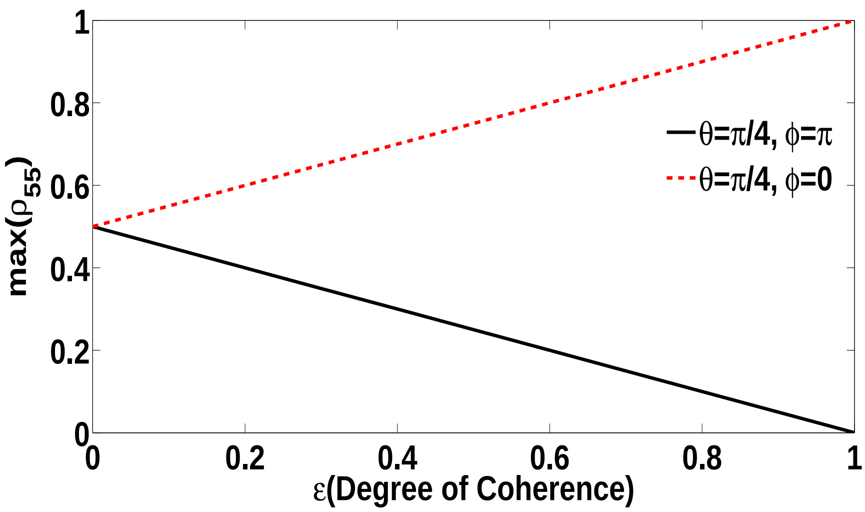

Figure 3.9 – Maximum value of probability of delocalization ρ_{55} that can be achieved during time evolution is shown as a function of ϵ. Continuous line corresponds to state $|-\rangle$ and dotted line corresponds to $|+\rangle$. Other parameters are $J/\omega_1 = 0.05$, $\Delta/\omega_1 = 0$.

3.5 Linearly coupled cavity array

In the context of two coupled cavities, $|11\rangle$ is the only one delocalized state. By including more number of cavities, number of delocalized states increases. In fact, the number of delocalized states is much more than the number of localized states for a large array. Hence, it is interesting to study the roles of the relative phase and entanglement on the localization-delocalization dynamics in an array of N cavities. Hamiltonian for a chain of N linearly coupled identical cavities is

$$\hat{H} = \omega \sum_{j=1}^{N} \hat{a}_j^\dagger \hat{a}_j + J \sum_{j=1}^{N-1} (\hat{a}_j^\dagger \hat{a}_{j+1} + \hat{a}_j \hat{a}_{j+1}^\dagger). \tag{3.48}$$

Here $\hat{a}_j$ and $\hat{a}_j^\dagger$ are respectively the annihilation and creation operators corresponding to the field mode in jth cavity. The coupling between two adjacent cavities is J. The time evolved annihilation operator for the jth cavity mode is

$$\hat{a}_j(t) = \sum_l G_{jl}(t) \hat{a}_l(0), \tag{3.49}$$

where $G_{jl}(t) = \sum_{k=1}^{N} e^{-i\Omega_k t} \tilde{S}(j,k)\tilde{S}(l,k)$, the normal mode frequency $\Omega_k = \omega + 2J\cos\left(\frac{\pi k}{N+1}\right)$ and the transformation matrix element $\tilde{S}(j,k) = \sqrt{\frac{2}{N+1}} \sin(\frac{j\pi k}{N+1})$. With these results, time-evolution of any physical quantity expressible in terms of the creation and annihilation operators can be determined.

Coupling, linear or otherwise, among the cavities leads to transport of photons from one cavity to another in the array. But realization of TPL or TPD is dependent on the initial state as well. In order to investigate the role of entanglement and relative phase in the initial state on the localization- delocalization phenomenon, consider states of the form

$$|\psi\rangle = \cos\theta\,|2\rangle_r\,|0\rangle_s + e^{i\phi}\sin\theta\,|0\rangle_r\,|2\rangle_s\,. \tag{3.50}$$

The notation $|p\rangle_r\,|q\rangle_s$ stands for p photons in the r-th cavity and q photons in the s-th cavity. Other cavities are in their respective vacuua. Here r and s vary from 1 to N. Hence, the probability of detecting two photons in the r-th and s-th cavities are $\cos^2\theta$ and $\sin^2\theta$ respectively. This is a two photon localized state according to the definition given earlier. The relative phase ϕ does not influence the measurement outcomes.

To study delocalization in the context of two photons, it is prudent to calculate the coincidence detection probability P_{mn}:

$$P_{m,n}(t) = \langle a_n^\dagger(t)a_m^\dagger(t)a_m(t)a_n(t)\rangle, \tag{3.51}$$

is the probability of detecting one photon each in two different cavities ($m \neq n$) at time t. As the number of photons is restricted to 2, the values of $P_{m,n}$ ranges from 0 to 1 for $m \neq n$. Here $\langle..\rangle$ refers to expectation value in the initial state. The time-developed operators used in Eqn. 3.51 are defined in Eqn. 3.49. Therefore,

$$P_{m,n}(t) = 2\,|\cos\theta G_{mr}(t)G_{nr}(t) + e^{i\phi}\sin\theta G_{ms}(t)G_{ns}(t)|^2. \tag{3.52}$$

The diagonal elements with a proportionality constant of this correlation matrix give the probability of localization and the off-diagonal elements represent the probability of delocalization. Degree of TPD, defined as

$$S = 1 - \frac{1}{2}\sum_{n=1}^{N} P_{n,n}(t), \tag{3.53}$$

is essentially the probability of detecting the photons, one each in two different cavities.

If $S = 0$ then the state is TPL state, and $S = 1$ corresponds to TPD state.

If there are two photons in the array, states of the form $|1\rangle_r |1\rangle_s$ $(r \neq s)$ or their superpositions are delocalized states. The initial state given in Eqn. 3.50 is an entangled state. To study the influence of initial entanglement on the localization-delocalization dynamics, the entanglement is quantified in terms of negativity. For any density matrix ρ, negativity $\mathcal{N}$ is

$$\mathcal{N}(\rho) = \sum_i \frac{|\lambda_i| - \lambda_i}{2}, \tag{3.54}$$

where λ_i are the eigenvalues of ρ^{PT}, the partial transposition of ρ [156]. For the state $|\psi\rangle$, $\mathcal{N} = \sin\theta\cos\theta$ which is independent of the relative phase ϕ in the initial state. If entanglement in the initial state is the only indicator of the degree of delocalization achievable [157], then S should be independent of ϕ. However, $P_{m,n}$ has an explicit dependence of ϕ which, in turn, implies that S depends on ϕ.

Time evolution of degree of delocalizations for different initial states are shown in Fig. 3.10. This clearly shows that the degree of TPD or TPL during time-evolution is dependent on the entanglement as well as the relative phase in the initial state. To bring out this feature more clearly, it is noted that the entanglement in state $|\psi\rangle$ depends on θ as indicated earlier. The maximum achievable S during time evolution has been shown as a function of θ for an array of two cavities in Fig. 3.11 (a) and for eight cavities in Fig. 3.11(b). Different curves correspond to different values of the relative phase ϕ in the range of 0 to π. It is seen that the delocalization probability not only depends on θ (entanglement) but also relative phase ϕ (interference).

3.6 Role of system size on TPD

It is to be noted from Fig. 3.11 that for a given initial state the maximum achievable degree of delocalization (S) is different for different sizes of the array. This indicates

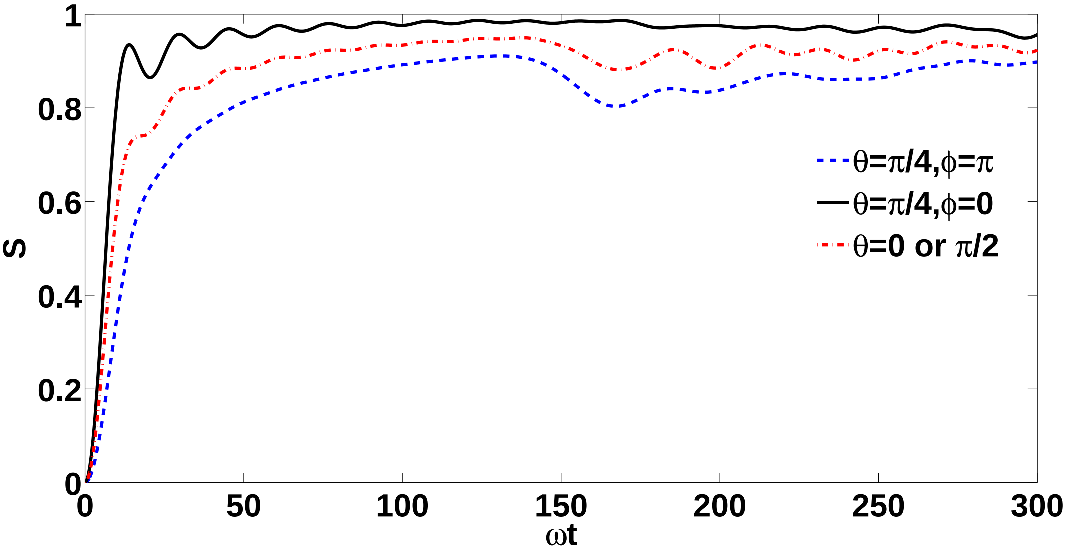

Figure 3.10 – Time evolution of degree of two photon delocalization S for different initial states with $J/\omega = 0.05$. Here $N = 29$.

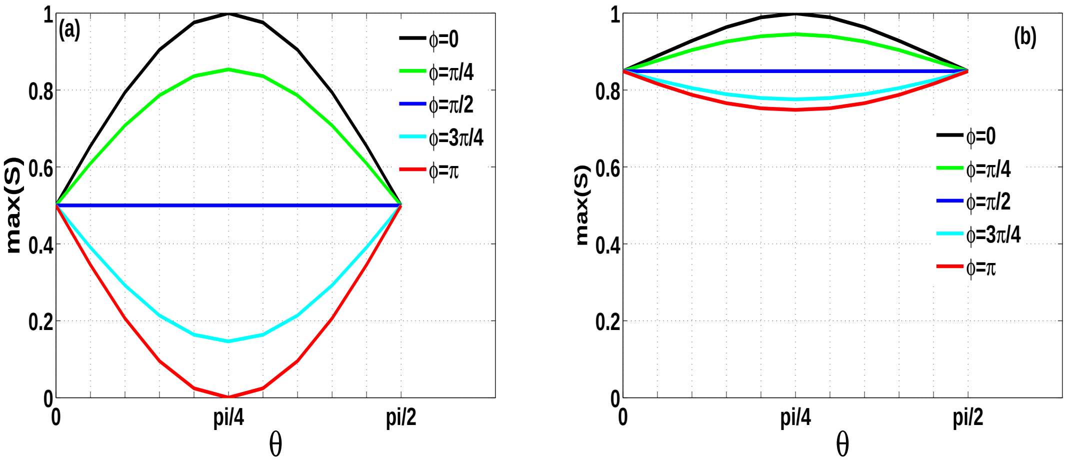

Figure 3.11 – Plot shows the maximum achievable value of degree of delocalization in time evolution is plotted as a function of θ for various values of ϕ for (a) $N = 2$ and (b) $N = 8$. Values used are $J/\omega = 0.05$. Here $r = N/2$ and $s = r + 1$.

that the strength of delocalization depends also on the size of the array, apart from θ and ϕ. The maximum achievable S as a function of N for different choices of ϕ and θ is shown in Fig. 3.12. For $\phi > \pi/2$, the maximum of S increases with N. If $\phi < \pi/2$, the maximum S is nearly unity and remain practically at the same value. If the size of the array is large, localized states completely delocalize during time evolution. This is consistent with the fact that the number of delocalized states is more than the number of localized states if N is large.

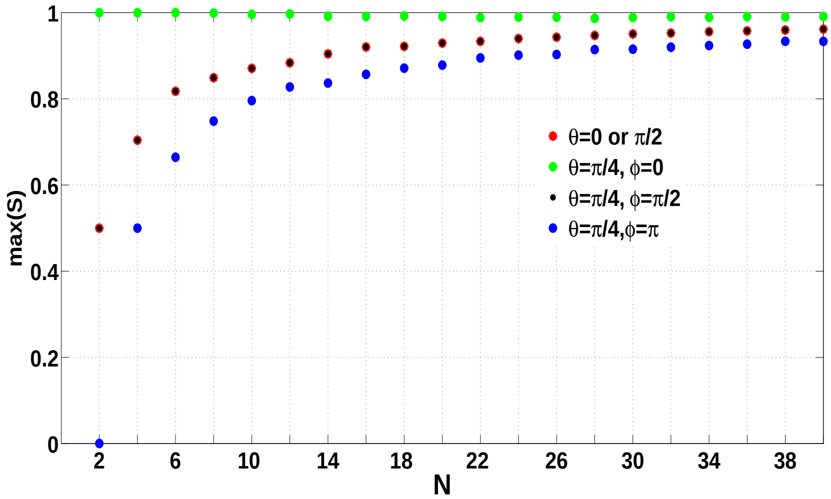

Figure 3.12 – Maximum value of S during time evolution as a function of number of cavities in the array (N) for various values of θ and ϕ. Here $J/\omega = 0.05$, $r = N/2$ and $s = r + 1$.

As an aside, an example of a state that never delocalizes during time evolution is

$$|\chi\rangle = \frac{1}{\sqrt{N}} \sum_{n=1}^{N} (-1)^n |2\rangle_n , \tag{3.55}$$

where $|2\rangle_n$ refers to two photons in the nth cavity and no photons in the other cavities. This state is a localized eigenstate of $\hat{H}$ given in Eqn. 3.48. Consequently, it will never delocalize during time evolution under $\hat{H}$.

3.7 Summary

Emergence of localization and delocalization of photons in an array of cavities is a consequence of quantum interference between various transition amplitudes. An initially localized entangled state remains localized or evolves to a delocalized state depending on the relative phase present in the initial state of the two coupled cavities. Localization occurs if the interference between the transition amplitudes is destructive whereas constructive interference delocalizes the state. On the other hand, a product state does not delocalize completely as there is no interference. Localization probability dominates over delocalization if the detuning between the cavities is larger than twice the coupling strength.

Dissipation leads to loss of energy and decay of localization probability. However, even in the presence of dissipation, localization probability does not vanish to zero due to quantum interference if the initial state is chosen properly.

Decoherence due to interaction with the environment reduces the magnitude of transition from localized states to delocalized states. This is consistent with the fact that the process of decoherence randomizes the relative phases which are very crucial for the interference of probability amplitudes.

Localization and delocalization probabilities depend on the entanglement and relative phase present in the initial localized state. This is true also for an array containing more than two cavities. If the array size is large, photons tend to delocalize rather than localize.

Chapter 4

Photon localization and delocalization in nonlinear cavities

4.1 Introduction

Cavities filled with nonlinear medium have become the workhorses to investigate quantum phenomena such as the photon blockade [86, 97–101], bunching and antibunching [102, 103], quantum phase transitions [104], etc. Strong interaction between individual photons is possible in the presence of nonlinear medium [86, 122]. Kerr cavities are useful as quantum scissors to truncate coherent states to generate finite superpositions of number states [158]. Often, optical nonlinearities are significant only at high intensities. Recently, several ways of generating optical nonlinearities in solids, even at the level of individual photons, have been proposed [86, 108, 109, 159, 160].

Interaction between two systems allows exchange of energy between them. Nonlinearity in the system strongly affects the exchange that may lead to localization of energy [147, 161–163]. The localization-delocalization dynamics of photons in the presence of nonlinearity provides a better understanding of some quantum many-body systems [164]. It is of interest to understand how nonlinearity and quantum interference affect the localization and delocalization process. Coupled cavity dynamics studied in the literature are mostly in the context of linear interaction between the cavities [60, 165] which contain non-linear Kerr medium [61]. As a generalization, intensity dependent coupling between the cavities is considered. This is the quantum equivalent of nonlinearly coupled classical nonlinear oscillators. A deformed algebra appears as a natural choice in studying the dynamics of the system.

The organization of this chapter is as follows. The Hamiltonian for two nonlinearly coupled cavities and the dynamics generated by it are discussed in Section. 4.2. Role of the nonlinearity on TPL and TPD is studied in Section. 4.3. Delocalization dynamics is explored in the presence of dissipation and dephasing in Section. 4.4. In Section. 4.5, localization and delocalization dynamics in an array of N nonlinear cavities is discussed. Results are summarized in Section. 4.6.

4.2 Nonlinearly coupled cavities

In this section, a system of two nonlinear cavities is described. The Hamiltonian for the system, setting $\hbar = 1$, is

$$\begin{aligned}\hat{H} = {} & \omega_1 \hat{a}_1^\dagger \hat{a}_1 + \omega_2 \hat{a}_2^\dagger \hat{a}_2 + \chi_1 \hat{a}_1^{\dagger 2} \hat{a}_1^2 + \chi_2 \hat{a}_2^{\dagger 2} \hat{a}_2^2 \\ & + J \left[\sqrt{1 + k\hat{a}_1^\dagger \hat{a}_1}\, \hat{a}_1 \hat{a}_2^\dagger \sqrt{1 + k\hat{a}_2^\dagger \hat{a}_2} + \hat{a}_1^\dagger \sqrt{1 + k\hat{a}_1^\dagger \hat{a}_1} \sqrt{1 + k\hat{a}_2^\dagger \hat{a}_2}\, \hat{a}_2 \right].\end{aligned} \tag{4.1}$$

Here $\hat{a}_m$ and $\hat{a}_m^\dagger$ are the annihilation and creation operators for the two cavities ($m = 1, 2$). The first two terms correspond to two independent linear cavities. The next two terms which depend on χ_1 and χ_2 account for the Kerr nonlinearity in the cavities. The interaction between the cavities is assumed to be intensity-dependent with coupling strength J. Such interaction terms have been considered in the context of intensity-dependent atom-field coupling [166–168]. In this work, the parameter k which describes the intensity dependent interaction is non-negative and limited to one. This ensures that the vacuum state is the only state annihilated by the deformed annihilation operator. All the coupling strengths, nonlinear strengths and frequencies are expressed in terms of frequency of the first cavity. In the plots, the frequency of the first cavity is set to unity.

The purpose of studying the system described by $\hat{H}$ is that many other well known interactions are special cases of $\hat{H}$. If k, χ_1 and χ_2 vanish, $\hat{H}$ is the Hamiltonian for two linearly coupled cavities,

$$\hat{H}_L = \omega_1 \hat{a}_1^\dagger \hat{a}_1 + \omega_2 \hat{a}_2^\dagger \hat{a}_2 + J(\hat{a}_1 \hat{a}_2^\dagger + \hat{a}_1^\dagger \hat{a}_2). \tag{4.2}$$

If $k\langle a^\dagger a\rangle >> 1$, then

$$\begin{aligned}\hat{H}_{BS} = {} & \omega_1 \hat{a}_1^\dagger \hat{a}_1 + \omega_2 \hat{a}_2^\dagger \hat{a}_2 + \chi_1 \hat{a}_1^{\dagger 2} \hat{a}_1^2 + \chi_2 \hat{a}_2^{\dagger 2} \hat{a}_2^2 \\ & + J\left[\sqrt{k\hat{a}_1^\dagger \hat{a}_1}\hat{a}_1 \hat{a}_2^\dagger \sqrt{k\hat{a}_2^\dagger \hat{a}_2} + \hat{a}_1^\dagger \sqrt{k\hat{a}_1^\dagger \hat{a}_1}\sqrt{k\hat{a}_2^\dagger \hat{a}_2}\hat{a}_2\right],\end{aligned} \tag{4.3}$$

which is the Buck-Sukumar Hamiltonian [169]. In the opposite limit $k\langle a^\dagger a\rangle << 1$,

$$\hat{H}_{Kerr} = \omega_1 \hat{a}_1^\dagger \hat{a}_1 + \omega_2 \hat{a}_2^\dagger \hat{a}_2 + \chi_1 \hat{a}_1^{\dagger 2} \hat{a}_1^2 + \chi_2 \hat{a}_2^{\dagger 2} \hat{a}_2^2 + J(\hat{a}_1 \hat{a}_2^\dagger + \hat{a}_1^\dagger \hat{a}_2), \tag{4.4}$$

which describes a Kerr interaction [158, 170–172].

To discuss the general case, consider the following deformed operators:

$$\begin{aligned}\hat{K}_m &= \sqrt{1 + k\hat{a}_m^\dagger \hat{a}_m}\hat{a}_m, \\ \hat{K}_m^\dagger &= \hat{a}_m^\dagger \sqrt{1 + k\hat{a}_m^\dagger \hat{a}_m},\end{aligned} \tag{4.5}$$

where $m = 1$ and 2 correspond to the first and second cavities respectively. These deformed operators satisfy $[\hat{K}_m, \hat{K}_m^\dagger] = 2\hat{K}_{0m}$, with $\hat{K}_{0m} = k\hat{a}_m^\dagger \hat{a}_m + \frac{1}{2}$ which becomes the identity operator when $k = 0$. Thus, these operators form a closed algebra, with

Heisenberg-Weyl algebra and SU(1,1) algebra as the limiting cases when $k \to 0$ and $k \to 1$ respectively [168]. The action of these operators on the number states is as follows:

$$\begin{aligned} &\hat{K}_m \left|n\right\rangle_m = \sqrt{n}\sqrt{1+k(n-1)}\left|n-1\right\rangle_m, \\ \text{and} \qquad &\hat{K}_m^\dagger \left|n\right\rangle_m = \sqrt{1+kn}\sqrt{n+1}\left|n+1\right\rangle_m, \end{aligned} \tag{4.6}$$

where $\left|n\right\rangle_m$ represents the state of mth cavity with number of photons n.

With $\chi_m = \omega_m k$, the Hamiltonian $\hat{H}$ given in Eqn. 4.1 is re-expressed in terms of the deformed operators to yield

$$\hat{H}_d = \omega_1 \hat{K}_1^\dagger \hat{K}_1 + \omega_2 \hat{K}_2^\dagger \hat{K}_2 + J(\hat{K}_1 \hat{K}_2^\dagger + \hat{K}_1^\dagger \hat{K}_2). \tag{4.7}$$

The deformations considered here are analogous to the Holstein-Primakoff realization of deformed boson operators to represent spin operators in the context of ferromagnetism [173]. The form of the intensity dependent interaction considered in the Hamiltonian in Eqn. 4.1 is not readily achievable. However, it allows to express the nonlinear Hamiltonian in a form that resembles the Jaynes-Cummings Hamiltonian.

Though the Hamiltonian includes intensity-dependent interaction as well as Kerr nonlinearity, it is still possible to identify a constant of motion, namely, the operator corresponding to the number of quanta $\hat{N} = \hat{a}_1^\dagger \hat{a}_1 + \hat{a}_2^\dagger \hat{a}_2$ so that $[\hat{H}, \hat{N}] = 0$. Existence of this constant of motion implies that there are invariant subspaces for the unitary dynamics generated by $\hat{H}$. The Hamiltonian can be diagonalized in the subspace of a given number of excitations.

Consider the initial state

$$|\psi(0)\rangle = C_1(0)\,|20\rangle + C_2(0)\,|11\rangle + C_3(0)\,|02\rangle\,, \tag{4.8}$$

where $|C_1(0)|^2 + |C_2(0)|^2 + |C_3(0)|^2 = 1$. Unitary evolution under $\hat{H}$ evolves the state $|\psi(0)\rangle$ to

$$|\psi(t)\rangle = C_1(t)\,|20\rangle + C_2(t)\,|11\rangle + C_3(t)\,|02\rangle\,, \tag{4.9}$$

where

$$\begin{aligned}
C_1(t) = &-[((2\omega_1 + 2\chi_1)^2 - 2(1+k)J)L_1 - i(2\omega_1 + 2\chi_1)L_2 + L_3)C_1(0) \\
&+ (\sqrt{2(1+k)}J(3\omega_1 + 2\chi_1 + \omega_2)L_1 - i\sqrt{2(1+k)}JL_2)C_2(0) \\
&+ 2(1+k)J^2 L_1 C_3(0)], \qquad (4.10) \\
C_2(t) = &-[(\sqrt{2(1+k)}J(3\omega_1 + 2\chi_1 + \omega_2)L_1 - i\sqrt{2(1+k)}JL_2)C_1(0) \\
&+ ((4(1+k)J^2 + (\omega_1 + \omega_2)^2)L_1 - i(\omega_1 + \omega_2)L_2 + L_3)C_2(0) \\
&+ ((\sqrt{2(1+k)}J(3\omega_2 + 2\chi_2 + \omega_1)L_1 - \sqrt{2(1+k)}JL_2)C_3(0)], \qquad (4.11) \\
C_3(t) = &-[((2\omega_2 + 2\chi_2)^2 - 2(1+k)J)L_1 - i(2\omega_2 + 2\chi_2)L_2 + L_3)C_3(0) \\
&+ (\sqrt{2(1+k)}J(3\omega_2 + 2\chi_2 + \omega_1)L_1 - i\sqrt{2(1+k)}JL_2)C_2(0) \\
&+ 2(1+k)J^2 L_1 C_1(0)]. \qquad (4.12)
\end{aligned}$$

Various terms occurring in the coefficients are

$$L_1 = \frac{e^{\lambda_1 t}}{(\lambda_1 - \lambda_2)(\lambda_1 - \lambda_3)} + \frac{e^{\lambda_2 t}}{(\lambda_2 - \lambda_1)(\lambda_2 - \lambda_3)} + \frac{e^{\lambda_3 t}}{(\lambda_3 - \lambda_1)(\lambda_3 - \lambda_2)}, \tag{4.13}$$

$$L_2 = \frac{e^{\lambda_1 t}(\lambda_2 + \lambda_3)}{(\lambda_1 - \lambda_2)(\lambda_1 - \lambda_3)} + \frac{e^{\lambda_2 t}(\lambda_3 + \lambda_1)}{(\lambda_2 - \lambda_1)(\lambda_2 - \lambda_3)} + \frac{e^{\lambda_3 t}(\lambda_2 + \lambda_1)}{(\lambda_3 - \lambda_1)(\lambda_3 - \lambda_2)}, \tag{4.14}$$

$$L_3 = \frac{e^{\lambda_1 t}(\lambda_2\lambda_3)}{(\lambda_1 - \lambda_2)(\lambda_1 - \lambda_3)} + \frac{e^{\lambda_2 t}(\lambda_3\lambda_1)}{(\lambda_2 - \lambda_1)(\lambda_2 - \lambda_3)} + \frac{e^{\lambda_3 t}(\lambda_2\lambda_1)}{(\lambda_3 - \lambda_1)(\lambda_3 - \lambda_2)}, \tag{4.15}$$

where λ_1, λ_2 and λ_3 are the eigenvalues of $-i\hat{H}$ in the two photon subspace. If $\Delta = 0$

and $\chi_1 = \chi_2$, then these eigenvalues are

$$\lambda_1 = -i(2\omega + 2\chi), \tag{4.16}$$

$$\lambda_2 = -i(2\omega + \chi - \sqrt{\chi^2 + 4(1+k)J^2}), \tag{4.17}$$

$$\lambda_3 = -i(2\omega + \chi + \sqrt{\chi^2 + 4(1+k)J^2}). \tag{4.18}$$

For the nonresonant case ($\Delta \neq 0$) with $\omega_1, \omega_2 >> \chi$, the approximate eigenvalues are

$$\lambda_1 \approx -i\left(\omega_1 + \omega_2 + 2\chi - \frac{\chi\Delta^2}{N_1(1+k)J^2}\right), \tag{4.19}$$

$$\lambda_2 \approx -i\left(\omega_1 + \omega_2 + 2\chi - R - \frac{\chi(\Delta - R)^2}{N_2(1+k)J^2}\right), \tag{4.20}$$

$$\lambda_3 \approx -i\left(\omega_1 + \omega_2 + 2\chi + R - \frac{\chi(\Delta + R)^2}{N_3(1+k)J^2}\right), \tag{4.21}$$

where

$$N_1 = 2 + \frac{\Delta^2}{2(1+k)J^2},$$

$$N_2 = 1 + \left(\frac{R(R-\Delta)}{2(1+k)J^2} - 1\right)^2 + \frac{(R-\Delta)^2}{2(1+k)J^2},$$

$$N_3 = 1 + \left(\frac{R(R+\Delta)}{2(1+k)J^2} - 1\right)^2 + \frac{(R+\Delta)^2}{2(1+k)J^2},$$

$$\text{and} \quad R = \sqrt{\Delta^2 + 4(1+k)J^2}.$$

Assuming $C_1(0) = \cos\theta$, $C_2(0) = 0$ and $C_3(0) = e^{i\phi}\sin\theta$, the initial state is

$$|\psi(0)\rangle = |\theta, \phi\rangle = \cos\theta\,|20\rangle + e^{i\phi}\sin\theta\,|02\rangle\,, \tag{4.22}$$

which is a TPL state. On detection, both the photons will be in one of the two cavities if $\theta \neq 0$ or $\pi/2$. In the next section, the delocalization features of this state are discussed.

4.3 Nonlinearity and delocalization

Considering the state $|\psi(0)\rangle$ given in Eqn. 4.22 and choosing $\theta = \frac{\pi}{4}$, the probability for TPD is

$$\begin{aligned} P_{|11\rangle}(t) &= |C_2(t)|^2, \\ &= \tilde{J}^2 | \left\{ (1+e^{i\phi}) \left[L_2 + iL_1(\omega_1+\omega_2) \right] + 2iL_1(\omega_1+\chi_1+e^{i\phi}(\omega_2+\chi_2)) \right\} |^2, \end{aligned} \tag{4.23}$$

where $\tilde{J} = \sqrt{(1+k)}J$.

This probability evolves in time as L_1 and L_2 are time-dependent. In the context of localization and delocalization, the quantity of interest is the maximum value attained by $P_{|11\rangle}$ during time evolution. If $\phi = 0$, the initial state is $|\psi(0)\rangle = |+\rangle = (|20\rangle + |02\rangle)/\sqrt{2}$. In Fig. 4.1, the maximum value of $P_{|11\rangle}$ is shown as a function of the nonlinear strength $\chi(=\chi_1 = \chi_2)$ for the resonant case ($\omega_1 = \omega_2$ such that $\Delta = 0$). Dashed line in Fig. 4.1 corresponds to $k = \chi/\omega$. To allow for independent variation of χ, maximum of $P_{|11\rangle}$ during time evolution is shown (continuous) in Fig. 4.1 for a fixed value of $k = 0.1$. The deviation between the two curves is insignificant. Hence, the condition $\chi = k\omega$ is not restrictive. However, it allows for expressing the Hamiltonian $\hat{H}$ given in Eqn. 4.1 as a deformed JC model.

It is noted that the maximum value decreases with increasing nonlinear strength. This comes from the fact that the cavity nonlinearity makes the average energies in the states $|20\rangle, |11\rangle$ and $|02\rangle$ unequal as shown in Fig. 4.2. This energy difference between states affects the transition from localized states to delocalized state.

On the other hand, if $\phi = \pi$, *i.e.*, $|\psi(0)\rangle = |-\rangle$,

$$P_{|11\rangle}(t) = 4\Delta^2 J^2 (1+k)|L_1|^2. \tag{4.24}$$

If the two cavities are resonant, *i.e.*, $\Delta = 0$, then $P_{|11\rangle}$ is 0 during time-evolution, independent of χ and k. Hence, the state $|-\rangle$ never delocalizes during time evolution. It is of interest to note that the state $|-\rangle$ is an eigenstate of $\hat{H}$ given in Eqn. 4.1 if the cavities are resonant. As a consequence, the state does not evolve.

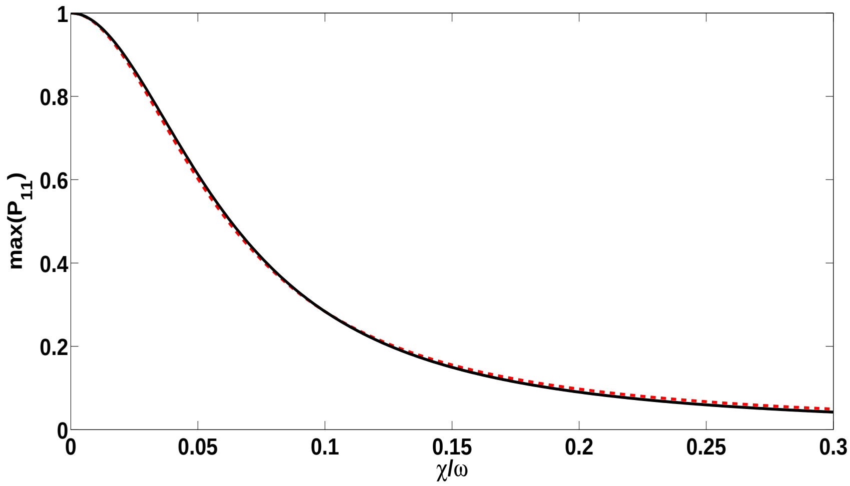

Figure 4.1 – Maximum achievable value of probability of delocalization $P_{|11\rangle}$ during time evolution is plotted a function of nonlinear strength χ/ω for the initial state $|+\rangle$. Parameters chosen are $\Delta/\omega = 0$ and $J/\omega = 0.03$. Continuous line corresponds to $k = 0.1$ and dashed line corresponds to $k = \chi/\omega$.

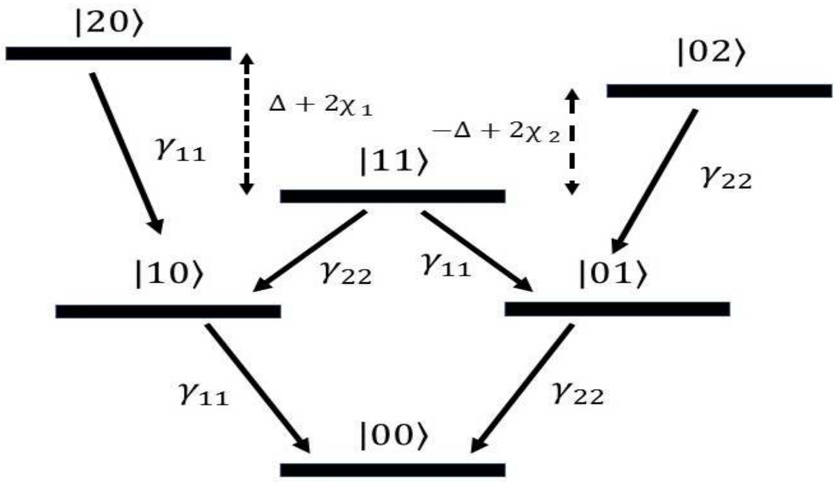

Figure 4.2 – Energy levels are labeled by the expectation value of the Hamiltonian $\hat{H}$ in the respective states. The inter-state decay rates are denoted by γ with appropriate suffixes.

If the initial state is a localized product state $|20\rangle$ or $|02\rangle$, obtained by setting $\theta = 0$

or $\pi/2$ in Eqn. 4.22 respectively, the corresponding delocalization probabilities are

$$P_{|11\rangle}(\theta = 0) = 2(1+k)J^2|(iL_1(3\omega_1 + 2\chi_1) + \omega_2) + L_2)|^2, \tag{4.25}$$

$$P_{|11\rangle}(\theta = \frac{\pi}{2}) = 2(1+k)J^2|(iL_1(3\omega_2 + 2\chi_2) + \omega_1) + L_2)|^2. \tag{4.26}$$

A condition to achieve complete delocalization starting from the product states $|20\rangle$ and $|02\rangle$ is derived. This condition ensures that the probabilities for the transitions $|20\rangle \to |11\rangle$ and $|02\rangle \to |11\rangle$ become unity. For the Hamiltonian given in Eqn. 4.1, the average energies in $|20\rangle$ and $|02\rangle$ shift by $\Delta + 2\chi_1$ and $-\Delta + 2\chi_2$ respectively from the average energy in the state $|11\rangle$ as shown in Fig. 4.2. For perfect transition to occur, the average energy levels must be same (degenerate). The average energies of the localized state ($|20\rangle$ or $|02\rangle$) and delocalized state ($|11\rangle$) are the same if

$$\begin{aligned} \Delta &= -2\chi_1, \quad \text{for } |20\rangle\,, \\ \text{and} \quad \Delta &= 2\chi_2, \qquad \text{for } |02\rangle\,. \end{aligned} \tag{4.27}$$

These are the state swiching conditions which ensure perfect delocalization from the states $|20\rangle$ and $|02\rangle$. When the system is detuned for one of the transitions, the other transition does not occur. For example, if the detuning is appropriate for the transition $|20\rangle \to |11\rangle$,*i.e.*, $\langle 20| H |20\rangle = \langle 11| H |11\rangle$, transition to $|02\rangle$ does not occur as the average energy in the state $|02\rangle$ is detuned by $2(\chi_1 + \chi_2)$ from $|20\rangle$ and $|11\rangle$. Thus, in the presence of Kerr nonlinearity, detuning can be used as a switch to block $|20\rangle \to |02\rangle$ transition. The time evolution of probabilities P_{20}, P_{11} and P_{02} are shown in Fig. 4.3 for the two localized states $|20\rangle$ and $|02\rangle$ as the initial states. The probability of delocalization is unity if the parameters satisfy the state switching condition given in Eqn. 4.27 for the corresponding initial state.

If the initial state is the delocalized state $|11\rangle$, the probability of localization P_{20+02}

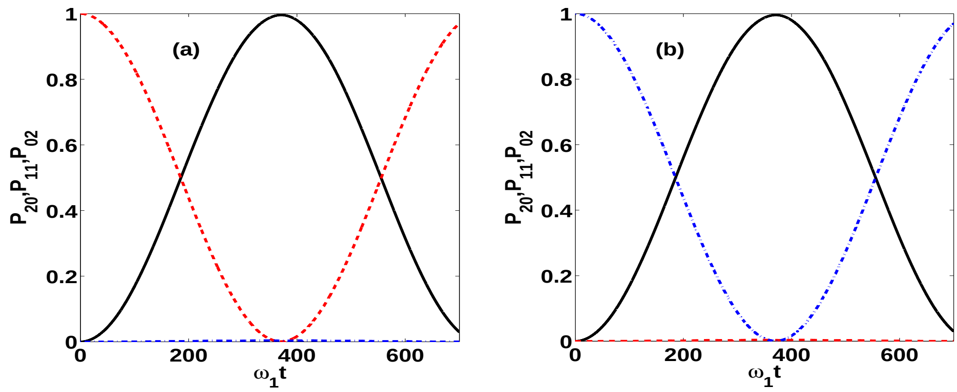

Figure 4.3 – The probabilities P_{20} (dashed), P_{11}(continuous) and P_{02}(dot-dashed) are plotted as a function of $\omega_1 t$ for the initial state $(a)\,|20\rangle$ with $\chi_1/\omega_1 = 0.02, \chi_2/\omega_1 = 0.015$ and $\Delta/\omega_1 = -0.04$ and $(b)\,|02\rangle$ with $\chi_1/\omega_1 = 0.015, \chi_2/\omega_1 = 0.02$ and $\Delta/\omega_1 = 0.04$. Other parameters are $J/\omega_1 = 0.003$ and $k = 0.001$.

is non-zero during time evolution in linear cavities. In the nonlinear case under consideration, transitions from $|11\rangle$ to $|02\rangle$ or $|20\rangle$ and vice-versa are nearly forbidden if $\chi_1, \chi_2 >> J$ and $\Delta = 0$. The time evolution of P_{20}, P_{11} and P_{02} are shown in Fig. 4.4 for two different values of $\chi(= \chi_1 = \chi_2)$ when the initial state is $|11\rangle$. Note that if the nonlinear strength χ is larger than the coupling strength J, then the state $|11\rangle$ is an approximate eigenstate of $\hat{H}$. As a consequence, it does not evolve to be a localized state. What happens in this limit is that the presence of a photon in a cavity blocks the inflow of photon from the other cavity, analogous to the photon blockade phenomenon in a driven cavity [86]. It is the Kerr nonlinearity which leads to the blockade, thereby stabilizing the delocalized state $|11\rangle$.

Now, the delocalization aspects of the superposition of the localized states $|20\rangle$ and $|02\rangle$ are considered. In particular, the symmetric and the anti-symmetric combinations ($|+\rangle$ and $|-\rangle$ respectively) are studied. If $|+\rangle$ or $|-\rangle$ is the initial state, then the evolved state does not have complete overlap with $|11\rangle$ for any detuning. The states do not delocalize completely. Essentially, the average energies of these localized states cannot be equal to the average energy of $|11\rangle$ for any values detuning in the presence of Kerr nonlinearity.

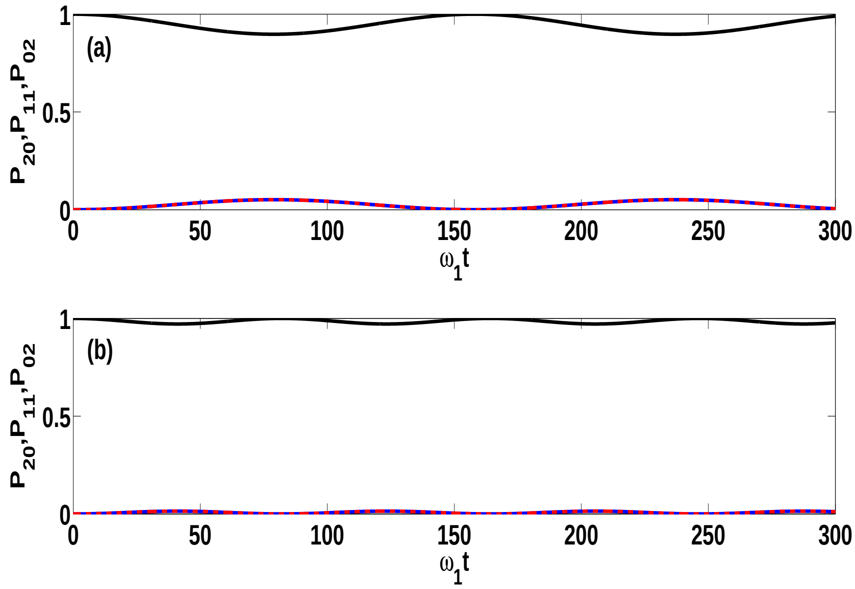

Figure 4.4 – The probabilities P_{20} (dashed), P_{11}(continuous) and P_{02}(dot-dashed) are plotted as a function of $\omega_1 t$ for the initial delocalized state $|11\rangle$ for $(a)\chi/\omega_1 = 0.03, k = 0.03$ and $(b)\chi/\omega_1 = 0.05, k = 0.05$. The detuning and coupling strength are set to be $\Delta/\omega_1 = 0$ and $J/\omega_1 = 0.005$.

4.4 Dissipative nonlinear cavities

As discussed in the previous section, Kerr nonlinearity shifts the energy levels of the cavities which, in turn, implies that the interference cannot be perfect. This feature has been used to explain the two-photon localization-delocalization in the coupled cavities. Yet another feature to be considered is dissipation. Interplay between the nonlinearity and interference when the system is subjected to dissipation (coupled with zero temperature reservoirs) is discussed in this section.

The evolution equations for the density matrix is obtained using the master equation

$$\frac{\partial \rho}{\partial t} = -i[\hat{H}, \rho] + \sum_{i,j=1}^{2} \frac{\gamma_{ij}}{2}(2\hat{a}_j \rho \hat{a}_i^\dagger - \hat{a}_i^\dagger \hat{a}_j \rho - \rho \hat{a}_i^\dagger \hat{a}_j). \tag{4.28}$$

Here γ_{11} and γ_{22} are decay rates of the first and second cavities respectively and, γ_{12} and γ_{21} are the cross-damping rates arising due to interference of transition amplitudes. The evolution equations for density matrix elements are

$$\frac{\partial \rho_{p,q}^{m,n}}{\partial t} = U + D + C; \tag{4.29}$$

where

$$\begin{aligned}
U =& -i[(m\omega_1 + m(m-1)\chi_1)\rho_{p,q}^{m,n} + (n\omega_2 + n(n-1)\chi_2)\rho_{p,q}^{m,n} \\
&+ J\sqrt{m(1+k(m-1))}\sqrt{(n+1)(1+kn)}\rho_{p,q}^{m-1,n+1} \\
&+ J\sqrt{n(1+k(n-1))}\sqrt{(m+1)(1+km)}\rho_{p,q}^{m+1,n-1} \\
&- (p\omega_1 + p(p-1)\chi_1)\rho_{p,q}^{m,n} - (q\omega_2 + q(q-1)\chi_2)\rho_{p,q}^{m,n} \\
&+ J\sqrt{p(1+k(p-1))}\sqrt{(q+1)(1+kq)}\rho_{p-1,q+1}^{m,n} \\
&+ J\sqrt{q(1+k(q-1))}\sqrt{(p+1)(1+kp)}\rho_{p+1,q-1}^{m,n}], \\
D =& \frac{\gamma_{11}}{2}[2\sqrt{(m+1)(p+1)}\rho_{p+1,q}^{m+1,n} - (m+p)\rho_{p,q}^{m,n}] \\
&+ \frac{\gamma_{22}}{2}[2\sqrt{(n+1)(q+1)}\rho_{p,q+1}^{m,n+1} - (n+q)\rho_{p,q}^{m,n}], \\
C =& \frac{\gamma_{12}}{2}[2\sqrt{(n+1)(p+1)}\rho_{p+1,q}^{m,n+1} - \sqrt{m(n+1)}\rho_{p,q}^{m-1,n+1} - \sqrt{q(p+1)}\rho_{p+1,q-1}^{m,n}] \\
&+ \frac{\gamma_{21}}{2}[2\sqrt{(m+1)(q+1)}\rho_{p,q+1}^{m+1,n} - \sqrt{n(m+1)}\rho_{p,q}^{m+1,n-1} - \sqrt{p(q+1)}\rho_{p-1,q+1}^{m,n}],
\end{aligned}$$

where $\rho_{i,j}^{g,h} = \langle g,h|\,\rho\,|i,j\rangle$. Here $m+n \leq 2$ and $p+q \leq 2$. Here U, D and C correspond to unitary, damping and cross damping parts.

The evolution equations for localization probabilities $\rho_{44} = \langle 20|\,\rho\,|20\rangle$ and $\rho_{66} = \langle 02|\,\rho\,|02\rangle$ are

$$\dot{\rho}_{44} = -i[\sqrt{2(1+k)}J(\rho_{54} - \rho_{45})] - 2\gamma_{11}\rho_{44} - \frac{\gamma_{12}}{\sqrt{2}}\rho_{54} - \frac{\gamma_{21}}{\sqrt{2}}\rho_{45}, \tag{4.30}$$

$$\dot{\rho}_{66} = -i[\sqrt{2(1+k)}J(\rho_{56} - \rho_{65})] - 2\gamma_{22}\rho_{66} - \frac{\gamma_{12}}{\sqrt{2}}\rho_{65} - \frac{\gamma_{21}}{\sqrt{2}}\rho_{56}. \tag{4.31}$$

The evolution of matrix elements ρ_{44} and ρ_{66} depend on the off diagonal elements. Evolution of these off diagonal elements depend on frequencies (ω_1, ω_2) and nonlinear strengths (χ_1, χ_2). Therefore, evolution of ρ_{44} and ρ_{66} are also dependent on these parameters.

Temporal evolution of TPL probability in the presence of dissipation for the initial state $|+\rangle$ is shown in Fig. 4.5. Linear $(\chi_1 = \chi_2 = 0)$ and nonlinear $(\chi_1 = \chi_2 = 0.1)$ cases are considered. Due to interference between the various transitions shown in Fig. 4.2, the probability of localization does not completely vanish in the absence of nonlinearity. Including nonlinearity $(\chi \neq 0)$ leads to complete decay of the state $|+\rangle$. Therefore, localization probability reduces in time. Essentially, nonlinearity reduces the transition amplitudes from $|20\rangle$ and $|02\rangle$ to $|11\rangle$. As a result perfect interference does not occur.

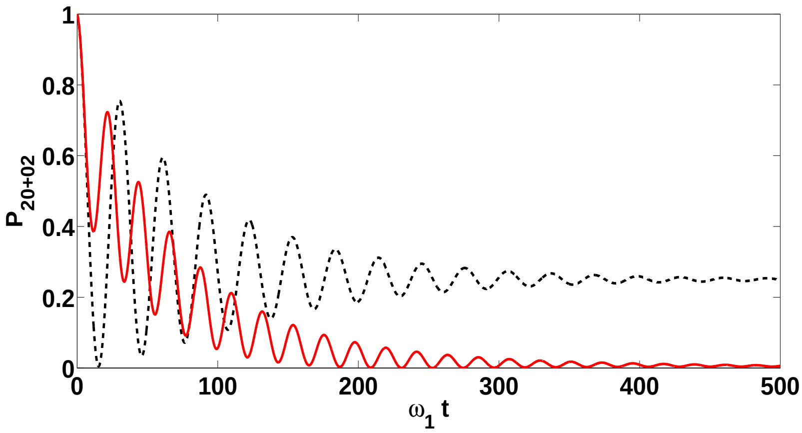

Figure 4.5 – Probability of localization $P_{|20\rangle+|02\rangle} = \rho_{44} + \rho_{66}$ is shown as a function of $\omega_1 t$ for the initial state $|+\rangle$. Values used are $J/\omega_1 = 0.05$,$\gamma/\omega_1 = 0.005$, $k = 0.05$ and $\Delta/\omega_1 = 0$. Here $\gamma = \gamma_{11} = \gamma_{22} = \gamma_{12} = \gamma_{21}$. Dashed curve corresponds to the linear case $\chi_1/\omega_1 = \chi_2/\omega_1 = 0$ and the continuous line for nonlinear case with $\chi_1/\omega_1 = \chi_2/\omega_1 = 0.1$.

The above features differ if the initial state is $|-\rangle$. The localization probability decays as $\sim e^{-2\gamma t}$, independent of χ, which provides the best fit for the numerical result. This decay pattern is shown in Fig. 4.6 for two different χ values. The curves corresponding to different χ values overlap, leading to the conclusion that the decay rate is independent of χ. As the state $|-\rangle$ is an eigenstate of $\hat{H}$ given in Eqn. 4.1, the transition from $|-\rangle$ to $|11\rangle$ is forbidden and interference does not occur between the various transition paths. This leads to the complete decay of the localized state $|-\rangle$.

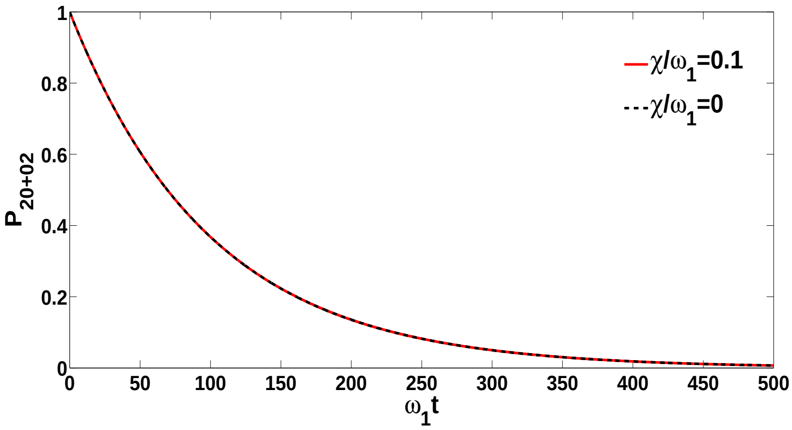

Figure 4.6 – Probability of localization $P_{|20\rangle+|02\rangle} = \rho_{44} + \rho_{66}$ is shown as a function of $\omega_1 t$ for the initial state $|-\rangle$. Here $J/\omega_1 = 0.05$,$\gamma/\omega_1 = 0.005$, $k = 0.05$ and $\Delta/\omega_1 = 0$. Here $\gamma = \gamma_{11} = \gamma_{22} = \gamma_{12} = \gamma_{21}$. Dashed curve corresponds to the linear case $\chi/\omega_1 = 0$ and the continuous line for nonlinear case with $\chi/\omega_1 = 0.1$.

Another consequence of interaction between a system and environment is the decoherence. Dephasing results in the decay of off-diagonal elements of the density operator. Essentially, dephasing affects the amplitudes of various transitions. As seen earlier, nonlinearity modifies the strength of TPL and TPD transition. It is of interest to understand the combined effect of dephasing and nonlinearity on delocalization.

Evolution equations for the density matrix elements can be obtained by using master equation

$$\frac{\partial \rho}{\partial t} = -i[\hat{H}, \rho] + \frac{\gamma_d}{2}\mathcal{D}[\hat{a}_1^\dagger \hat{a}_1]\rho + \frac{\gamma_d}{2}\mathcal{D}[\hat{a}_2^\dagger \hat{a}_2]\rho, \tag{4.32}$$

where $\mathcal{D}[\hat{o}]\rho = 2\hat{o}\rho\hat{o}^\dagger - \hat{o}^\dagger\hat{o}\rho - \rho\hat{o}^\dagger\hat{o}$.

Evolution equation for density matrix elements is

$$\frac{d}{dt}\begin{bmatrix}\rho_{44}\\ \rho_{45}\\ \rho_{46}\\ \rho_{54}\\ \rho_{55}\\ \rho_{56}\\ \rho_{64}\\ \rho_{65}\\ \rho_{66}\end{bmatrix} = \begin{bmatrix} 0 & B & 0 & -B & 0 & 0 & 0 & 0 & 0\\ B & A & B & 0 & -B & 0 & 0 & 0 & 0\\ 0 & B & C & 0 & 0 & -B & 0 & 0 & 0\\ -B & 0 & 0 & A^* & B & 0 & -B & 0 & 0\\ 0 & -B & 0 & B & 0 & B & 0 & -B & 0\\ 0 & 0 & -B & 0 & B & D & 0 & 0 & -B\\ 0 & 0 & 0 & -B & 0 & 0 & C^* & B & 0\\ 0 & 0 & 0 & 0 & -B & 0 & B & D^* & B\\ 0 & 0 & 0 & 0 & 0 & -B & 0 & B & 0 \end{bmatrix}\begin{bmatrix}\rho_{44}\\ \rho_{45}\\ \rho_{46}\\ \rho_{54}\\ \rho_{55}\\ \rho_{56}\\ \rho_{64}\\ \rho_{65}\\ \rho_{66}\end{bmatrix}, \quad (4.33)$$

where $A = -i(\Delta + 2\chi_1)) - \gamma_d$, $B = iJ\sqrt{2(1+k)}$, $C = -2i(\Delta + \chi_1 - \chi_2) - 4\gamma_d$, $D = -i(\Delta - 2\chi_2) - \gamma_d$.

The probability of TPD ρ_{55} for different values $\chi(=\chi_1 = \chi_2)$ are shown in Fig. 4.7. Comparing the results corresponding to different values of χ, it is clear that the rate of attaining the steady state density matrix is slow in the presence of Kerr nonlinearity.

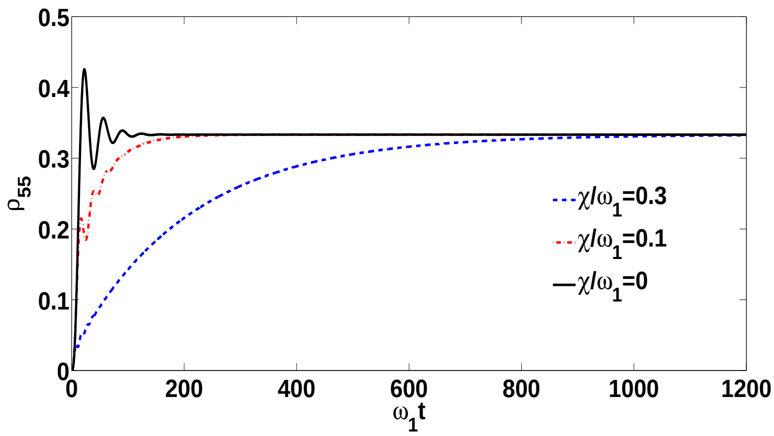

Figure 4.7 – Delocalization probability as a function of $\omega_1 t$ for $|-\rangle$ for various χ. Continuous line is for ($\chi/\omega_1 = 0$,$k = 0$), dot-dashed line is for ($\chi/\omega_1 = 0.1, k = 0.1$) and dashed line is for ($\chi/\omega_1 = 0.3, k = 0.3$) with $J/\omega_1 = 0.05$, $\Delta/\omega_1 = 0$ and $\gamma_d/\omega_1 = 0.05$. Non-linearity slows down the process of attaining steady state density operator.

The first and last rows of the matrix given in Eqn. 4.33 have two non-zero entries. This makes $\rho_{45} = \rho_{54}$ and $\rho_{56} = \rho_{65}$ respectively in the steady state. The remaining steady state equations are

$$[-i(\Delta + 2\chi_1) - \gamma_d]\rho_{45} - iJ\sqrt{2(1+k)}(\rho_{55} - \rho_{44} - \rho_{46}) = 0, \tag{4.34}$$

$$[-2i(\Delta + \chi_1 - \chi_2) - 4\gamma_d]\rho_{46} - iJ\sqrt{2(1+k)}(\rho_{56} - \rho_{45}) = 0, \tag{4.35}$$

$$[i(\Delta + 2\chi_1) - \gamma_d]\rho_{45} + iJ\sqrt{2(1+k)}(\rho_{55} - \rho_{44} - \rho_{64}) = 0, \tag{4.36}$$

$$[-i(\Delta - 2\chi_2) - \gamma_d]\rho_{56} - iJ\sqrt{2(1+k)}(\rho_{46} + \rho_{66} - \rho_{55}) = 0, \tag{4.37}$$

$$[2i(\Delta + \chi_1 - \chi_2) - 4\gamma_d]\rho_{64} + iJ\sqrt{2(1+k)}(\rho_{56} - \rho_{45}) = 0, \tag{4.38}$$

$$[i(\Delta - 2\chi_2) - \gamma_d]\rho_{56} + iJ\sqrt{2(1+k)}(\rho_{64} + \rho_{66} - \rho_{55}) = 0. \tag{4.39}$$

Using the Cramer's rule for solving the above of linear equations, with the constraint $\rho_{44} + \rho_{55} + \rho_{66} = 1$, the steady state solutions are

$$\rho_{44} = \frac{1}{3}, \rho_{45} = 0, \rho_{46} = 0, \rho_{55} = \frac{1}{3}, \rho_{56} = 0, \rho_{64} = 0, \rho_{66} = \frac{1}{3}, \tag{4.40}$$

which are indeed independent of nonlinear strengths.

4.5 Array of nonlinearly coupled cavities

In this section, localization and delocalization of two photons in an array of Kerr cavities is considered. All the cavities are in resonant. The Hamiltonian given in Eqn.

4.1 can be generalized to an array of N cavities. The Hamiltonian is

$$\hat{H} = \sum_{j=1}^{N} \omega \hat{a}_j^\dagger \hat{a}_j + \chi \hat{a}_j^{\dagger 2} \hat{a}_j^2$$
$$+ J \sum_{j=1}^{N-1} \left[\sqrt{1 + k\hat{a}_j^\dagger \hat{a}_j}\, \hat{a}_j \hat{a}_{j+1}^\dagger \sqrt{1 + k\hat{a}_{j+1}^\dagger \hat{a}_{j+1}} + \hat{a}_j^\dagger \sqrt{1 + k\hat{a}_j^\dagger \hat{a}_j} \sqrt{1 + k\hat{a}_{j+1}^\dagger \hat{a}_{j+1}}\, \hat{a}_{j+1} \right]. \tag{4.41}$$

Here $\hat{a}_j$ and $\hat{a}_j^\dagger$ are the annihilation and creation operators for the jth cavity. The photon hopping strength between two adjacent cavities is J. All the cavities are having equal Kerr strengths χ. In order to investigate the role of nonlinearity, consider states of the form $|\psi\rangle = \cos\theta\, |2\rangle_r |0\rangle_s + e^{i\phi} \sin\theta\, |0\rangle_r |2\rangle_s$. The notation $|p\rangle_r |q\rangle_s$ stands for p photons in the r-th cavity and q photons in the s-th cavity. Other cavities are in their respective vacuua. Here r and s vary from 1 to N.

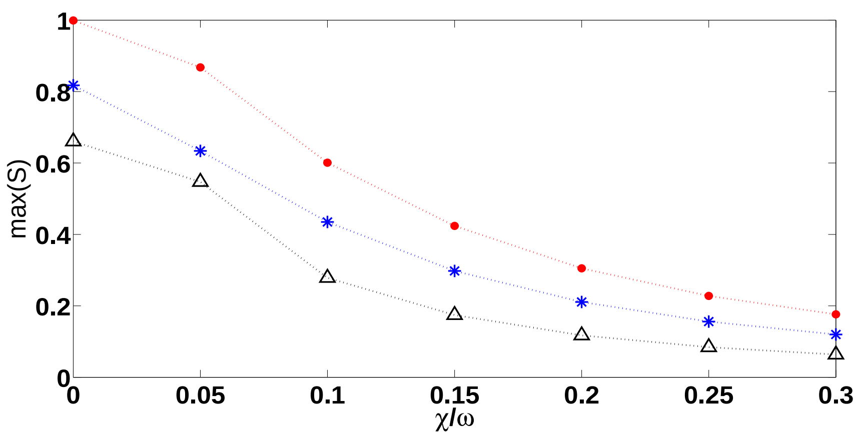

Figure 4.8 – Maximum achievable value of S during time evolution as a function of nonlinear strength χ/ω for the initial states $|+\rangle$(circle), $|20\rangle$(star) and $|-\rangle$(triangle). Here $J/\omega = 0.05$, $k = \chi/\omega$, $N = 6$, $r = N/2$ and $s = r + 1$.

The maximum achievable value of the degree of TPD (S), defined in Eqn. 3.53, is shown as a function of the nonlinear strength χ in Fig. 4.8 for an array of six cavities. It is seen that delocalization probability decreases if the strength of nonlinearity increases. This comes from the fact that nonlinearity localizes the energy (photons), so that $|20\rangle$, $|02\rangle$ and their superpositions are more probable. If the initial state is $|-\rangle$, the evolved state is more localized compared to the state evolving from $|+\rangle$. Hence, degree of delocalization S depends on the relative phase present in the initial state in the nonlinear case too.

4.6 Summary

In this chapter, dynamics of localization and delocalization due to intensity-dependent coupling of two Kerr cavities has been studied. As in the linear case localization and delocalization probabilities depend on the entanglement and relative phase present in the initial state.

Due to nonlinearity, the energy levels of the cavities are anharmonic (unequally spaced) and the average energies of the localized and delocalized states are different. As a consequence, transition from localized state to delocalized state is blocked if the cavities are resonant. For transition to occur from a localized product state to a delocalized state, the average energies in these states are to be nearly equal which is achieved by adjusting the strength of nonlinearity and detuning. If the initial state is the delocalized state $|11\rangle$ then transition to localized states can be forbidden, analogous to photon blockade, by suitably choosing the nonlinear strength.

The entangled state $(|20\rangle + |02\rangle)/\sqrt{2}$ does not achieve complete delocalization in the presence of nonlinearity. The state $(|20\rangle - |02\rangle)/\sqrt{2}$ remains localized independent of the strength of nonlinearity. Essentially, the average energies of the localized entangled states and delocalized state are not equal for any value of detuning in the presence of nonlinearity.

Chapter 5

Atomic switch for control of heat transfer in coupled cavities

Dynamics of an isolated system is unitary and the total energy of the system is constant. In practical situations, interaction of system with environment is unavoidable. Simplest of this situation corresponds to coupling the system to a reservoir at absolute zero temperature. This implies that the reservoir cannot transfer energy to the system while the system can transfer to the environment. As a consequence, the system suffers an irreversible dissipation. The dissipative dynamics studies presented in the previous chapters are based on the interaction of the cavities in the array and reservoirs at zero temperature. However, if coupled to reservoirs at non-zero absolute temperatures, cavities can exchange energy with the reservoirs. In this context, a linear array of cavities whose ends are connected to two reservoirs is considered. This array forms a conduit for energy transport between the two reservoirs [174–177]. For a conventional bulk material, steady state heat transport is governed by

$$\mathbf{J} = -\kappa \nabla T, \tag{5.1}$$

which is the Fourier's law of heat conduction. Here $\mathbf{J}$ is the thermal current density and ∇T is the temperature gradient. The proportionality constant κ is the thermal conductivity which is positive for bulk matter. This law is valid if the system is close to its equilibrium, in which case linear response theory is applicable [178–182].

A system away from equilibrium may violate the Fourier's empirical law [179, 180]. There is no universal theory of heat transfer applicable to all nonequilibrium systems. A chain of coupled oscillators is known to violate the Fourier's law of heat conduction in the sense that the thermal current is independent of system size and the heat transport is ballistic [176, 179, 183]. Diffusive transport can be recovered by including anharmonicity and dephasing [114, 176, 184, 185]. Another interesting phenomenon is thermal rectification which is essential for realizing thermal diodes and transistors [186, 187]. A system shows thermal rectification if it possesses structural asymmetry for allowing higher thermal current in one direction. Thermal rectifiers based on nanotubes [188], quantum spin chains [189–191], anharmonic oscillators [192], two-level systems [193], etc. have been proposed in the literature.

In this chapter, heat transfer in a system of two coupled cavities containing a single atom is discussed. The system-reservoir interaction is assumed to be of Lindblad type [70]. Both magnitude and direction of current are shown to be controllable by suitably choosing the atomic state and the system-reservoir coupling parameters. The system exhibits large thermal rectification for proper choices of the cavity-reservoir and cavity-atom couplings.

The present chapter is organized as follows. In Section. 5.1, details of the system and its theoretical model are discussed to arrive at an expression for heat current. Also, various special cases of importance are indicated. Based on the dependence of the current on the reservoirs' temperatures and coupling parameters, violation of second law of thermodynamics is established in Section. 5.2. Thermal rectification in the system is explored in Section. 5.3. Generalization to N cavities is discussed in

Section. 5.4. Results are summarized in Section. 5.5.

5.1 System and its model

Consider a system of two linearly coupled cavities (right and left, for brevity) and a two-level atom in one of the cavities. The resonance frequencies of the cavities are ω_L and ω_R respectively. The cavity coupling strength is J. The right cavity interacts dispersively with the two-level atom embedded in it. The coupling strength between the atom and the cavity field is g. The atomic transition frequency is ω_0. In the dispersive limit, *i.e.*, $\Delta = (\omega_0 - \omega_R) >> g$, the Hamiltonian is [83, 194]

$$\hat{H} = \frac{\omega_0}{2}\hat{\sigma}_z + \omega_L \hat{a}_L^\dagger \hat{a}_L + \omega_R \hat{a}_R^\dagger \hat{a}_R + \chi(\hat{\sigma}_+\hat{\sigma}_- + \hat{a}_R^\dagger \hat{a}_R \hat{\sigma}_z) + J(\hat{a}_L^\dagger \hat{a}_R + \hat{a}_L \hat{a}_R^\dagger), \tag{5.2}$$

where $\chi = g^2/\Delta$ is assumed to be positive. Here $\hbar = 1$. The states $|e\rangle$ and $|g\rangle$ are respectively the excited and ground states of the two-level atom. The operators $\hat{\sigma}_+ = |e\rangle\langle g|$ and $\hat{\sigma}_- = |g\rangle\langle e|$ are the raising and lowering operators for the atom. The energy operator for the atom is $\hat{\sigma}_z = |e\rangle\langle e| - |g\rangle\langle g|$. The Hamiltonian $\hat{H}$ conserves the respective total excitation numbers for the cavity fields and the atom, *i.e.*, $[\hat{a}_L^\dagger \hat{a}_L + \hat{a}_R^\dagger \hat{a}_R, \hat{H}] = 0$ and $[\hat{\sigma}_z, \hat{H}] = 0$. As a consequence, the atom and the field cannot exchange energy in the dispersive limit [194], they independently conserve their respective number of quanta.

The system is coupled to two reservoirs, each modeled as a collection of independent oscillators [68]. The reservoir Hamiltonian is taken to be

$$\hat{H}_x = \sum_j \omega_{xj} \hat{b}_{xj}^\dagger \hat{b}_{xj}, \tag{5.3}$$

where $x = L, R$ is the index referring to the left reservoir and the right reservoir respectively. The creation and annihilation operators of the reservoirs obey the bosonic commutation relation $[\hat{b}_{xj}, \hat{b}^\dagger_{yk}] = \delta_{jk}\delta_{xy}$. The arrangement of the cavities and reservoirs is shown in Fig. 5.1. The interaction Hamiltonian for the cavity-reservoir component is

$$\hat{H}_I = \left(\sum_j g_{Lj}(\hat{a}^\dagger_L + \hat{a}_L)(\hat{b}_{Lj} + \hat{b}^\dagger_{Lj}) + \sum_j g_{Rj}(\hat{a}^\dagger_R + \hat{a}_R)(\hat{b}_{Rj} + \hat{b}^\dagger_{Rj}) \right), \tag{5.4}$$

where $g_{Lj}(g_{Rj})$ is the coupling strength of the left (right) cavity to jth mode of the left (right) reservoir.

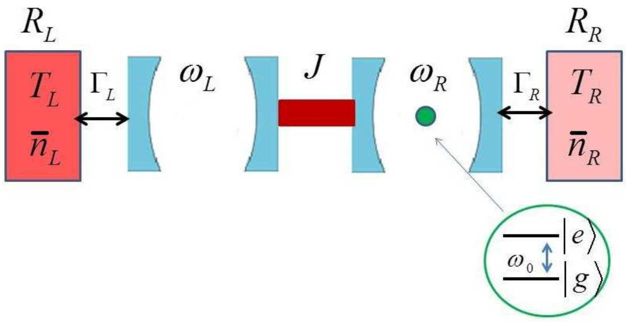

Figure 5.1 – Schematic representation of system of coupled cavities with a two-level atom embedded in the right cavity. The cavities are also coupled with their respective reservoirs.

Under the Born-Markov and rotating wave approximations [68], the reduced joint density matrix for the two cavities (traced over the reservoirs) obeys

$$\frac{\partial \rho}{\partial t} = -i[\hat{H}, \rho] + \mathcal{D}_L(\rho) + \mathcal{D}_R(\rho), \tag{5.5}$$

where the Lindblad operators are defined as

$$\mathcal{D}_x(\rho) = \frac{\Gamma_x(\bar{n}_x + 1)}{2}(2\hat{a}_x\rho\hat{a}^\dagger_x - \hat{a}^\dagger_x\hat{a}_x\rho - \rho\hat{a}^\dagger_x\hat{a}_x) + \frac{\Gamma_x\bar{n}_x}{2}(2\hat{a}^\dagger_x\rho\hat{a}_x - \hat{a}_x\hat{a}^\dagger_x\rho - \rho\hat{a}_x\hat{a}^\dagger_x), \tag{5.6}$$

for $x = L, R$. The parameters Γ_L and Γ_R are related to the coupling strengths as [72]

$$\Gamma_x = 2\pi \sum_j g_{xj}^2 \delta(\omega_{xj} - \omega_x). \tag{5.7}$$

The two terms in Eqn. 5.6 correspond to energy flow from the system to the reservoir and vice-versa respectively. The dynamics generated by the master equation satisfies the detailed balance condition and gives the correct steady state if the different components of the system are weakly coupled [195–198]. The reservoirs R_L and R_R are assumed to be in thermal equilibrium at temperatures T_L and T_R respectively. The density operators of the reservoirs are

$$\varrho_x = \frac{e^{-\hat{H}_x/k_B T_x}}{\mathrm{Tr}\left(e^{-\hat{H}_x/k_B T_x}\right)}, \tag{5.8}$$

with mean photon numbers $\bar{n}_x = 1/[\exp(\omega_x/k_B T_x) - 1]$, where $x = L, R$. The dynamics of the system can be understood from the temporal evolution of expectation values of suitable operators. The expectation values satisfy

$$\tfrac{d}{dt}\langle \hat{a}_L^\dagger \hat{a}_L \rangle = iJ(\langle \hat{a}_L \hat{a}_R^\dagger \rangle - \langle \hat{a}_L^\dagger \hat{a}_R \rangle) - \Gamma_L \langle \hat{a}_L^\dagger \hat{a}_L \rangle + \Gamma_L \bar{n}_L, \tag{5.9a}$$

$$\tfrac{d}{dt}\langle \hat{a}_R^\dagger \hat{a}_R \rangle = -iJ(\langle \hat{a}_L \hat{a}_R^\dagger \rangle - \langle \hat{a}_L^\dagger \hat{a}_R \rangle) - \Gamma_R \langle \hat{a}_R^\dagger \hat{a}_R \rangle + \Gamma_R \bar{n}_R, \tag{5.9b}$$

$$\tfrac{d}{dt}\langle \hat{a}_L^\dagger \hat{a}_R \rangle = i\Delta_c \langle \hat{a}_L^\dagger \hat{a}_R \rangle - iJ(\langle \hat{a}_L^\dagger \hat{a}_L \rangle - \langle \hat{a}_R^\dagger \hat{a}_R \rangle) - i\chi \langle \hat{a}_L^\dagger \hat{a}_R \hat{\sigma}_z \rangle - \gamma \langle \hat{a}_L^\dagger \hat{a}_R \rangle, \tag{5.9c}$$

$$\tfrac{d}{dt}\langle \hat{a}_L \hat{a}_R^\dagger \rangle = -i\Delta_c \langle \hat{a}_L \hat{a}_R^\dagger \rangle + iJ(\langle \hat{a}_L^\dagger \hat{a}_L \rangle - \langle \hat{a}_R^\dagger \hat{a}_R \rangle) + i\chi \langle \hat{a}_L \hat{a}_R^\dagger \hat{\sigma}_z \rangle - \gamma \langle \hat{a}_L \hat{a}_R^\dagger \rangle, \tag{5.9d}$$

$$\tfrac{d}{dt}\langle \hat{a}_L^\dagger \hat{a}_L \hat{\sigma}_z \rangle = iJ(\langle \hat{a}_L \hat{a}_R^\dagger \hat{\sigma}_z \rangle - \langle \hat{a}_L^\dagger \hat{a}_R \hat{\sigma}_z \rangle) - \Gamma_L \langle \hat{a}_L^\dagger \hat{a}_L \hat{\sigma}_z \rangle + \Gamma_L \bar{n}_L \langle \hat{\sigma}_z \rangle, \tag{5.9e}$$

$$\tfrac{d}{dt}\langle \hat{a}_R^\dagger \hat{a}_R \hat{\sigma}_z \rangle = -iJ(\langle \hat{a}_L \hat{a}_R^\dagger \hat{\sigma}_z \rangle - \langle \hat{a}_L^\dagger \hat{a}_R \hat{\sigma}_z \rangle) - \Gamma_R \langle \hat{a}_R^\dagger \hat{a}_R \hat{\sigma}_z \rangle + \Gamma_R \bar{n}_R \langle \hat{\sigma}_z \rangle, \tag{5.9f}$$

$$\begin{aligned}\tfrac{d}{dt}\langle \hat{a}_L^\dagger \hat{a}_R \sigma_z \rangle = {} & i\Delta_c \langle \hat{a}_L^\dagger \hat{a}_R \hat{\sigma}_z \rangle - iJ(\langle \hat{a}_L^\dagger \hat{a}_L \hat{\sigma}_z \rangle - \langle \hat{a}_R^\dagger \hat{a}_R \hat{\sigma}_z \rangle) \\ & - i\chi \langle \hat{a}_L^\dagger \hat{a}_R \rangle - \gamma \langle \hat{a}_L^\dagger \hat{a}_R \hat{\sigma}_z \rangle,\end{aligned} \tag{5.9g}$$

$$\begin{aligned}\tfrac{d}{dt}\langle \hat{a}_L \hat{a}_R^\dagger \hat{\sigma}_z \rangle = {} & -i\Delta_c \langle \hat{a}_L \hat{a}_R^\dagger \hat{\sigma}_z \rangle + iJ(\langle \hat{a}_L^\dagger \hat{a}_L \hat{\sigma}_z \rangle - \langle \hat{a}_R^\dagger \hat{a}_R \sigma_z \rangle) \\ & + i\chi \langle \hat{a}_L \hat{a}_R^\dagger \rangle - \gamma \langle \hat{a}_L \hat{a}_R^\dagger \hat{\sigma}_z \rangle,\end{aligned} \tag{5.9h}$$

where $\gamma = (\Gamma_L + \Gamma_R)/2$ and $\Delta_c = \omega_L - \omega_R$. Here $\langle \hat{A} \rangle = \mathrm{Tr}[\rho \hat{A}]$, where ρ satisfies the master equation given in Eqn. 5.5. The operators in Eqn. 5.9$(a-h)$ collectively represent the energies of the various components, coherences and interaction energies.

As $[\hat{\sigma}_z, \hat{H}] = [\hat{\sigma}_z, \mathcal{D}_L(\rho)] = [\hat{\sigma}_z, \mathcal{D}_R(\rho)] = 0$, the evolution equation for $\langle \hat{\sigma}_z \rangle$ is $d\langle \hat{\sigma}_z \rangle/dt = 0$. This indicates that the value of $\langle \hat{\sigma}_z \rangle$ remains constant during time evolution as a consequence of the fact that the atom is dispersively coupled with the cavity field.

Steady state current is defined *via* the continuity equation

$$\frac{d}{dt}\langle \hat{H} \rangle = 0, \tag{5.10}$$

which expresses the conservation of total energy of the system. With $\langle \hat{H} \rangle$ =Tr$[\rho \hat{H}]$ and using Eqn. 5.5 for evolving ρ, the continuity equation given in Eqn. 5.10 yields

$$0 = \mathrm{Tr}[\hat{H}\mathcal{D}_L(\rho) + \hat{H}\mathcal{D}_R(\rho)] =: I_L + I_R. \tag{5.11}$$

Here $I_x = \mathrm{Tr}[\hat{H}\mathcal{D}_x(\rho)],\ x = L, R$. Further, I_L refers to the thermal current from the left reservoir R_L to the system and I_R indicates the current from the right reservoir R_R to the system. Using Eqn. 5.5, the steady state heat current from the left reservoir to the right reservoir through the system is

$$I_L = \mathrm{Tr}[\hat{H}\mathcal{D}_L(\rho)] = \Gamma_L(I_{nd} - I_{coh}). \tag{5.12}$$

Here $I_{nd} = (\bar{n}_L - \langle \hat{a}_L^\dagger \hat{a}_L \rangle_{ss})\omega_L$ is the current due to the average excitation number difference between the left reservoir and the left cavity, $I_{coh} = \frac{1}{2}J(\langle \hat{a}_L^\dagger \hat{a}_R \rangle_{ss} + \langle \hat{a}_L \hat{a}_R^\dagger \rangle_{ss})$ is the current due to the total coherence in the system. The steady state expectation values are represented as $\langle \cdot \rangle_{ss}$. A similar expression for the steady state heat current from the right reservoir to the left reservoir is

$$I_R = \mathrm{Tr}[\hat{H}\mathcal{D}_R(\rho)] = \Gamma_R(\bar{n}_R - \langle \hat{a}_R^\dagger \hat{a}_R \rangle_{ss})(\omega_R + \langle \hat{\sigma}_z \rangle \chi) - \Gamma_R I_{coh}. \tag{5.13}$$

Steady state solutions obtained by equating the time derivatives in Eqns. 5.9$(a-h)$ to zero are

$$\langle \hat{a}_L^\dagger \hat{a}_L \rangle_{ss} = \tfrac{C(\Gamma_L \bar{n}_L + \Gamma_R \bar{n}_R) + \Gamma_L \Gamma_R \bar{n}_L}{C(\Gamma_L + \Gamma_R) + \Gamma_L \Gamma_R}, \tag{5.14a}$$

$$\langle \hat{a}_R^\dagger \hat{a}_R \rangle_{ss} = \tfrac{C(\Gamma_L \bar{n}_L + \Gamma_R \bar{n}_R) + \Gamma_L \Gamma_R \bar{n}_R}{C(\Gamma_L + \Gamma_R) + \Gamma_L \Gamma_R}, \tag{5.14b}$$

$$\delta N = \langle \hat{a}_L^\dagger \hat{a}_L \rangle_{ss} - \langle \hat{a}_R^\dagger \hat{a}_R \rangle_{ss} = \tfrac{\Gamma_L \Gamma_R (\bar{n}_L - \bar{n}_R)}{C(\Gamma_L + \Gamma_R) + \Gamma_L \Gamma_R}, \tag{5.14c}$$

$$\langle \hat{a}_L^\dagger \hat{a}_R \rangle_{ss} = -J \tfrac{\chi \langle \hat{\sigma}_z \rangle + \Delta_c + i\gamma}{\chi^2 - \Delta_c^2 + \gamma^2 - 2i\gamma\Delta_c} \delta N, \tag{5.14d}$$

with

$$C = 2J^2 \gamma \frac{\Delta_c^2 + \chi^2 + 2\Delta_c \chi \langle \hat{\sigma}_z \rangle + \gamma^2}{(\chi^2 - \Delta_c^2 + \gamma^2)^2 + 4\gamma^2 \Delta_c^2}.$$

Using these steady state solutions in Eqn. 5.12 yields

$$I_L = J^2 \delta N \frac{\begin{array}{r}\Gamma_L \chi \langle \hat{\sigma}_z \rangle (\chi^2 - \Delta_c^2 + \gamma^2) + (\omega_L \Gamma_R + \omega_R \Gamma_L)(\Delta_c^2 + \gamma^2) \\ + \chi^2 (2\omega_L \gamma + \Delta_c \Gamma_L) + 4\Delta_c \chi \langle \hat{\sigma}_z \rangle \omega_L \gamma\end{array}}{(\chi^2 - \Delta_c^2 + \gamma^2)^2 + 4\gamma^2 \Delta_c^2}. \tag{5.15}$$

In the absence of inter-cavity coupling ($J = 0$), the cavities equilibrate with their respective reservoirs with mean photon numbers $\bar{n}_L$ and $\bar{n}_R$. The currents I_L and I_R vanish since energy cannot flow from one cavity to another as $J = 0$. If the coupling is non-zero and the reservoirs are at different temperatures, energy flows from one reservoir to the other through the cavities.

Interestingly, expression in Eqn. 5.15 shows that the current through the system explicitly depends on $\langle\hat{\sigma}_z\rangle$ which, in turn, depends on the state of the atom. This dependency arises as the atom modifies the cavity resonance frequency as well as the coherences $\langle\hat{a}_L^\dagger\hat{a}_R\rangle_{ss}$ and $\langle\hat{a}_L\hat{a}_R^\dagger\rangle_{ss}$. By proper choice of the atomic state, $\langle\hat{\sigma}_z\rangle$ can be tuned from $+1$ corresponding to the atom in its excited state to -1 if the atom is in its ground state. This feature can be used to control the energy flow (current) between the reservoirs.

Consider the cavities to be coupled ($J \neq 0$) and resonant, *i.e.*, $\omega_L = \omega_R = \omega$, so that $\Delta_c = 0$. In the absence of the atom, the total coherence $\langle\hat{a}_L^\dagger\hat{a}_R\rangle_{ss} + \langle\hat{a}_L\hat{a}_R^\dagger\rangle_{ss}$ given in Eqn. 5.14d vanishes under steady state condition. The current through the cavities is

$$I_L = \frac{4\omega J^2\Gamma_L\Gamma_R}{(4J^2+\Gamma_L\Gamma_R)(\Gamma_L+\Gamma_R)}(\bar{n}_L - \bar{n}_R), \tag{5.16}$$

which is proportional to the difference in the mean photon numbers. Equivalently, current is proportional to the temperature difference between the two reservoirs for a fixed system size, which is like the Fourier's law.

If the temperatures of the two reservoirs are equal ($\bar{n}_L = \bar{n}_R = \bar{n}$), the system equilibrates with the reservoirs and no current flows through the system. The mean number of photons in the cavities are $\langle\hat{a}_L^\dagger\hat{a}_L\rangle_{ss} = \langle\hat{a}_R^\dagger\hat{a}_R\rangle_{ss} = \bar{n}$. Also, the states of the cavity fields satisfy the zero coherence condition, namely, $\langle\hat{a}_L^\dagger\hat{a}_R\rangle_{ss} = \langle\hat{a}_R^\dagger\hat{a}_L\rangle_{ss} = 0$. To know the states of the fields in the cavities, the fidelity $F(\rho_{th}, \rho_x)$,

$$F(\rho_{th}, \rho_x) = \mathrm{Tr}\left(\sqrt{\sqrt{\rho_{th}}\rho_x\sqrt{\rho_{th}}}\right), \tag{5.17}$$

between the thermal field and the cavity field is calculated. Here

$$\rho_{th} = \frac{1}{1+\bar{n}}\sum_{n=0}^{\infty}\left(\frac{\bar{n}}{1+\bar{n}}\right)^{n}|n\rangle\langle n|, \tag{5.18}$$

is the single mode Gibbs thermal state; $\rho_x(x = L, R)$ are the steady state reduced density matrices for the left- and right-cavities respectively. The steady state fidelity $F(\rho_{th}, \rho_x)$ is numerically calculated to be unity. Therefore, the respective states of the cavity fields are Gibbs thermal states. The zero-time delay second order correlation function

$$g_x^{(2)}(0) = \frac{\mathrm{Tr}(\rho_x \hat{a}_x^{\dagger 2}\hat{a}_x^2)}{\left[\mathrm{Tr}(\rho_x \hat{a}_x^{\dagger}\hat{a}_x)\right]^2}, \tag{5.19}$$

in the steady state ρ_x is numerically estimated to be 2, same as that of the thermal state. This confirms that the cavity states are indeed the thermal states ρ_{th}.

If the reservoirs are at different temperatures, the high temperature reservoir is the source of energy to the system and the low temperature reservoir is the sink for the energy to establish a steady state. As a consequence, heat continuously flows from the high temperature reservoir to the low temperature reservoir. The system reaches a non-equilibrium steady state with effective mean photon numbers $\langle\hat{a}_L^{\dagger}\hat{a}_L\rangle_{ss}$ and $\langle\hat{a}_R^{\dagger}\hat{a}_R\rangle_{ss}$ in the left- and right- cavities respectively. Analytical expressions for these mean photon numbers are given in Eqn. 5.14a and Eqn. 5.14b.

In the presence of an atom in one of the cavities as shown in Fig. 5.1, the expression for current obtained from Eqn. 5.15 is

$$I_L = \frac{\Gamma_L \Gamma_R}{\bar{c}(\Gamma_L + \Gamma_R) + \Gamma_L \Gamma_R} \frac{\bar{c}}{\gamma} \left(\gamma\omega + \frac{\Gamma_L}{2} \chi \langle \hat{\sigma}_z \rangle \right) (\bar{n}_L - \bar{n}_R), \tag{5.20}$$

where $\bar{c} = 2J^2\gamma/(\chi^2 + \gamma^2)$.

For $\Gamma_L = \Gamma_R = \Gamma$ and finite J, an alternate expression for the current is

$$\begin{aligned} I_L &= \frac{(I_L - I_R)}{2}, \\ &= \frac{\Gamma}{2} \left[(\bar{n}_L - \langle \hat{a}_L^\dagger \hat{a}_L \rangle_{ss})\omega - (\bar{n}_R - \langle \hat{a}_R^\dagger \hat{a}_R \rangle_{ss})(\omega + \langle \hat{\sigma}_z \rangle \chi) \right]. \end{aligned} \tag{5.21}$$

On substituting the steady state values from Eqns. 5.14a and 5.14b,

$$I_L = 2J^2 \frac{\Gamma}{4J^2 + \chi^2 + \Gamma^2} \left(\omega + \frac{\chi}{2} \langle \hat{\sigma}_z \rangle \right) (\bar{n}_L - \bar{n}_R). \tag{5.22}$$

Scaled current I_L/ω^2 as a function of Γ/ω is shown in Fig. 5.2. Maximum current flows through the system if $\Gamma = \sqrt{4J^2 + \chi^2}$. This special value $\sqrt{4J^2 + \chi^2}$ corresponds to the Rabi frequency of the oscillation of the mean number of photons when the cavity detuning is χ and the cavities are not coupled to the reservoirs. The detuning between the cavity frequencies arises due to the atom in one of the cavities. The competition between the cavity-reservoir energy exchange rate Γ and the cavity-cavity energy exchange rate $\sqrt{4J^2 + \chi^2}$ affects the current through the system. If the two rates are equal, then

$$I_L = \frac{J^2}{\sqrt{4J^2 + \chi^2}} \left(\omega + \frac{\chi}{2} \langle \hat{\sigma}_z \rangle \right) (\bar{n}_L - \bar{n}_R), \tag{5.23}$$

which is the maximum current. If $\Gamma >> \sqrt{4J^2 + \chi^2}$, the cavities and their respective reservoirs exchange energy faster than the inter-cavity exchange. In the opposite limit, the cavities exchange energy with each other faster than with their respective reservoirs. This mismatch between the energy exchange rates reduces the current. From Eqn. 5.22, it is seen that for small Γ, $I_L \propto \Gamma$ and for large Γ, $I_L \propto \Gamma^{-1}$.

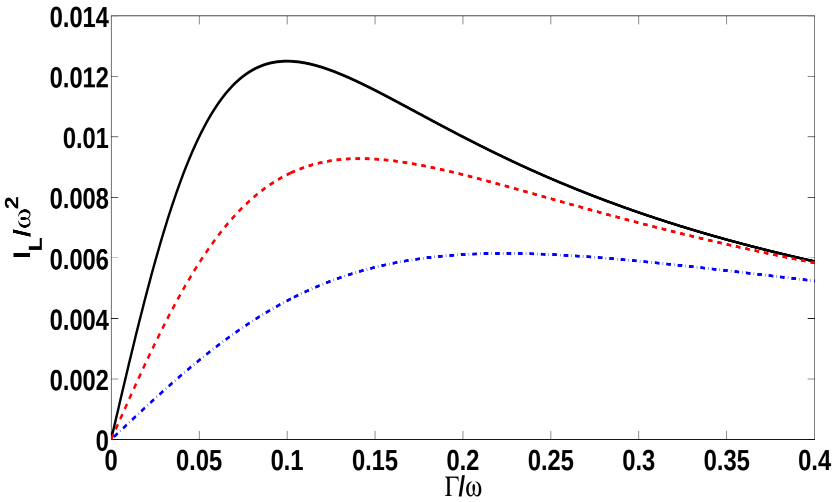

Figure 5.2 – Current I_L/ω^2 shown as a function of reservoir coupling strength Γ/ω for different atom-cavity coupling strengths $\chi/\omega = 0$ (continuous), 0.1 (dashed) and 0.2 (dot-dashed). The system-reservoir parameters are $J/\omega = 0.05, \bar{n}_L - \bar{n}_R = 0.5$ and $\langle\hat{\sigma}_z\rangle = 1$.

5.2 Switching action of atom

According to the Fourier's law given in Eqn. 5.1, current density is proportional to temperature gradient. Using the fact that $\delta N \propto (\bar{n}_L - \bar{n}_R)$ as given in Eqn. 5.14*c*, the expression for I_L in Eqn. 5.15 is written in the form

$$I_L = \tilde{\kappa}(\bar{n}_L - \bar{n}_R), \tag{5.24}$$

for comparing with the Fourier's law. Here $\tilde{\kappa}$ is the effective thermal conductivity. It is to be noted that thermal conductivity can be tuned by choosing the atomic state. Two important cases corresponding to the atom being in the excited state and the ground state are considered, *i.e.*, $\langle\hat{\sigma}_z\rangle = \pm 1$. The corresponding currents are

$$I_L = J^2 \delta N \frac{\Omega}{(\chi^2 - \Delta_c^2 + \gamma^2)^2 + 4\gamma^2\Delta_c^2}((\Delta_c \pm \chi)^2 + \gamma^2). \tag{5.25}$$

where $\Omega = \omega_L\Gamma_R+\Gamma_L(\omega_R\pm\chi)$. For subsequent discussion, it is assumed that $\bar{n}_L > \bar{n}_R$, *i.e.*, $\delta N > 0$ without loss of generality. Under this assumption, I_L and Ω have the same sign. If the atom is in its ground state, sign of Ω is changeable by properly choosing the ratios Γ_R/Γ_L and $(\chi - \omega_R)/\omega_L$. Consequently, direction of current can also be changed. It is to be pointed out that $\omega_R - \chi$ is the resonance frequency of the right cavity modified by the atom. If the atom is in its excited state, *i.e.*, $\langle\hat{\sigma}_z\rangle = +1$, I_L is always positive, meaning that the thermal current flows from the high temperature reservoir to the low temperature reservoir (conventional flow) and reversal of current is not possible.

In order to exhibit the switching action by the atom, consider $\chi > \omega_R$. If the system-reservoir parameters satisfy

$$\frac{\Gamma_R}{\Gamma_L} > \frac{(\chi - \omega_R)}{\omega_L}, \tag{5.26}$$

to make $\Omega > 0$, then the thermal current flows from the high temperature reservoir to the low temperature reservoir, independent of the atomic state.

If the ratios are equal, *i.e.*,

$$\frac{\Gamma_R}{\Gamma_L} = \frac{(\chi - \omega_R)}{\omega_L}, \tag{5.27}$$

and the atom is in the ground state, so that $\Omega = 0$, then the thermal current vanishes even if the reservoirs are at different temperatures. The system completely blocks the heat flow like a thermal insulator. On driving the atom to its excited state, the system changes from a thermal insulator to a thermal conductor.

Table 5.1 – Conditions for positive and negative thermal currents.

	$\langle\hat{\sigma}_z\rangle = +1$	$\langle\hat{\sigma}_z\rangle = -1$
$\alpha > 1$	$I_L > 0$	$I_L > 0$
$\alpha = 1$	$I_L > 0$	$I_L = 0$
$\alpha < 1$	$I_L > 0$	$I_L < 0$

If the atom is in its ground state and the system-reservoir parameters are such that

$$\frac{\Gamma_R}{\Gamma_L} < \frac{(\chi - \omega_R)}{\omega_L}, \tag{5.28}$$

then $\Omega < 0$ and the direction of thermal current reverses, *i.e.*, current flows from the low temperature reservoir to the high temperature reservoir (unconventional flow). This phenomenon has been interpreted to be a violation of the second law of thermodynamics [199–201]. Alternatively, the thermal conductivity of the system can be interpreted to be negative in which case heat flows from the low temperature reservoir to high temperature reservoir. On driving the atom from the ground state to its excited state, the unconventional flow of thermal current switches to the conventional flow. Thus, the atom acts as a thermal switch which brings about a controllable current flow through the cavities.

To summarize, defining

$$\alpha = \frac{\Gamma_R/\Gamma_L}{(\chi - \omega_R)/\omega_L}, \tag{5.29}$$

the three conditions given in Eqns. (5.26-5.28) are equivalent to setting α greater than, equal to or less than unity respectively. The signs of the respective currents established in the system are indicated in Table. 5.1.

Scaled current I_L/I_0 for the case of the atom in its ground state is shown as a function

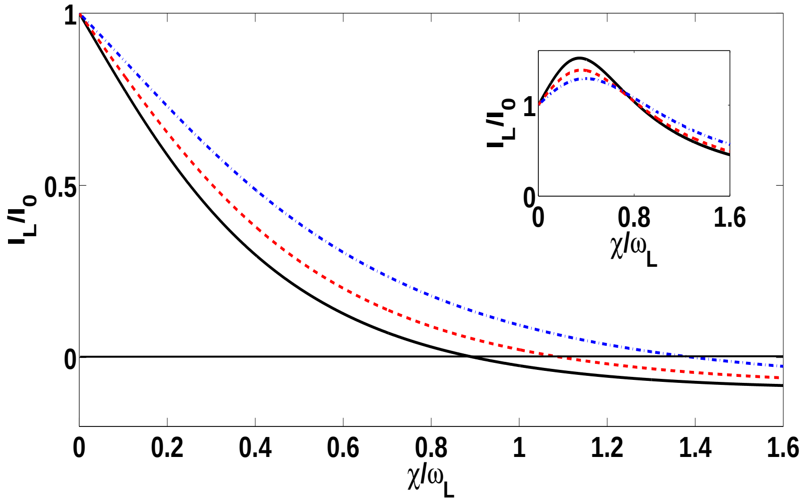

Figure 5.3 – Scaled currents I_L/I_0 shown as a function of χ/ω_L for different cavity-reservoir coupling ratio $\Gamma_R/\Gamma_L = 0.1$ (continuous), 0.3 (dashed) and 0.6 (dot-dashed). The system-reservoir parameters are $J/\omega_L = 0.05, \bar{n}_L - \bar{n}_R = 0.5, \omega_R/\omega_L = 0.8$ and $\langle\hat{\sigma}_z\rangle = -1$. Scaled current in the system is shown in the inset for the same values of the parameters and $\langle\hat{\sigma}_z\rangle = +1$.

of χ/ω_L in Fig. 5.3 for three different values of the cavity-reservoir coupling ratios Γ_R/Γ_L : 0.1 (continuous), 0.3 (dash) and 0.6 (dot-dash). Here I_0 is the magnitude of current flowing through the system when $\chi = 0$. The inset figure shows the scaled current in the system when the atom is in its excited state. Note that the current is always positive if the atom is in the excited state (inset figure). If the system and reservoir parameters satisfy Eqn. 5.27, then the current vanishes. Negative current occurs at different values of χ/ω_L depending on the ratio Γ_R/Γ_L that satisfy Eqn. 5.28.

From Eqn. 5.12, it is seen that if the contribution from the coherence part I_{coh} is more than the current due to mean excitation number difference I_{nd}, then I_L becomes negative. Dimensionless quantities $I_{nd}/\omega_L^2, I_{coh}/\omega_L^2$ and I_L/ω_L^2 are shown in Fig. 5.4 as a function of the atom-field coupling strength χ/ω_L. If the parameters are chosen to satisfy Eqn. 5.27, in which case $I_{nd} = I_{coh}$, the system completely blocks the current which corresponds to the intersection of zero current axis and I_L/ω_L^2 in Fig. 5.4. Current reverses its direction from the low temperature reservoir to the high temperature reservoir when $I_{coh} > I_{nd}$. In this sense, the coherence in the system drives energy to flow to the high temperature reservoir.

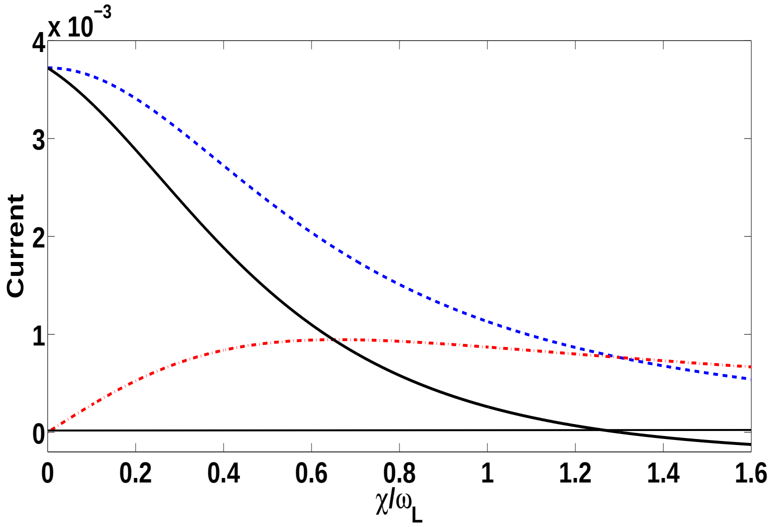

Figure 5.4 – Dimensionless currents I_L/ω_L^2(continuous), I_{nd}/ω_L^2 (dashed) and I_{coh}/ω_L^2 (dot-dashed) shown as function of χ/ω_L. Here $\Gamma_R/\Gamma_L = 0.3$, $J/\omega_L = 0.05, \bar{n}_L - \bar{n}_R = 0.5, \omega_R/\omega_L = 1$ and $\langle\hat{\sigma}_z\rangle = -1$.

5.3 Thermal rectification

A system exhibits thermal rectification if thermal current depends on the direction of heat flow. Symbolically,

$$I(\Delta n) \neq -I(-\Delta n), \tag{5.30}$$

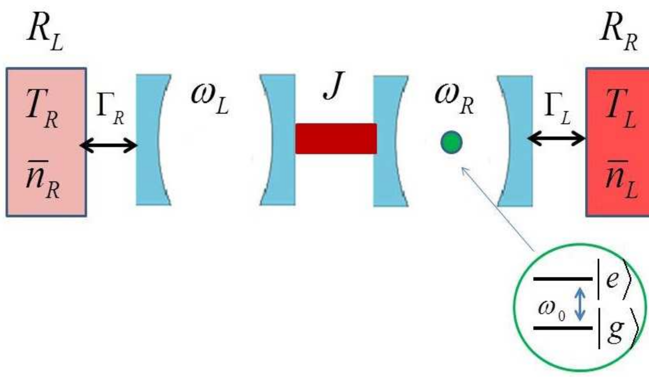

Figure 5.5 – Reverse configuration of system-reservoirs. reservoir temperatures and the system-reservoir coupling strengths are interchanged.

where $\Delta n = \bar{n}_L - \bar{n}_R$ is the difference in the average number of photons in the left and right reservoirs. This means that by swapping the thermal reservoirs, current changes its sign and magnitude.

If the system is symmetric under the exchange of cavities so that $I(\Delta n) = -I(-\Delta n)$, then thermal rectification is not possible. If the system is asymmetric, thermal rectification is a possibility. In the system under discussion, symmetry is broken due to the presence of the atom in one of the cavities. Thermal rectification arises by interchanging the reservoirs and system-reservoir coupling strengths. The reverse configuration is shown in Fig. 5.5. The relevant Lindblad operators for the reverse configuration are

$$\begin{aligned} \mathcal{D}_L(\rho) =& \frac{\Gamma_R(\bar{n}_R+1)}{2}(2\hat{a}_L\rho\hat{a}_L^\dagger - \hat{a}_L^\dagger\hat{a}_L\rho - \rho\hat{a}_L^\dagger\hat{a}_L) \\ &+ \frac{\Gamma_R\bar{n}_R}{2}(2\hat{a}_L^\dagger\rho\hat{a}_L - \hat{a}_L\hat{a}_L^\dagger\rho - \rho\hat{a}_L\hat{a}_L^\dagger), \\ \text{and} \quad \mathcal{D}_R(\rho) =& \frac{\Gamma_L(\bar{n}_L+1)}{2}(2\hat{a}_R\rho\hat{a}_R^\dagger - \hat{a}_R^\dagger\hat{a}_R\rho - \rho\hat{a}_R^\dagger\hat{a}_R) \\ &+ \frac{\Gamma_L\bar{n}_L}{2}(2\hat{a}_R^\dagger\rho\hat{a}_R - \hat{a}_R\hat{a}_R^\dagger\rho - \rho\hat{a}_R\hat{a}_R^\dagger). \end{aligned} \tag{5.31}$$

The atom is taken to be in its ground state so that $\langle\sigma_z\rangle = -1$. Steady state solutions for the expectation values of the operators are obtained by the transformations $\Gamma_L \longrightarrow \Gamma_R$, $\bar{n}_L \longrightarrow \bar{n}_R$ and vice-versa in Eqns. 5.14$(a-d)$.

Current from the left reservoir R_L to the right reservoir R_R in the system shown in Fig. 5.1 is called forward current. The expression for the forward current is

$$I_f(\Delta n, \Gamma_L, \Gamma_R) = J^2\delta N \frac{(\omega_L\Gamma_R + \Gamma_L(\omega_R-\chi))}{(\chi^2-\Delta_c^2+\gamma^2)^2 + 4\gamma^2\Delta_c^2}((\Delta_c-\chi)^2+\gamma^2). \tag{5.32}$$

On exchanging $(\bar{n}_L, \Gamma_L)$ with $(\bar{n}_R, \Gamma_R)$, reverse current from the right reservoir R_R to

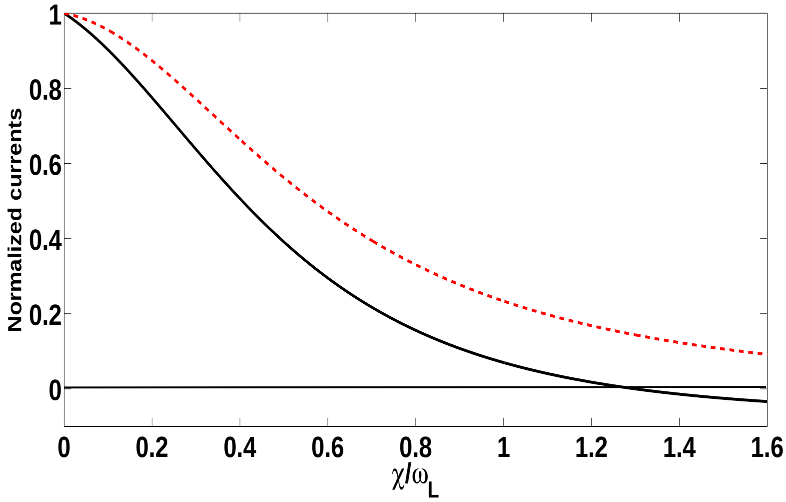

Figure 5.6 – Normalized forward current I_f (continuous line) and reverse current I_r (dashed line) as a function of χ/ω_L for $\Gamma_R/\Gamma_L = 0.3$. Currents are normalized with their respective values at $\chi = 0$. The system-reservoir parameters are $J/\omega_L = 0.05, \bar{n}_L - \bar{n}_R = 0.5, \omega_R/\omega_L = 1$ and $\langle\hat{\sigma}_z\rangle = -1$.

the left reservoir R_L in the configuration shown in Fig. 5.5 is

$$I_r(-\Delta n, \Gamma_R, \Gamma_L) = -J^2 \delta N \frac{(\omega_L \Gamma_L + \Gamma_R(\omega_R - \chi))}{(\chi^2 - \Delta_c^2 + \gamma^2)^2 + 4\gamma^2\Delta_c^2}((\Delta_c - \chi)^2 + \gamma^2). \tag{5.33}$$

The reverse current is negative as the direction of flow is opposite to the forward current.

The currents I_f and I_r, normalized with their corresponding values for $\chi = 0$ and $\Delta_c = 0$, are shown as functions of the atom-field coupling strength χ in Fig. 5.6. For non-zero χ, the magnitudes of the forward and reverse currents are different. Therefore, the system shows thermal rectification. Importantly, if the parameters satisfy the condition given in Eqn. 5.28, the forward current changes the sign. As a result, both I_f and I_r flow in same direction.

Thermal rectification of a system is quantified in terms of its rectification coefficient

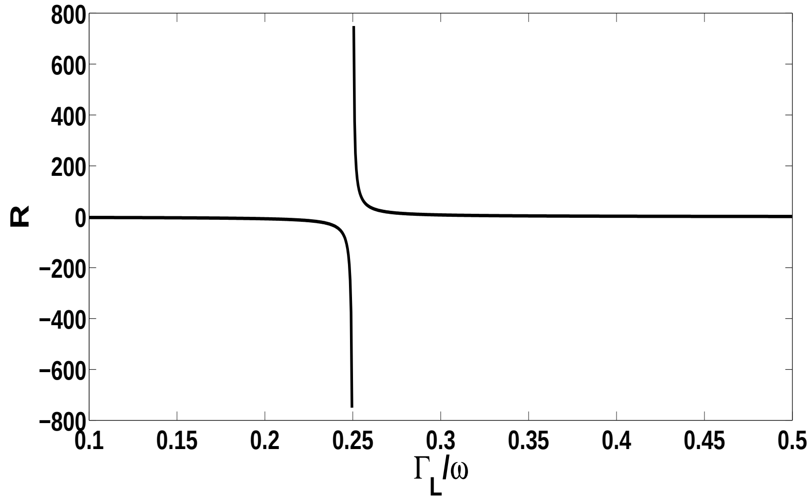

Figure 5.7 – Rectification R as a function of Γ_L/ω for $\Gamma_R/\omega = 0.5$. Here $\chi/\omega = 1.5$ and $\langle\hat{\sigma}_z\rangle = -1$.

R defined as

$$R = -\frac{I_f}{I_r}. \tag{5.34}$$

If $R = 1$, there is no rectification. For the system under consideration

$$R = \frac{\omega_L\Gamma_R + \Gamma_L(\omega_R - \chi)}{\omega_L\Gamma_L + \Gamma_R(\omega_R - \chi)}. \tag{5.35}$$

If $\Gamma_L = \Gamma_R$ or $\omega_L = |\omega_R - \chi|$, the rectification coefficient R becomes unity. Rectification coefficient R is shown as a function of Γ_L/ω in Fig. 5.7 for the resonant case ($\Delta_c = 0$). Rectification is positive, zero, or negative depending on the parameters. The system shows large rectification if

$$\frac{\Gamma_L}{\Gamma_R} = \frac{\chi - \omega_R}{\omega_L}, \tag{5.36}$$

as seen in Fig. 5.7. This comes from the fact that if Eqn. 5.36 holds then the atom completely blocks the current in one direction (thermally insulating) and allows in the other direction (thermally conducting) so that R becomes unbounded. Even though the system size is finite, rectification becomes infinity, theoretically. If Γ_L/ω is increased from values less than that satisfying Eqn. 5.36 to higher values, R jumps from negative values of large magnitude to large positive values. Thus, R is very sensitive to changes in the parameters in that region. Asymmetry can also be introduced with non-resonant cavities without an atom ($\chi = 0$) in any of the cavities. In this case,

$$R = \frac{\omega_L \Gamma_R + \Gamma_L \omega_R}{\omega_L \Gamma_L + \Gamma_R \omega_R}, \tag{5.37}$$

obtained from Eqn. 5.35. The denominator cannot be made arbitrarily large. So, large rectification is not possible if atom is not present.

5.4 Heat transport in cavity array

In the case of linearly coupled, homogeneous arrays, heat current does not depend on the number of cavities in the array. However, size dependent current can be realized by embedding atoms in the cavities. It would be interesting to study the steady state heat transfer in N coupled cavities containing a two-level atom in one of the cavities. The Hamiltonian for the system is

$$\tilde{H} = \frac{\omega_0}{2}\hat{\sigma}_z + \omega \sum_{j=1}^{N} \hat{a}_j^\dagger \hat{a}_j + J \sum_{j=1}^{N-1} (\hat{a}_j^\dagger \hat{a}_{j+1} + \hat{a}_j \hat{a}_{j+1}^\dagger) + \chi(\hat{\sigma}_+ \hat{\sigma}_- + \hat{a}_m^\dagger \hat{a}_m \hat{\sigma}_z). \tag{5.38}$$

The atom is embedded in the mth cavity and considered to dispersively interact with the cavity-field. The right most and left most cavities in the array are coupled with two thermal reservoirs R_L and R_R respectively. The density matrix $\tilde{\rho}$ of the system obeys

$$\frac{\partial \tilde{\rho}}{\partial t} = -i[\tilde{H}, \tilde{\rho}] + \mathcal{D}_L(\tilde{\rho}) + \mathcal{D}_R(\tilde{\rho}), \tag{5.39}$$

where

$$\mathcal{D}_L(\tilde{\rho}) = \frac{\Gamma_L(\bar{n}_L+1)}{2}(2\hat{a}_1\tilde{\rho}\hat{a}_1^\dagger - \hat{a}_1^\dagger\hat{a}_1\tilde{\rho} - \tilde{\rho}\hat{a}_1^\dagger\hat{a}_1) + \frac{\Gamma_L\bar{n}_L}{2}(2\hat{a}_1^\dagger\tilde{\rho}\hat{a}_1 - \hat{a}_1\hat{a}_1^\dagger\tilde{\rho} - \tilde{\rho}\hat{a}_1\hat{a}_1^\dagger),$$

and

$$\mathcal{D}_R(\tilde{\rho}) = \frac{\Gamma_R(\bar{n}_R+1)}{2}(2\hat{a}_N\tilde{\rho}\hat{a}_N^\dagger - \hat{a}_N^\dagger\hat{a}_N\tilde{\rho} - \tilde{\rho}\hat{a}_N^\dagger\hat{a}_N) + \frac{\Gamma_R\bar{n}_R}{2}(2\hat{a}_N^\dagger\tilde{\rho}\hat{a}_N - \hat{a}_N\hat{a}_N^\dagger\tilde{\rho} - \tilde{\rho}\hat{a}_N\hat{a}_N^\dagger). \tag{5.40}$$

Here $\bar{n}_L$ and $\bar{n}_R$ are the mean number of photons in the reservoirs R_L and R_R respectively. Without loss of generality, assume $\bar{n}_L > \bar{n}_R$.

Using Eqn. 5.39, the equation of motion for expectation values of operators is expressible as

$$\frac{d\langle G\rangle}{dt} = \frac{d}{dt}\mathrm{Tr}(\tilde{\rho}G) = i[M_1, \langle G\rangle] + \{M_2, \langle G\rangle\} + M_3, \tag{5.41}$$

where $\langle G\rangle = \langle A^\dagger A\rangle$ is the matrix whose elements are the expectation values of the operator elements of $A^\dagger A$. Here

$$A = \mathrm{Row}(\hat{a}_1, \hat{a}_2, ...\hat{a}_N, \hat{a}_1\hat{\sigma}_z, ..., \hat{a}_N\hat{\sigma}_z), \tag{5.42}$$

$$A^\dagger = \mathrm{Column}(\hat{a}_1^\dagger, \hat{a}_2^\dagger, ...\hat{a}_N^\dagger, \hat{a}_1^\dagger\hat{\sigma}_z, ..., \hat{a}_N^\dagger\hat{\sigma}_z). \tag{5.43}$$

Further $[M_1, \langle G\rangle] = M_1\langle G\rangle - \langle G\rangle M_1$ and $\{M_2, \langle G\rangle\} = M_2\langle G\rangle + \langle G\rangle M_2$. The transformation matrices are

$$
\begin{aligned}
M_1 =& I_{2\times 2} \otimes H_c + \sigma_x \otimes X, && (5.44)\\
M_2 =& I_{2\times 2} \otimes \text{Diag}\left(-\frac{1}{2}\Gamma_L, 0, ...0, -\frac{1}{2}\Gamma_R\right)_{N\times N}, && (5.45)\\
M_3 =& I_{2\times 2} \otimes \text{Diag}\left(\Gamma_L \bar{n}_L, 0, ...0, \Gamma_R \bar{n}_R\right)_{N\times N} \\
& + \hat{\sigma}_x \otimes \text{Diag}(\Gamma_L \bar{n}_L \langle \hat{\sigma}_z \rangle, 0, ...0, \Gamma_R \bar{n}_R \langle \hat{\sigma}_z \rangle)_{N\times N}, && (5.46)
\end{aligned}
$$

where $I_{2\times 2}$ is the identity matrix of dimension 2, σ_x is the Pauli matrix,

$$
H_c = \begin{pmatrix} \omega & J & 0 & \ldots\ldots & 0 \\ J & \omega & J & \ldots\ldots & 0 \\ \vdots & \vdots & \ddots & \vdots & \vdots \\ 0 & 0 & \ldots & \omega & J \\ 0 & 0 & \ldots & J & \omega \end{pmatrix}_{N\times N},
$$

and $(X)_{N\times N}$ is a matrix whose elements vanish except the element $X_{m,m}$ which is equal to χ.

Using $\tilde{H}$ given in Eqn. 5.38 in the continuity equation (refer Eqn. 5.10), the expression for current in the array is

$$
I_L = \Gamma_L \left[(\bar{n}_L - \langle \hat{a}_1^\dagger \hat{a}_1 \rangle_{ss})(\omega + \chi \langle \hat{\sigma}_z \rangle \delta_{m,1}) - \frac{J}{2}(\langle \hat{a}_1^\dagger \hat{a}_2 \rangle_{ss} + \langle \hat{a}_1 \hat{a}_2^\dagger \rangle_{ss}) \right]. \tag{5.47}
$$

Here $\delta_{m,1}$ is Kronecker delta. If there is no atom in the array, the coherence term $\langle \hat{a}_j^\dagger \hat{a}_{j+1} \rangle$ is purely imaginary [176]. The contribution of the coherence term to the current vanishes as $I_{coh} = \frac{J}{2}(\langle \hat{a}_1^\dagger \hat{a}_2 \rangle_{ss} + \langle \hat{a}_1 \hat{a}_2^\dagger \rangle_{ss}) = 0$. Consequently, current in the

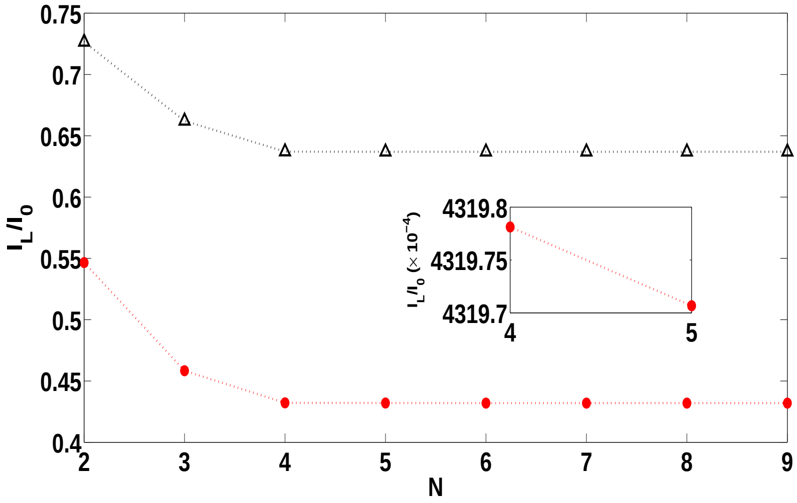

Figure 5.8 – Ratio of currents I_L/I_0 as a function of N for $\chi/\omega = 0.15$ (circle) and 0.1 (triangle). The atom is embedded in the last cavity ($m = N$). Here $J/\omega = 0.05, \bar{n}_L - \bar{n}_R = 0.5, \langle\hat{\sigma}_z\rangle = -1, \Gamma_L/\omega = \Gamma_R/\omega = 0.15$. Enlarged view of current in the array for $N = 4$ and 5 is in inset for $\chi/\omega = 0.15$ to show size dependence of current.

cavity array is

$$I_L(\chi = 0) = I_0 = \frac{4\omega J^2 \Gamma_L \Gamma_R}{(4J^2 + \Gamma_L\Gamma_R)(\Gamma_L + \Gamma_R)}(\bar{n}_L - \bar{n}_R). \tag{5.48}$$

Note that the current I_0 is independent of the size of the array, in violation of the Fourier's law. This feature is similar to the system-size independent current in the case of ballistic transport [176, 202, 203]. This comparison indicates that the mean free path of the photons scales in proportion to the number of cavities N.

If there is no atom in the array, then a photon travels across the array without getting scattered. The length of the array is the mean free path of the photon. However, the mean free path is different from the array size if an atom is embedded in one of the cavities. In the present case, the atom is embedded in the last cavity of the array, *i.e.*, $m = N$, to keep the mean free path as close to the size of the array. This helps in understanding the emergence of diffusive character if there is a single scatterer. The normalized current I_L/I_0 as a function of the size of the array (N) is shown in Fig. 5.8 for a fixed temperature difference ($\bar{n}_L - \bar{n}_R$). On increasing the size of the array,

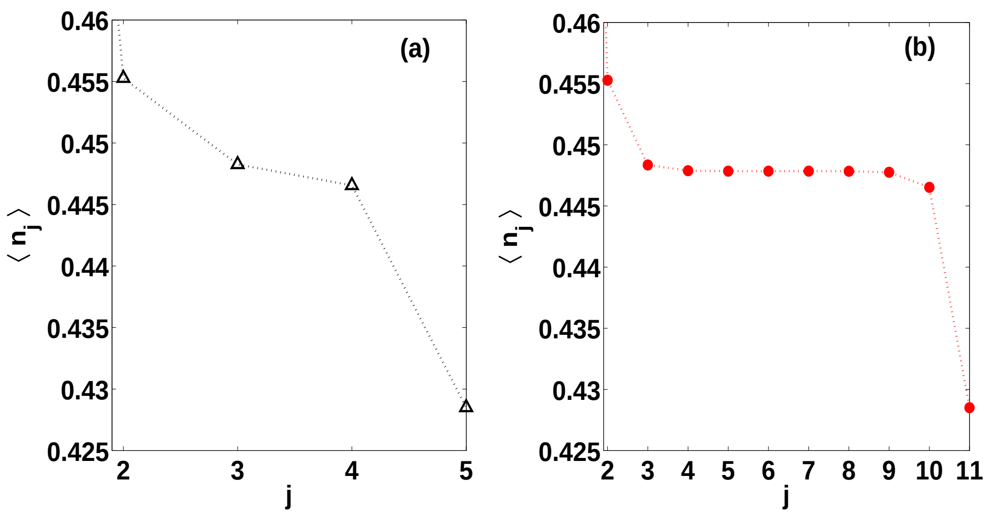

Figure 5.9 – Steady state mean photon number in the intermediate cavities for arrays of length $(a)N = 6$ and $(b)N = 12$. The atom-field coupling strength is chosen to be $\chi/\omega = 0.1$. Here $J/\omega = 0.05, \bar{n}_L - \bar{n}_R = 0.5, \langle\hat{\sigma}_z\rangle = -1, \Gamma_L/\omega = \Gamma_R/\omega = 0.15$.

the steady state current significantly decreases and asymptotically approaches a constant value. Hence, current is size dependent for smaller array as the atom is able to introduce diffusive character in the heat transport. It saturates with further increase in size and becomes nearly size independent as in the case of ballistic transport. This is not consistent with Fourier's law.

The transition from diffusive to ballistic transport as size of the array increases is understood by calculating the mean photon numbers $\langle\hat{n}_j\rangle = \langle\hat{a}_j^\dagger\hat{a}_j\rangle$ (known as local temperature [176]) of the respective cavities in the array. The steady state mean photon number $\langle n_j\rangle$ in the intermediate cavities in arrays containing 6 and 12 cavities are shown in Fig. 5.9(a) and (b) respectively. Gradient in the mean photon number is noticed in Fig. 5.9(a). This implies that the transport is diffusive [183, 184]. For larger size array, for instance $N = 12$, the gradient in mean photon number approaches zero and the current is independent of the system size. Essentially, the change in mean free path in the presence of a single scatterer at the end of the array is insignificant in a large array and the transport is almost ballistic.

5.5 Summary

Mesoscopic systems offer interesting possibilities when it comes to thermal properties. A system of two coupled cavities connected between thermal reservoirs provides a conduit for heat flow between the reservoirs. Many of the transport properties can be modified by dispersively coupling an atom to any one of the cavities. The heat current in the system depends on the state of the atom. For instance, the system changes from a thermal insulator to a conductor on driving the atom from its ground state to excited state. In addition, if the atomic state changes from the excited state to the ground state, current through the system becomes zero or reversed depending on the system-reservoir coupling strengths and the cavity frequencies. The vanishing current in the system corresponds to a thermally insulating phase. Reversal of current demonstrates the violation of second law of thermodynamics in this system.

The presence of atom provides a structural asymmetry. As a consequence, the magnitude of the current changes by exchanging the reservoirs along with the coupling strengths. This makes it possible to achieve thermal rectification. Large rectification is possible if the parameters are chosen to make the system thermally insulating.

In an array of N linearly coupled resonant cavities, current is independent of the array size which is characteristic of ballistic transport. If the array contains a two-level atom in one of the cavities, the magnitude of current depends on the number of cavities. This size-dependence indicates that the thermal current through the array is analogous to the diffusive heat transport. With only one atom in a large sized array, it is not possible to completely recover diffusive transport. One atom does not provide enough dephasing to recover the diffusive character.

Chapter 6

Summary and future directions

6.1 Summary

The main focus of the this thesis is to study controlled transfer of photons in coupled cavity arrays. The results obtained in the thesis are expected to be of relevance in realizing quantum information processing, study of quantum-classical divide, etc. A brief review of the basic facts relevant to the thesis such as the field quantization, quantum states of the electromagnetic field, physics of microcavities and arrays, open quantum systems is presented in the first chapter.

Analysis of controlled transfer of photons is carried out in Chapter 2. Homogeneously coupled cavities do not allow perfect transfer if there are more than three cavities in the array. This is a serious limitation if arrays are to be used as conduit for photon transport. It has been established that a suitable choice of inhomogeneity in terms of inter-cavity couplings and resonance frequencies can overcome the limitation in the homogeneous case. An apt choice for these parameters is determined on the basis of a duality relation between an array with one photon and a system of two coupled cavities with suitable number of photons. These values for the parameters enable perfect transfer between any two symmetrically located cavities in the array. To further improve the controllability so that photon transfer can happen between any two cavities, Kerr cavities are considered. By extending the duality notion to an array of coupled Kerr cavities containing a photon and a system of two coupled Kerr cavities sharing a suitable number of photons, condition for the perfect transfer of a photon between any two cavities in the array has been established. With this, perfect transfer a photonic qubit which is realized on superposing the vacuum and the one photon state is also shown to be possible.

Localization of particles due to scattering in a random medium is a well known effect. In the case of two coupled cavities, a pair of photons can be either localized in a cavity or distributed (delocalized) in the two cavities. The main interest is to identify the factors that affect the delocalization and localization. This is the focus of the third and fourth chapters. In the third chapter, two linearly coupled cavities are considered. It is argued that the relative phase and entanglement in the initial state are the important factors that dictate the emergence of localization and delocalization. These two phenomena are understood in terms of quantum interference. Constructive and destructive interference among the quantum amplitudes for the transitions between the levels of the two-cavity two-photon system is related to the occurrence localization and delocalization.

In continuation of discussion presented in third chapter, nonlinearity is incorporated in the cavities to bring forth additional controllability in the system. Two new features that emerge are the possibility of photon blockade and delocalization of localized product state which is not possible in linear cavities. These two are particularly interesting in the context many-body physics and quantum information processing.

Interaction between a quantum system and environment also needs to be controlled for effective utilization of cavity network. In chapter five, the possibility of configuring two coupled cavities as a thermal rectifier is discussed. The system consists of two coupled cavities, where each one connected to its own independent thermal reservoir. The two reservoirs are taken to be at two different temperatures. The system has to be asymmetrical to ensure that the thermal current is not the same when the reservoirs are exchanged. This is accomplished by embedding a dispersively interacting atom in one of the cavities.

Interestingly, thermal current in the system depends on the atomic state. By choosing the atomic state properly, the system is made either thermally insulating or conducting. If the atom is in its ground state, the direction also can be reversed making the current flow from the low temperature reservoir to the high temperature reservoir, a clear violation of the second law of thermodynamics. The magnitude of the thermal current changes on exchanging the reservoirs and the cavity-reservoir couplings. The parameters in the system, namely, the atomic state, detuning and coupling coefficients, can be chosen so that the system allows thermal current in one direction and blocks in other direction. This leads to thermal rectification. As the coupled cavity system transports energy between the reservoirs, the nature of the transport has been analyzed in the array of N cavities. The transport is not entirely ballistic as there is an atom in one of the cavities. It is not entirely diffusive since a single atom is inadequate to introduce enough dephasing of the scattering amplitudes. In short, this simple system has been shown to exhibit many interesting features: violation of the second law of thermodynamics, thermal rectification and a mix of ballistic and diffusive modes of thermal transport.

6.2 Future directions

Some issues that could be pursued are presented here. The focus so far has been on cavity arrays in one dimension. It is desirable to identify the right choice of the system parameters so that controlled transfer of photon can be accomplished in two-dimensional and three-dimensional networks. Extending the duality notion to these higher dimensional arrays is an interesting approach. This is a pertinent issue as any realistic configuration for quantum information processing will require higher dimensional networks. Design of suitable networks to implement specific quantum algorithms is another topic worth pursuing.

An enigmatic question in physics is the quantum-classical divide. While quantum theory is considered to be universally applicable, most of the macroscopic properties are well described by classical physics. On the other hand, microscopic systems wholly need a quantum approach. It is believed that mesoscopic systems, which are between the microscopic and the macroscopic, are the best candidates to study quantum-classical divide. Cavity arrays of suitable size belong to this mesoscopic category. Incorporating nonlinearity allows one to explore quantum aspects of classically nonlinear systems.

Many quantum information protocols involve quantum operations on qubit. Superposition of the vacuum state and a single photon state is used as qubit. Another class of qubits is being considered as a better allternative. These are the cat states, which involve superposition of coherent states with opposite phases. Superposition of cat states are desirable as they decohere much lesser compared to the conventional photonic qubits. Hence, generation and maneuvering of superposed cat states in cavities are of interest.

References

[1] A. Pathak, *Elements of Quantum Computation and Quantum Communication* (Taylor and Francis, 2013).

[2] C. N. Cohen-Tannoudji, Rev. Mod. Phys. **70**, 707 (1998).

[3] S. Chu, Rev. Mod. Phys. **70**, 685 (1998).

[4] W. Paul, Rev. Mod. Phys. **62**, 531 (1990).

[5] H. J. Kimble, M. Dagenais, and L. Mandel, Phys. Rev. Lett. **39**, 691 (1977).

[6] G. Nogues, A. Rauschenbeutel, S. Osnaghi, M. Brune, J. M. Raimond, and S. Haroche, Nature **400**, 239 (1999).

[7] M. O. Scully and M. S. Zubairy, *Quantum Optics* (Cambridge University Press, 1997).

[8] P. Meystre and M. Sargent, *Elements of Quantum Optics* (Springer, 2007).

[9] P. W. Milonni and C. Eberlein, American Journal of Physics **62**, 1154 (1994).

[10] C. Gerry and P. Knight, *Introductory Quantum Optics* (Cambridge University Press, 2004), ISBN 052152735X.

[11] M. Khudaverdyan, W. Alt, I. Dotsenko, T. Kampschulte, K. Lenhard, A. Rauschenbeutel, S. Reick, K. Schorner, A. Widera, and D. Meschede, New Journal of Physics **10**, 073023 (2008).

[12] K. Djordjev, S.-J. Choi, S.-J. Choi, and P. D. Dapkus, Journal of Lightwave Technology **20**, 105 (2002), ISSN 0733-8724.

[13] K. Djordjev, S.-J. Choi, S.-J. Choi, and R. D. Dapkus, IEEE Photonics Technology Letters **14**, 828 (2002), ISSN 1041-1135.

[14] M. Fox, *Quantum Optics: An Introduction* (Oxford Master Series in Physics, 2006).

[15] S. Haroche, AIP Conference Proceedings **329**, 30 (1995).

[16] C. K. Law and J. H. Eberly, Phys. Rev. Lett. **76**, 1055 (1996).

[17] K. Vogel, V. M. Akulin, and W. P. Schleich, Phys. Rev. Lett. **71**, 1816 (1993).

[18] B. M. Garraway, B. Sherman, H. Moya-Cessa, P. L. Knight, and G. Kurizki, Phys. Rev. A **49**, 535 (1994).

[19] A. S. Parkins, P. Marte, P. Zoller, and H. J. Kimble, Phys. Rev. Lett. **71**, 3095 (1993).

[20] R. W. Heeres, B. Vlastakis, E. Holland, S. Krastanov, V. V. Albert, L. Frunzio, L. Jiang, and R. J. Schoelkopf, Phys. Rev. Lett. **115**, 137002 (2015).

[21] Y. Wang, J. Wan, B. Zou, J. Zhang, and Y. Zhu, Journal of Physics: Conference Series **414**, 012001 (2013).

[22] K. Rojan, D. M. Reich, I. Dotsenko, J.-M. Raimond, C. P. Koch, and G. Morigi, Phys. Rev. A **90**, 023824 (2014).

[23] G. Rempe, R. J. Thompson, H. J. Kimble, and R. Lalezari, Opt. Lett. **17**, 363 (1992).

[24] C. J. Hood, H. J. Kimble, and J. Ye, Phys. Rev. A **64**, 033804 (2001).

[25] J. M. Gerard, D. Barrier, J. Y. Marzin, R. Kuszelewicz, L. Manin, E. Costard, V. Thierry-Mieg, and T. Rivera, Applied Physics Letters **69**, 449 (1996).

[26] V. Lefevre-Seguin and S. Haroche, Materials Science and Engineering: B **48**, 53 (1997), ISSN 0921-5107.

[27] M. L. Gorodetsky, A. A. Savchenkov, and V. S. Ilchenko, Opt. Lett. **21**, 453 (1996).

[28] J. Vučković, M. Lončar, H. Mabuchi, and A. Scherer, Phys. Rev. E **65**, 016608 (2001).

[29] A. Majumdar, A. Rundquist, M. Bajcsy, V. D. Dasika, S. R. Bank, and J. Vučković, Phys. Rev. B **86**, 195312 (2012).

[30] K. Vahala, *Optical Microcavities* (World Scientific, 2004).

[31] K. J. Vahala, Nature **424**, 839 (2003).

[32] A. V. Kavokin, J. J. Baumberg, G. Malpuech, and F. P. Laussy, *Microcavities* (Oxford University, 2017).

[33] H. J. Kimble, Physica Scripta **1998**, 127 (1998).

[34] H. Mabuchi, Q. A. Turchette, M. S. Chapman, and H. J. Kimble, Opt. Lett. **21**, 1393 (1996).

[35] G. Rempe, Applied Physics B **60**, 233 (1995), ISSN 1432-0649.

[36] Y. Shimizu, N. Shiokawa, N. Yamamoto, M. Kozuma, T. Kuga, L. Deng, and E. W. Hagley, Phys. Rev. Lett. **89**, 233001 (2002).

[37] J. M. Raimond, M. Brune, and S. Haroche, Rev. Mod. Phys. **73**, 565 (2001).

[38] F. Vollmer, D. Braun, A. Libchaber, M. Khoshsima, I. Teraoka, and S. Arnold, Applied Physics Letters **80**, 4057 (2002).

[39] M. A. Cooper, Nature Reviews Drug Discovery **1**, 515 (2002).

[40] E. Krioukov, D. J. W. Klunder, A. Driessen, J. Greve, and C. Otto, Opt. Lett. **27**, 512 (2002).

[41] T. E. Northup and R. Blatt, Nature Photonics **8**, 356 (2014).

[42] S. Bose, Phys. Rev. Lett. **91**, 207901 (2003).

[43] A. Reiserer and G. Rempe, Rev. Mod. Phys. **87**, 1379 (2015).

[44] Z.-R. Zhong, Scientific Reports **6**, 8 (2016), ISSN 2045-2322.

[45] T. Pellizzari, Phys. Rev. Lett. **79**, 5242 (1997).

[46] G. D. de Moraes Neto, F. M. Andrade, V. Montenegro, and S. Bose, Phys. Rev. A **93**, 062339 (2016).

[47] J. I. Cirac, P. Zoller, H. J. Kimble, and H. Mabuchi, Phys. Rev. Lett. **78**, 3221 (1997).

[48] M. C. de Oliveira, S. S. Mizrahi, and V. V. Dodonov, Journal of Optics B: Quantum and Semiclassical Optics **1**, 610 (1999).

[49] G. W. Lin, X. B. Zou, X. M. Lin, and G. C. Guo, Applied Physics Letters **95**, 224102 (2009).

[50] Z.-D. Hu, Y.-Q. Zhang, and J.-B. Xu, Journal of Physics A: Mathematical and Theoretical **44**, 425303 (2011).

[51] V. Ilchenko, M. Gorodetsky, and S. Vyatchanin, Optics Communications **107**, 41 (1994), ISSN 0030-4018.

[52] A. Majumdar, A. Rundquist, M. Bajcsy, and J. Vučković, Phys. Rev. B **86**, 045315 (2012).

[53] B. Peropadre, D. Zueco, F. Wulschner, F. Deppe, A. Marx, R. Gross, and J. J. García-Ripoll, Phys. Rev. B **87**, 134504 (2013).

[54] Y. Sato, Y. Tanaka, J. Upham, Y. Takahashi, T. Asano, and S. Noda, Nature Photonics **6**, 56 (2011).

[55] M. J. Hartmann, Journal of Optics **18**, 104005 (2016).

[56] W. T. M. Irvine, K. Hennessy, and D. Bouwmeester, Phys. Rev. Lett. **96**, 057405 (2006).

[57] K. Ebeling, *Integrated optoelectronics* (Springer, Berlin, 1997).

[58] L. E. Estes, T. H. Keil, and L. M. Narducci, Phys. Rev. **175**, 286 (1968).

[59] A. S. M. de Castro, V. V. Dodonov, and S. S. Mizrahi, Journal of Optics B: Quantum and Semiclassical Optics **4**, S191 (2002).

[60] S. Felicetti, G. Romero, D. Rossini, R. Fazio, and E. Solano, Phys. Rev. A **89**, 013853 (2014).

[61] A. Biella, L. Mazza, I. Carusotto, D. Rossini, and R. Fazio, Phys. Rev. A **91**, 053815 (2015).

[62] H. Du, X. Zhang, G. Chen, J. Deng, F. S. Chau, and G. Zhou, Scientific Reports **6**, 24766 (2016).

[63] G. Milburn and M. Woolley, Acta Physica Slovaca **61**, 483 (2011).

[64] A. Mazzei, S. Götzinger, L. de S. Menezes, G. Zumofen, O. Benson, and V. Sandoghdar, Phys. Rev. Lett. **99**, 173603 (2007).

[65] K. R. Brown, C. Ospelkaus, Y. Colombe, A. C. Wilson, D. Leibfried, and D. J. Wineland, Nature **471**, 196 (2011).

[66] L. Frunzio, A. Wallraff, D. Schuster, J. Majer, and R. Schoelkopf, IEEE Transactions on Applied Superconductivity **15**, 860 (2005), ISSN 1051-8223.

[67] J.-M. Pirkkalainen, S. U. Cho, F. Massel, J. Tuorila, T. T. Heikkilä, P. J. Hakonen, and M. A. Sillanpää, Nature Communications **6**, 6981 (2015).

[68] H. J. Carmichael, *Statistical Methods in Quantum Optics 1: Master Equations and Fokker-Planck Equations* (Springer, 1999).

[69] A. REDFIELD, in *Advances in Magnetic Resonance*, edited by J. S. Waugh (Academic Press, 1965), vol. 1 of *Advances in Magnetic and Optical Resonance*, pp. 1 – 32.

[70] G. Lindblad, Commun.Math. Phys. **48**, 195452 (1976).

[71] I. R. Senitzky, Phys. Rev. **119**, 670 (1960).

[72] S.-A. Biehs and G. S. Agarwal, J. Opt. Soc. Am. B **30**, 700 (2013).

[73] G. Solomon, M. Pelton, and Y. Yamamoto, physica status solidi **178**, 341 (2000).

[74] E. M. Purcell, Physical Review **69**, 681+ (1946).

[75] P. R. Berman, *Cavity quantum electrodynamics* (Academic Press New York, 1993).

[76] H. Walther, B. T. H. Varcoe, B.-G. Englert, and T. Becker, Reports on Progress in Physics **69**, 1325 (2006).

[77] R. J. Thompson, G. Rempe, and H. J. Kimble, Phys. Rev. Lett. **68**, 1132 (1992).

[78] H. Matsueda, Lasers and Electro-Optics p. 274 (1995).

[79] L. H. Pedersen and C. Rangan, Quantum Information Processing **7**, 33 (2008), ISSN 1573-1332.

[80] I. I. Rabi, Phys. Rev. **49**, 324 (1936).

[81] I. I. Rabi, Phys. Rev. **51**, 652 (1937).

[82] E. T. Jaynes and F. W. Cummings, Proceedings of the IEEE **51**, 89 (1963), ISSN 0018-9219.

[83] M. Brune, S. Haroche, J. M. Raimond, L. Davidovich, and N. Zagury, Phys. Rev. A **45**, 5193 (1992).

[84] B. Vlastakis, G. Kirchmair, Z. Leghtas, S. E. Nigg, L. Frunzio, S. M. Girvin, M. Mirrahimi, M. H. Devoret, and R. J. Schoelkopf, Science **342**, 607 (2013), ISSN 0036-8075.

[85] S. Krastanov, V. V. Albert, C. Shen, C.-L. Zou, R. W. Heeres, B. Vlastakis, R. J. Schoelkopf, and L. Jiang, Phys. Rev. A **92**, 040303 (2015).

[86] A. Imamoglu, H. Schmidt, G. Woods, and M. Deutsch, Phys. Rev. Lett. **79**, 1467 (1997).

[87] L. Zhou, Z. R. Gong, Y.-x. Liu, C. P. Sun, and F. Nori, Phys. Rev. Lett. **101**, 100501 (2008).

[88] W. Qin and F. Nori, Phys. Rev. A **93**, 032337 (2016).

[89] Z. R. Gong, H. Ian, L. Zhou, and C. P. Sun, Phys. Rev. A **78**, 053806 (2008).

[90] A. Tomadin and R. Fazio, J. Opt. Soc. Am. B **27**, A130 (2010).

[91] A. D. Greentree, C. Tahan, J. H. Cole, and L. C. L. Hollenberg, Nature Physics **2**, 856 (2006).

[92] M. J. Hartmann, F. G. S. L. Brandao, and M. B. Plenio, Nature Physics **2**, 849 (2006).

[93] D. G. Angelakis, M. F. Santos, and S. Bose, Phys. Rev. A **76**, 031805 (2007).

[94] S. Schmidt, D. Gerace, A. A. Houck, G. Blatter, and H. E. Türeci, Phys. Rev. B **82**, 100507 (2010).

[95] F. Lombardo, F. Ciccarello, and G. M. Palma, Phys. Rev. A **89**, 053826 (2014).

[96] S. Bose, D. G. Angelakis, and D. Burgarth, Journal of Modern Optics **54**, 2307 (2007).

[97] K. M. Birnbaum, A. Boca, R. Miller, A. D. Boozer, T. E. Northup, and H. J. Kimble, Nature **436**, 87 (2005).

[98] J. Tang, W. Geng, and X. Xu, Scientific Reports **5**, 9252 (2015).

[99] H. Z. Shen, Y. H. Zhou, and X. X. Yi, Phys. Rev. A **91**, 063808 (2015).

[100] A. Miranowicz, J. c. v. Bajer, M. Paprzycka, Y.-x. Liu, A. M. Zagoskin, and F. Nori, Phys. Rev. A **90**, 033831 (2014).

[101] A. Miranowicz, J. c. v. Bajer, N. Lambert, Y.-x. Liu, and F. Nori, Phys. Rev. A **93**, 013808 (2016).

[102] Y. Zhang, J. Zhang, and C.-s. Yu, Scientific Reports **6**, 24098 (2016).

[103] C. Gies, F. Jahnke, and W. W. Chow, Phys. Rev. A **91**, 061804 (2015).

[104] M. Hartmann, F. Brandao, and M. Plenio, Laser & Photonics Reviews **2**, 527 (2008), ISSN 1863-8899.

[105] T. N. Dey and G. S. Agarwal, Phys. Rev. A **76**, 015802 (2007).

[106] H. Azuma, Journal of Physics D: Applied Physics **41**, 025102 (2008).

[107] P. D. Drummond and D. F. Walls, Journal of Physics A: Mathematical and General **13**, 725 (1980).

[108] S. Ferretti and D. Gerace, Phys. Rev. B **85**, 033303 (2012).

[109] I. Fushman, D. Englund, A. Faraon, N. Stoltz, P. Petroff, and J. Vučković, Science **320**, 769 (2008), ISSN 0036-8075.

[110] S. M. Giampaolo and F. Illuminati, Phys. Rev. A **80**, 050301 (2009).

[111] G. M. A. Almeida, F. Ciccarello, T. J. G. Apollaro, and A. M. C. Souza, Phys. Rev. A **93**, 032310 (2016).

[112] B. P. Williams, R. J. Sadlier, and T. S. Humble, Phys. Rev. Lett. **118**, 050501 (2017).

[113] A. Muller, J. Breguet, and N. Gisin, EPL (Europhysics Letters) **23**, 383 (1993).

[114] K. Debnath, E. Mascarenhas, and V. Savona, New Journal of Physics **19**, 115006 (2017).

[115] T. C. H. Liew and V. Savona, New Journal of Physics **15**, 025015 (2013).

[116] M. Alexanian, Phys. Rev. A **84**, 052302 (2011).

[117] K. Kamide, Y. Ota, S. Iwamoto, and Y. Arakawa, Phys. Rev. A **96**, 013853 (2017).

[118] J. Cho, D. G. Angelakis, and S. Bose, Phys. Rev. A **78**, 062338 (2008).

[119] J.-Q. Liao, Z. R. Gong, L. Zhou, Y.-x. Liu, C. P. Sun, and F. Nori, Phys. Rev. A **81**, 042304 (2010).

[120] R. Konoike, H. Nakagawa, M. Nakadai, T. Asano, Y. Tanaka, and S. Noda, Science Advances **2** (2016).

[121] J.-Q. Liao, J.-F. Huang, Y.-x. Liu, L.-M. Kuang, and C. P. Sun, Phys. Rev. A **80**, 014301 (2009).

[122] D. E. Chang, V. Vuletic, and M. D. Lukin, Nature Photonics **8**, 685 (2014).

[123] K. M. Gheri, W. Alge, and P. Grangier, Phys. Rev. A **60**, R2673 (1999).

[124] B. M. Anderson, R. Ma, C. Owens, D. I. Schuster, and J. Simon, Phys. Rev. X **6**, 041043 (2016).

[125] M. Hennrich, A. Kuhn, and G. Rempe, Phys. Rev. Lett. **94**, 053604 (2005).

[126] M. F. Atiyah (2007), URL http://www.iecl.univ-lorraine.fr/~Wolfgang.Bertram/Atiyah-Duality.pdf.

[127] M. S. Kim, W. Son, V. Bužek, and P. L. Knight, Phys. Rev. A **65**, 032323 (2002).

[128] M. Calic, P. Gallo, M. Felici, K. A. Atlasov, B. Dwir, A. Rudra, G. Biasiol, L. Sorba, G. Tarel, V. Savona, et al., Phys. Rev. Lett. **106**, 227402 (2011).

[129] A. Huggenberger, S. Heckelmann, C. Schneider, S. Hofling, S. Reitzenstein, L. Worschech, M. Kamp, and A. Forchel, Applied Physics Letters **98**, 131104 (2011).

[130] A. Surrente, M. Felici, P. Gallo, B. Dwir, A. Rudra, G. Biasiol, L. Sorba, and E. Kapon, Nanotechnology **22**, 465203 (2011).

[131] S. D. Huver, C. F. Wildfeuer, and J. P. Dowling, Phys. Rev. A **78**, 063828 (2008).

[132] S. Noda, in *Optical Fiber Communication Conference* (Optical Society of America, 2016), p. Th1K.1.

[133] M. Notomi, T. Tanabe, A. Shinya, E. Kuramochi, H. Taniyama, S. Mitsugi, and M. Morita, Opt. Express **15**, 17458 (2007).

[134] A. F. van Loo, A. Fedorov, K. Lalumière, B. C. Sanders, A. Blais, and A. Wallraff, Science **342**, 1494 (2013), ISSN 0036-8075.

[135] M. Delbecq, L. Bruhat, J. Viennot, S. Datta, A. Cottet, and T. Kontos, Nature Communications **4**, 1400 (2013).

[136] J. Bourassa, F. Beaudoin, J. M. Gambetta, and A. Blais, Phys. Rev. A **86**, 013814 (2012).

[137] S. E. Harris, Phys. Rev. Lett. **62**, 1033 (1989).

[138] S. E. Harris, J. E. Field, and A. Imamoğlu, Phys. Rev. Lett. **64**, 1107 (1990).

[139] K.-J. Boller, A. Imamoğlu, and S. E. Harris, Phys. Rev. Lett. **66**, 2593 (1991).

[140] G. Alzetta, A. Gozzini, L. Moi, and G. Orriols, Il Nuovo Cimento B (1971-1996) **36**, 5 (1976), ISSN 1826-9877.

[141] C. K. Hong, Z. Y. Ou, and L. Mandel, Phys. Rev. Lett. **59**, 2044 (1987).

[142] P. W. Anderson, Phys. Rev. **109**, 1492 (1958).

[143] T. Schwartz, G. Bartal, S. Fishman, and M. Segev, Nature **446**, 52 (2007).

[144] S. John, Phys. Rev. Lett. **53**, 2169 (1984).

[145] S. John, Phys. Rev. Lett. **58**, 2486 (1987).

[146] Y. Lahini, Y. Bromberg, D. N. Christodoulides, and Y. Silberberg, Phys. Rev. Lett. **105**, 163905 (2010).

[147] M. Segev, Y. Silberberg, and D. N. Christodoulides, Nature Photonics **7**, 197 (2013).

[148] X. T. Zou and L. Mandel, Phys. Rev. A **41**, 475 (1990).

[149] G. S. Agarwal, *Quantum statistical theories of spontaneous emission and their relation to other approaches* (Springer Berlin Heidelberg, Berlin, Heidelberg, 1974), pp. 1–128, ISBN 978-3-540-37918-8.

[150] C. W. Gardiner, Phys. Rev. Lett. **70**, 2269 (1993).

[151] H. J. Carmichael, Phys. Rev. Lett. **70**, 2273 (1993).

[152] Z. Ficek and S. Swain, *Quantum Interference and Coherence* (Springer-Verlag New York, 2005).

[153] A. R. Bosco de Magalhães and M. C. Nemes, Phys. Rev. A **70**, 053825 (2004).

[154] F. Caruso, A. W. Chin, A. Datta, S. F. Huelga, and M. B. Plenio, The Journal of Chemical Physics **131**, 105106 (2009).

[155] R. de J Leon-Montiel, A. Valles, H. M. Moya-Cessa, and J. P. Torres, Laser Physics Letters **12**, 085204 (2015).

[156] K. Życzkowski, P. Horodecki, A. Sanpera, and M. Lewenstein, Phys. Rev. A **58**, 883 (1998).

[157] T. Shi-Qing, Y. Ji-Bing, W. Xin-Wen, and K. Le-Man, Chinese Physics Letters **32**, 040303 (2015).

[158] W. Leonski and A. Miranowicz, Journal of Optics B: Quantum and Semiclassical Optics **6**, S37 (2004).

[159] K. Jacobs and A. J. Landahl, Phys. Rev. Lett. **103**, 067201 (2009).

[160] A. Auffèves-Garnier, C. Simon, J.-M. Gérard, and J.-P. Poizat, Phys. Rev. A **75**, 053823 (2007).

[161] J. Eilbeck, P. Lomdahl, and A. Scott, Physica D: Nonlinear Phenomena **16**, 318 (1985), ISSN 0167-2789.

[162] A. S. Pikovsky and D. L. Shepelyansky, Phys. Rev. Lett. **100**, 094101 (2008).

[163] S. Flach, D. O. Krimer, and C. Skokos, Phys. Rev. Lett. **102**, 024101 (2009).

[164] D. Belitz and T. R. Kirkpatrick, Rev. Mod. Phys. **66**, 261 (1994).

[165] C. D. Ogden, E. K. Irish, and M. S. Kim, Phys. Rev. A **78**, 063805 (2008).

[166] J.-r. Liu and Y.-z. Wang, Phys. Rev. A **54**, 2326 (1996).

[167] R. L. de Matos Filho and W. Vogel, Phys. Rev. A **58**, R1661 (1998).

[168] S. Sivakumar, International Journal of Theoretical Physics **43**, 2405 (2004), ISSN 1572-9575.

[169] B. Buck and C. Sukumar, Physics Letters A **81**, 132 (1981), ISSN 0375-9601.

[170] G. S. Agarwal and R. R. Puri, Phys. Rev. A **39**, 2969 (1989).

[171] B. Yurke and D. Stoler, Phys. Rev. Lett. **57**, 13 (1986).

[172] G. Kirchmair, B. Vlastakis, Z. Leghtas, S. E. Nigg, H. Paik, E. Ginossar, M. Mirrahimi, L. Frunzio, S. M. Girvin, and R. J. Schoelkopf, Nature **495**, 205 (2013).

[173] T. Holstein and H. Primakoff, Phys. Rev. **58**, 1098 (1940).

[174] D. Manzano and E. Kyoseva, Scientific Reports **6**, 31161 (2016).

[175] A. Xuereb, A. Imparato, and A. Dantan, New Journal of Physics **17**, 055013 (2015).

[176] A. Asadian, D. Manzano, M. Tiersch, and H. J. Briegel, Phys. Rev. E **87**, 012109 (2013).

[177] A. Purkayastha, A. Dhar, and M. Kulkarni, Phys. Rev. A **94**, 052134 (2016).

[178] P. L. Garrido, P. I. Hurtado, and B. Nadrowski, Phys. Rev. Lett. **86**, 5486 (2001).

[179] A. Dhar, Advances in Physics **57**, 457 (2008).

[180] K. Saito, EPL (Europhysics Letters) **61**, 34 (2003).

[181] M. Michel, G. Mahler, and J. Gemmer, Phys. Rev. Lett. **95**, 180602 (2005).

[182] Y. Dubi and M. Di Ventra, Phys. Rev. E **79**, 042101 (2009).

[183] Z. Rieder, J. L. Lebowitz, and E. Lieb, Journal of Mathematical Physics **8**, 1073 (1967).

[184] B. Hu, B. Li, and H. Zhao, Phys. Rev. E **57**, 2992 (1998).

[185] T. N. Shah and P. Gajjar, Communications in Theoretical Physics **59**, 361 (2013).

[186] C. Starr, Physics **7**, 15 (1936).

[187] B. Li, L. Wang, and G. Casati, Phys. Rev. Lett. **93**, 184301 (2004).

[188] C. W. Chang, D. Okawa, A. Majumdar, and A. Zettl, Science **314**, 1121 (2006), ISSN 0036-8075.

[189] L. Zhang, Y. Yan, C.-Q. Wu, J.-S. Wang, and B. Li, Phys. Rev. B **80**, 172301 (2009).

[190] Y. Yan, C.-Q. Wu, and B. Li, Phys. Rev. B **79**, 014207 (2009).

[191] T. Werlang, M. A. Marchiori, M. F. Cornelio, and D. Valente, Phys. Rev. E **89**, 062109 (2014).

[192] M. Terraneo, M. Peyrard, and G. Casati, Phys. Rev. Lett. **88**, 094302 (2002).

[193] D. Segal and A. Nitzan, Phys. Rev. Lett. **94**, 034301 (2005).

[194] M. Brune, E. Hagley, J. Dreyer, X. Maître, A. Maali, C. Wunderlich, J. M. Raimond, and S. Haroche, Phys. Rev. Lett. **77**, 4887 (1996).

[195] A. Rivas, A. D. K. Plato, S. F. Huelga, and M. B. Plenio, New Journal of Physics **12**, 113032 (2010).

[196] A. Purkayastha, A. Dhar, and M. Kulkarni, Phys. Rev. A **93**, 062114 (2016).

[197] D. Manzano, M. Tiersch, A. Asadian, and H. J. Briegel, Phys. Rev. E **86**, 061118 (2012).

[198] J. P. Santos and G. T. Landi, Phys. Rev. E **94**, 062143 (2016).

[199] M. H. Partovi, Phys. Rev. E **77**, 021110 (2008).

[200] K. Micadei, J. P. S. Peterson, A. M. Souza, R. S. Sarthour, I. S. Oliveira, G. T. Landi, T. B. Batalhão, R. M. Serra, and E. Lutz, ArXiv e-prints (2017), 1711.03323.

[201] D. Jennings and T. Rudolph, Phys. Rev. E **81**, 061130 (2010).

[202] U. Zürcher and P. Talkner, Phys. Rev. A **42**, 3278 (1990).

[203] C. Gaul and H. Büttner, Phys. Rev. E **76**, 011111 (2007).